The Johns Hopkins University

Final Report on NASA Contract #NAS5-32029

High Speed QPPM Direct Detection Optical Communication Receivers for FSDD Intersatellite Links

Frederic M. Davidson
Xiaoli Sun

August 1993

ELECTRICAL & COMPUTER ENGINEERING

Final Report
on NASA Contract #NAS5-32029
High Speed QPPM Direct Detection Optical Communication Receivers for FSDD Intersatellite Links

Frederic M. Davidson
Xiaoli Sun

August 1993

Department of Electrical and Computer Engineering
The Johns Hopkins University, Baltimore, MD 21218-2686

SUMMARY

This final report consists of four separate reports, one for each project involved in this contract. The first report is entitled "325 Mbps QPPM Direct Detection Free Space Optical Communication Encoder and Receiver," which was our primary work. The second report is entitled "Test Results of the 325 Mbps QPPM High Speed Data Transmission GaAs ASICs," which describes our work in connection with Galaxy Microsystems Inc. who produced these ASICs for NASA. The third report, "Receiver Performance Analysis of BPPM Optical Communication Systems Using 1.3 μm Wavelength Transmitter and InGaAs PIN Photodiodes," was prepared at the request of the NASA/Photonics Branch for their efforts in upgrading the 1773 optical fiber data bus. The forth report, "Photomultiplier Tubes for Use at 1.064μm Wavelength," was also prepared at the request of the NASA/Photonics Branch as a research project.

325 Mbps QPPM Direct Detection Free Space Optical Communication Encoder and Receiver Manual

Xiaoli Sun
Frederic M. Davidson

Department of Electrical and Computer Engineering
The Johns Hopkins University
Baltimore, Maryland 21218-2686

August 1993

1. Introduction

This manual contains a detailed description of the operation and the design of the 325 megabit per second (Mbps) quaternary pulse position modulation (QPPM) direct detection optical communication system. This system was built for NASA as a demonstration system for potential use in optical intersatellite communication links. The system consists of three parts, the QPPM encoder, the optical link, and the QPPM receiver. The QPPM encoder receives binary data and encodes them into QPPM signals at a source binary data rate of 325 Mbps. The optical link includes a laser diode, collimating and focusing optics, neutral density attenuators to simulate free-space propagation loss, interference filters, and a silicon avalanche photodiode (APD). The QPPM receiver regenerates the QPPM signal from the noise contaminated APD output signal and then demodulates the recovered QPPM signal back to binary data. The receiver timing recovery subsystem is currently not included. One has to establish receiver synchronization by sharing the same timing signals with the transmitter.

The next section of this manual describes how to set up the system. Section 3 gives a detailed description of the QPPM transmitter and receiver electronics. Section 4 contains the test results. A parts list and copies of the data sheets of all the major components are given in Appendix.

2. System Setup and Operation

2.1. System Setup

Figure 1 shows the system set up. A bit error rate test set (BERT) is used as the binary data source which generates 1 volt peak-to-peak unipolar binary data and the clock. The coax cables for the data and the clock have to have exactly the same length. The ECL level PPM output from the encoder is used if the laser transmitter requires an ECL level drive signal or requires AC coupling (e.g. input to a bias tee). The unipolar 0-1 V PPM output requires 50Ω to ground termination and it may be connected to an oscilloscope for monitoring purposes. The binary clock and the word sync outputs from the QPPM encoder are directly connected to the corresponding QPPM receiver input ports through equal length coax cables. The cable length between the APD preamplifier and the QPPM receiver has to be adjusted according to the procedure described later. A coaxial RF attenuator is used before the QPPM receiver to adjust the input signal level since there is no automatic gain control (AGC) mechanism. The regenerated binary data from the QPPM receiver is connected to a BERT receiver. The inverted clock output from the BERT transmitter is used as the clock input to the BERT receiver.

2.2. System Operation

Connect the system as shown in Figure 1. The polarity of the QPPM encoder output is positive. An inverting transformer has to be inserted if the laser diode requires a negative polarity driving signal. The QPPM receiver also requires a positive polarity input signal. Therefore, if the APD preamplifier has negative polarity output, an inverting transformer or an inverting amplifier has to be inserted before the receiver.

Follow the procedure described below to start the system, synchronize the timing between the QPPM encoder and the receiver, and optimize the system performance.

a). Turn on the QPPM encoder, the BERT transmitter, and receiver. Check the QPPM encoder output signals with an oscilloscope. The waveforms should be the same as those shown in Figure 2.

b). Turn on the laser transmitter and adjust the laser diode bias current to slightly above its lasing threshold. Use a high speed photodiode and an oscilloscope to measure the laser pulse shape after the collimating lens. The pulse rise and fall times of the laser transmitter should be less than 500 ps (10%-90%).

c). Align the laser collimating lens, the neutral density attenuators, the interference filter, and the focusing lens. The interference filter may need to be tilted to tune to the laser wavelength. Do not align the APD at this time since it may be damaged by the excess optical power at the input by accident.

d). Connect the APD preamplifier output to an oscilloscope through a DC blocking capacitor (such as Picosecond Pulse Lab- Model 5500, or simply a bias tee). Turn on the power for the APD and adjust the APD bias voltage to a few volts below the break-down point.

e). Gradually bring the APD into the focal point of the signal beam. Align the APD by monitoring its output until the pulse amplitude reaches its maximum. The amount of attenuation of the neutral density filters may have to be set to very little in the beginning and gradually increased as the APD is brought into the focal point of the signal

beam. The peak to peak voltage of the APD preamplifier output should always be kept well below the damage threshold (100 μA times the gain of the transimpedance preamplifier).

f). Increase the APD gain by adjusting the APD bias voltage closer to the break-down point until the noise on the waveform begins to grow faster than the signal. The input optical signal level may have to be reduced by inserting more neutral density filters.

g). Connect the APD preamplifier output to a 15-20 dB wide band (1-1000 MHz) low noise amplifier, such as MiniCircuit ZFL-1000LN, then a variable RF attenuator. Connect the output of the RF attenuator output to the oscilloscope.

h). Adjust the optical input signal level to about 10 nW. Adjust the RF attenuator until its average output pulse amplitude is 50-100 mV. Figure 3 shows an example of the waveform. The RF attenuator output is the input to the QPPM receiver.

i). Find a pair of back-to-back QPPM pulses on the screen of the oscilloscope. Adjust the length of the coax cable between the QPPM transmitter and the laser transmitter so that the back-to-back QPPM pulse pair and the binary clock and the QPPM word sync signal at the input to the QPPM receiver are aligned as shown in Figure 4. Connect all three signals to the corresponding ports on the front panel of the QPPM receiver.

j). The system should start to work and the BERT receiver should be able to establish synchronization and measure the receiver BER. Begin with a short PN code (e.g. 2^7-1 bits long) at the BERT transmitter. Connect

the inverted data output from the QPPM receiver to the oscilloscope and one should see the recovered binary data.

k). Reduce the input optical power further such that the receiver BER is about 10^{-4} to 10^{-5}. Adjust the APD position and adjust the length of the coax cable from the QPPM encoder to the laser transmitter for the lowest receiver BER.

l). Adjust the input optical power such that the receiver BER is kept at about 10^{-5} to 10^{-6}. Optimize the APD gain for minimum receiver BER. The RF attenuator also needs to be adjusted slightly for each APD gain setting such that the average input signal level into the QPPM receiver is nearly constant (50-75 mV peak-to-peak).

m). The optimization process may have to be iterated several time until the input optical signal power required to achieve a BER of 10^{-6} is finally minimized.

3. System Description

3.1 The 325 Mbps QPPM Encoder Electronics

Both the QPPM encoder and the Receiver electronics were similar to our previous 220 Mbps QPPM system described in [1] and [2].

Figure 5 shows a schematic circuit diagram of the QPPM encoder. The circuit was built with GaAs digital ICs manufactured by Triquint Semiconductors, Inc. (formerly GigaBit Logic). The circuit was constructed on a GigaBit Logic 90GUPB-40 high speed prototyping board

with the matching 90GPPS power supply card. The board provided the chips with all the necessary DC power supplies and decoupling capacitors right at the chip sites. Miniature semirigid coaxial cables were used for all high speed signals between chips and between chips and input and output SMA connectors.

In Figure 5, the buffered binary data clock was used to clock the data in and also to generate the QPPM slot clock through a frequency doubler. The lowpass filters before and after the frequency doubler were necessary to reduce the effects of higher order harmonics. The amplifier after the doubler was used to make up the loss of the frequency doubler. The QPPM encoder also worked at data rates other than 325 Mbps, though it was not specifically tuned to operate over a wide range.

The dual D-flip-flop chip (10G021A) in Figure 5 was used as a two bit shift register for the binary data. The quad NOR chip encoded every two bits into the corresponding QPPM format in parallel form and the 4 bit shift register (10G022) loaded the parallel QPPM word and then shifted it out in series. The counter (10G061) was used to divide the QPPM slot clock and generate the QPPM word sync signal.

Figure 6 shows the correspondence between the binary bit patterns and the QPPM patterns. Figure 7 shows the timing diagram. Figures 8 and 9 show the top and bottom views of the assembled QPPM encoder. Figure 10 shows the chip location on the board. Figure 11 shows the pulse shapes of the QPPM output signals from the encoder.

3.1 The 325 Mbps QPPM Receiver Electronics

Figures 12 and 13 show the schematic circuit diagram of the QPPM receiver. The components shown in Figure 12 were all mounted on the chassis and those shown in Figure 13 were on the circuit board.

The APD preamplifier output was followed immediately by a low noise wide band amplifier. The RF attenuator after that was used to adjust the input signal level since there is no AGC mechanism in the receiver front end. The signal was further amplified and filtered inside the receiver box. The combination of the amplifiers and the Bessel lowpass filter had a system response close to a raised cosine filter described in [3]. The filtered output was then split and delayed before being fed into the comparator bank and the subsequent decision logic. Since the coax delay cables were cut to the lengths for 325 Mbps QPPM signal, the receiver could only operate at this data rate.

The high speed QPPM signals were split through the on board 3-way resistive power splitter and then sent to the comparators (10G012B). The quad 3 input NOR chip (10G000A) after the comparator performed the function of choosing the QPPM slot that contained the largest signal output. One of the gates on the chip was not necessary for this purpose because its output would be redundant. The gate was used to buffer the word sync signal. The two NOR gates (10G001) and the shift register (10G022) demodulated the regenerated QPPM signal back to binary data.

Figure 14 shows the timing diagram of the QPPM detection and demodulation circuit. Figure 15 shows a picture of the top view of the QPPM receiver box. There is nothing mounted on the bottom of the chassis. Figure 16 shows the chip locations on the circuit board.

3.3 The Optical Link

The optical link consisted of an AlGaAs laser diode at about 830 nm wavelength, collimating and focusing optics, neutral density attenuators, an interference filter, and a silicon avalanche photodiode (APD) with its preamplifier. The entire optic setup is already shown in Figure 1.

The laser diode must have a fast rise and fall time, less than 500ps from 10% to 90% of the average pulse amplitude. Most of the laser diodes tend to have a longer trailing edge than the rising edge, which is acceptable provided they are both within 500 ps. For test purposes, a low power AlGaAs laser diode is suggested since it is easier to operate to achieve high speed and good pulse shapes.

The neutral density attenuators which consisted of a set of fixed attenuators and a variable one were used to simulate free-space propagation loss. The interference filter was used to block out broad band back ground radiation noise and spontaneous emission from the laser. The interference filter had to be tilted at certain angle with respect to the incident laser beam to tune the center of the pass band to the laser wavelength. The focusing lens before the APD had to be able to focus the signal beam well within the APD active area.

The Si APD and the preamplifier should ideally should have greater than 800 MHz electrical bandwidth. The preamplifier should be extremely low noise in order to achieve a high receiver sensitivity. A transimpedance preamplifier is usually used for high stability and wide dynamic range. The preamplifier output should be connected to the

subsequent amplifier with as short a cable as possible in order to avoid oscillation and maintain the signal to noise ratio.

4. Test Results

The system was tested both in the lab at the Johns Hopkins University and in the lab at the Photonics Branch of NASA Goddard Space Flight Center. Similar test results were obtained at both locations although the components of the optical link were different. The laser transmitters and the APD preamplifier modules used in the tests are described in this section. The test data from the raised cosine filter are also included. The measured system performance is presented at the end of this section.

4.1. The Laser Transmitter

The first laser transmitter used was a medium power AlGaAs laser diode, SDL-5420-C by Spectral Diode Lab. The temperature controller and the laser diode mount were made by NASA. The bias current supply was made by ILX (LDX-3207). The QPPM signal was combined with the bias current with the use of a bias tee (Picosecond Pulse Lab 5575A). The QPPM signal from the encoder had to be amplified to 2.3 volts peak-to-peak before being fed into the bias tee in order to obtain clean laser pulse shapes. Figure 17 shows the QPPM driving pulse shape. Figure 18 shows the output laser pulse shape measured with a high speed PIN photodiode (Opto-Electronics, PD-10).

4.2. APD and Preamplifier

The photodetectors used in our test were the so called *Slik* APDs developed by EG&G Canada [4] which feature a "super low ionization coefficient," $k_{eff} \approx 0.005$ as compared to $k_{eff} \approx 0.020$ of the commercial grade devices. Typical quantum efficiency at 800 nm wavelength is about $\eta = 90\%$. The diameter of the active area of the APD is 100 μm.

Two transimpedance preamplifiers were used, one was an Anadigics ATA12000 and the other was a GigaBit Logic 16G072-10X. The APDs and their preamplifiers were integrated into sealed hybrid circuit modules by EG&G Canada. The transimpedance of the preamplifiers were 1.5 kΩ and 10 kΩ, respectively. The former had a bandwidth of about 900 MHz and the latter had a bandwidth of about 350 MHz after being integrated with the APDs.

We primarily used the photodetector module with the Anadigics ATA12000 preamplifier since it gave much better pulse shapes. The preamplifier also contained an AGC circuit although the AGC threshold current was relatively high (100 μ A) as compared with our normal operation signal level (≈1 μA at 10 nW input optical signal level). The APD high voltage bias supply consisted of a programmable DC to DC converter (Analog Modules 522-2). It had an internal temperature compensation circuit and the rms output ripple was 5 mV.

The characteristics of the APD preamplifier module (EG&G Canada C30964E/CD1796, serial number 0011) was first determined experimentally. The preamplifier noise current density was found by measuring the noise power spectrum while keeping the APD completely in the dark. The only noise sources under this condition were the APD dark current and the preamplifier circuit noise. The APD dark current

noise was found to be so small that it caused little change in the noise spectrum when the APD bias voltage varied from well below to near the breakdown voltage. Figure 19 shows the measured noise power spectrum. Note a low noise and broad band amplifier (MiniCircuit ZFL-1000LN, 23.5 dB) was used before the spectrum analyzer. At 500 MHz, the noise density measured by the spectrum analyzer was -126.4 dBm/Hz. The noise power density at the preamplifier output was therefore -149.9 dBm/Hz or $1.02X10^{-18}$ Watts/Hz. Multiplying it by 50Ω and taking the square root, the voltage noise density was 7.15 $nV/Hz^{1/2}$. Dividing it by the transimpedance (1.5 kΩ), the current noise density was equal to 4.8 pA/√Hz.

The APD ionization coefficient, k_{eff}, was found by measuring the APD output excess noise factor under a relatively strong CW incident laser light such that the APD excess noise became dominant. The APD excess noise factor, F, is defined as the ratio of the mean square to the square of mean of the APD gain and is related to k_{eff} by [5]

$$F = k_{eff}G + (2 - \frac{1}{G})(1 - k_{eff})$$

where G is the average APD gain. The excess noise factor is also the solution to the equation

$$\frac{d\langle i^2\rangle_{ncw}}{df} = 2qFG^2\frac{\eta P_{cw}}{hf}$$

where $d\langle i^2\rangle_{ncw}/df$ is the spectral noise current density, q is the electron charge, P_{cw} is the incident CW laser optical power, and hf is the photon energy.

The spectral noise current density was measured directly using a spectrum analyzer, similar to how the preamplifier noise current density was measured. The incident CW laser optical power was held at 15 nW, which was well below the preamplifier AGC threshold.

The average APD gain was determined by modulating the laser diode with a QPPM signal and measuring the pulse amplitude, V_{p-p}, of the output from the APD preamplifier. The average APD gain is the solution to the equation

$$V_{p-p} = Gq \frac{\eta P_{p-p}}{hf} R_f A$$

where P_{p-p} is the peak-to-peak incident optical signal power, R_f is the preamplifier transimpedance, and A is the gain of the amplifier after the preamplifier. The laser ON-OFF extinction ratio was kept high such that P_{p-p} was equal to the average optical signal power, P_{av}, divided by the PPM signal duty cycle, 25%. The average optical signal power was measured directly using an optical power meter. The APD gain was held at $G \approx 100$ during the measurements. The APD ionization coefficient was obtained by substituting the above two equations into the previous one. The resultant ionization coefficient was about $k_{eff}=0.0050$.

We also calculated k_{eff} by the measuring statistics of the pulse amplitude fluctuations. It has been shown [6] that the variance of the pulse amplitude fluctuation can be written as

$$\sigma_A^2(t) = G^2 F \int_0^\infty \frac{\eta P_s(t-\tau)}{hf} h^2(\tau) d\tau$$

where $P_S(t)$ is the received optical signal power and h(t) is the combined impulse response of the APD and the preamplifier. One can find k_{eff} by measuring σ_A^2 for two different values of the average APD gain at a fixed time under a given input signal power. The ratio of the two measurements is

$$\frac{\sigma_{A1}^2}{\sigma_{A2}^2} = \frac{G_1^2 F_1 \int_0^\infty \frac{\eta P_s(t-\tau)}{hf} h^2(\tau) d\tau}{G_2^2 F_2 \int_0^\infty \frac{\eta P_s(t-\tau)}{hf} h^2(\tau) d\tau} = \frac{G_1^2 F_1}{G_2^2 F_2}$$

$$= \frac{G_1^2 [k_{eff} G_1 + \left(2 - \frac{1}{G_1}\right)(1 - k_{eff})]}{G_2^2 [k_{eff} G_2 + \left(2 - \frac{1}{G_2}\right)(1 - k_{eff})]}$$

Once the values of G_1 and G_2 are determined, the value of k_{eff} can be obtained by solving the above equation. The value of k_{eff} for the APD used was found to be 0.0048 based on this method.

Figure 20 shows the average pulse shape output from the APD preamplifier at 50 nW average input optical signal power at a relatively low gain. Figure 21 shows the APD preamplifier output amplified by the ZFL-1000LN amplifier at 6.5 nW average input optical signal power at an average APD gain of about 120.

4.3. Raised Cosine Filter

Theoretical analysis and simulation suggested the used of a 7th order 845 MHz 3dB bandwidth Bessel lowpass filter as the raised cosine filter. However, the response of the APD preamplifier and other amplifiers we used were far from ideal and the pulse shape output from the Bessel lowpass filter did not look like a raised cosine filter output.

We found during the experiment that the receiver performance was better when we added in series another 7th order 570 MHz 3 dB bandwidth Bessel lowpass filter. The actual filter assembly was constructed by trial and error with all the components at hand. The actual filter consisted of an amplifier (MiniCircuit ZFL-500), the 570 MHz Bessel lowpass filter, a 1 dB attenuator, another amplifier (MiniCircuit ZFL-1000VH), and the 845 MHz Bessel lowpass filter, as shown in Figure 12. The amplifiers were used both to boost the received QPPM signal level and to buffer between filters for better impedance match. The attenuator was also used to improve the impedance matching. Figure 22 shows the frequency response of the filter assembly measured by a spectrum analyzer while illuminating the APD with a relatively strong CW light.

4.4. Receiver BER versus the Input Optical Signal Power.

The receiver BER was measured as a function of the average received optical power. Figure 23 shows the measurement results. Figure 24 is the same as Figure 24 but the received optical signal power is expressed in average signal photons per bit. The average APD gain was optimized around BER= 10^{-6} by adjusting the APD bias voltage until the BER reached its minimum for a given input optical signal. The value of optimal APD gain was found to be about 130. The theoretical results shown in Figure 24 was based on the algorithm described in [3]. The value of the optimal average APD gain predicted by the theory was 200. The interference between pulses behaved to some degree as background radiation noise and resulted in a lower optimal average APD gain in practice. The laser ON-OFF extinction ratio was taken to be 100 in the

calculation. The APD preamplifier module used was an EG&G *Slik* silicon APD with an Anadigics ATA12000 transimpedance preamplifier.

Figure 25 shows the measurement results using a different APD preamplifier module which contained a *Slik* APD and a GigaBit Logic 16G072-10X transimpedance preamplifier. This preamplifier had lower noise, about 3.1 $pA/Hz^{1/2}$, but a narrower electrical bandwidth, 350 MHz, after integrated with the APD into a hybrid circuit. The optimal average APD gain in this case was about 54. Once again, the theoretically predicted optimal average APD gain was higher, $G_{opt}=150$.

Table 1 shows the tabulated data plotted in Figures 23 through 25.

The discrepancy between the theoretical calculations and the measurement data was believed to be caused by the intersymbol interference due to poor APD preamplifier output pulse shape.

References

[1] X. Sun and F. M. Davidson, 'Direct Detection Optical Intersatellite Link at 220 Mbps Using AlGaAs Laser Diode and Silicon APD with 4-ary PPM signaling,' Interim progress report on NASA grant #NAG5-356 "Optical Communication with semiconductor laser diode" for the period Sept. 1989 - Feb. 1990. Department of Electrical and Computer Engineering, the Johns Hopkins University, Baltimore, MD 21218.

[2] F. M. Davidson and X. Sun, 'Performance Measurement Results for a 220 Mbps QPPM Optical Communication Receiver with an EG&G

Slik APD,' Progress report on NASA grant #NAG5-510, "Reduced electrical bandwidth receivers for direct detection 4-ary PPM optical communication intersatellite links", for the period Oct. 16, 1991 to July 15, 1992, Department of Electrical and Computer Engineering, the Johns Hopkins University, Baltimore, MD 21218.

[3] F. M. Davidson, X. Sun, and M. A. Krainak, 'Bandwidth requirements for direct detection optical communication receivers with PPM signaling,' in *Free-Space Laser communication Technologies III*, David L. Begley and Bernard D. Seery, Eds., proc. SPIE 1417, 1991.

[4] A. D. MacGregor, B. Dion, C. Noldeke, and O. Duchmann, '39 photons/bit direct detection receiver at 810 nm, BER=1x10^{-6}, 60 Mb/s QPPM,' in *Free-Space Laser communication Technologies III*, David L. Begley and Bernard D. Seery, Eds., proc. SPIE 1417, 1991.

[5] P. P. Webb and R. J. McIntyre, 'Properties of Avalanche Photodiodes,' RCA Reviews, vol. 35, pp. 234-278, June 1974.

[6] D. L. Snyder, *Random Point Processes*, New York: Wiley, 1975, ch. 4.

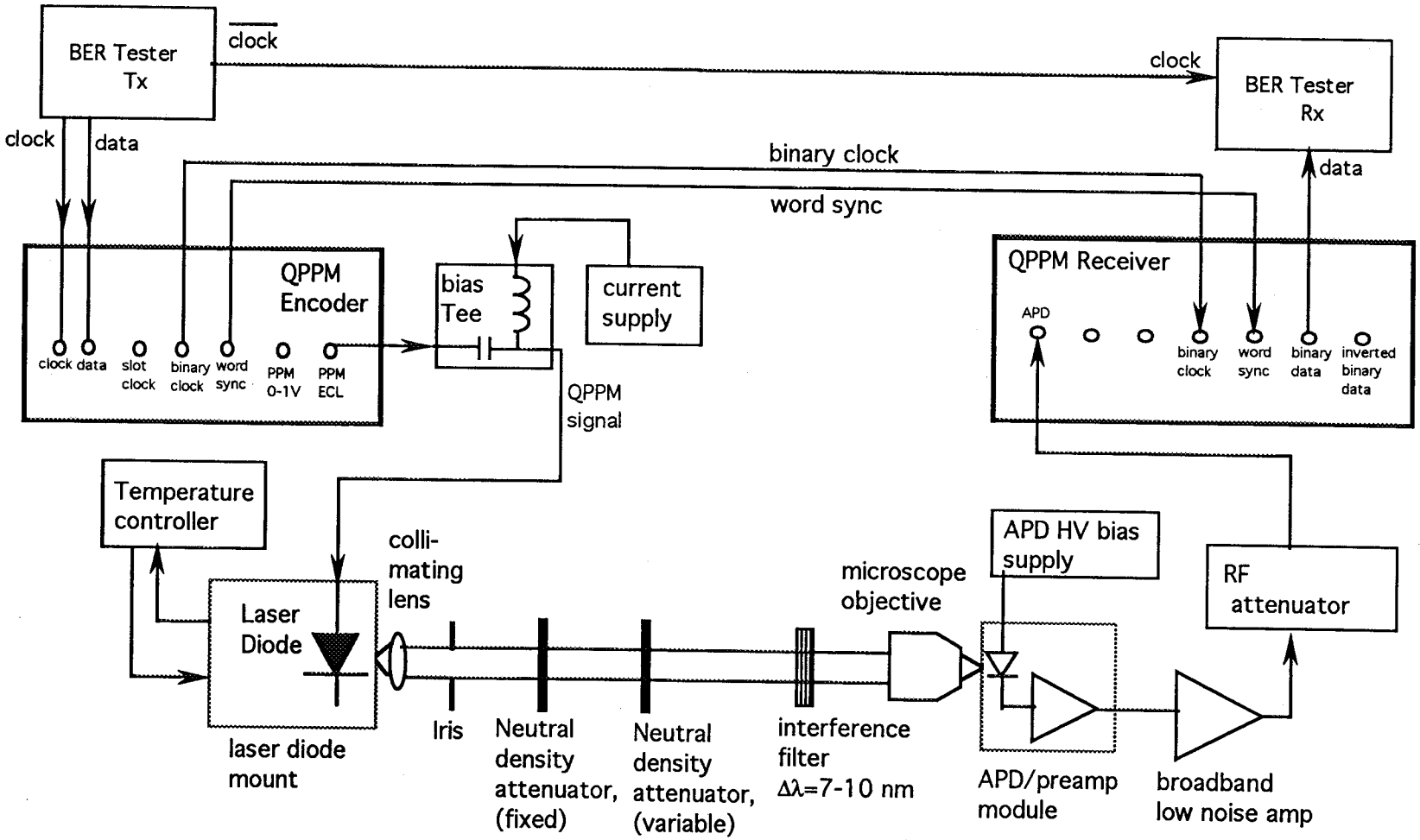

Figure 1. 325 Mbps QPPM direct detection optical communication system setup

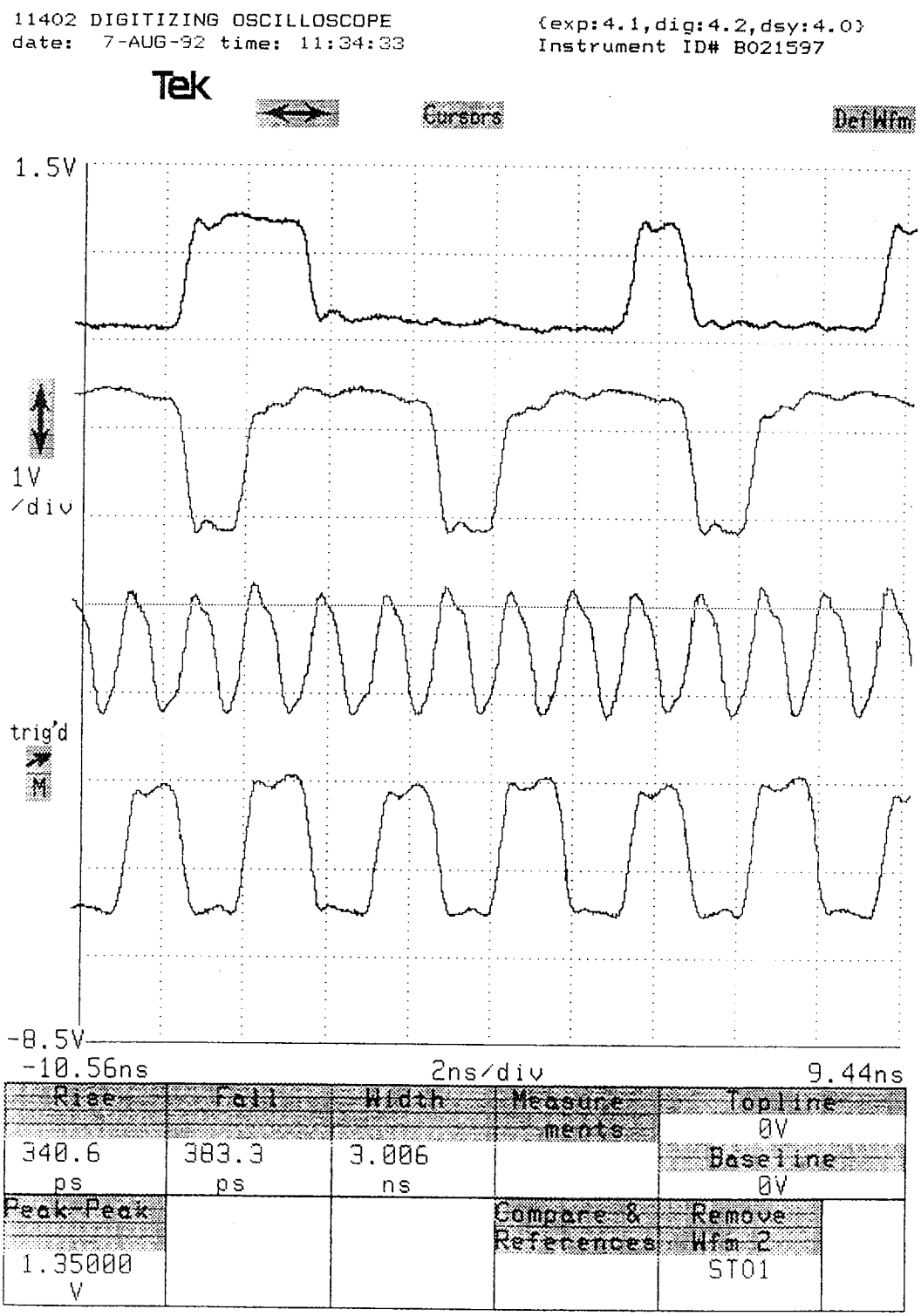

Figure 2. The waveforms of the QPPM encoder outputs. They are, from the top down, the binary data, the inverted QPPM signal output, the QPPM slot clock, and the binary data clock.

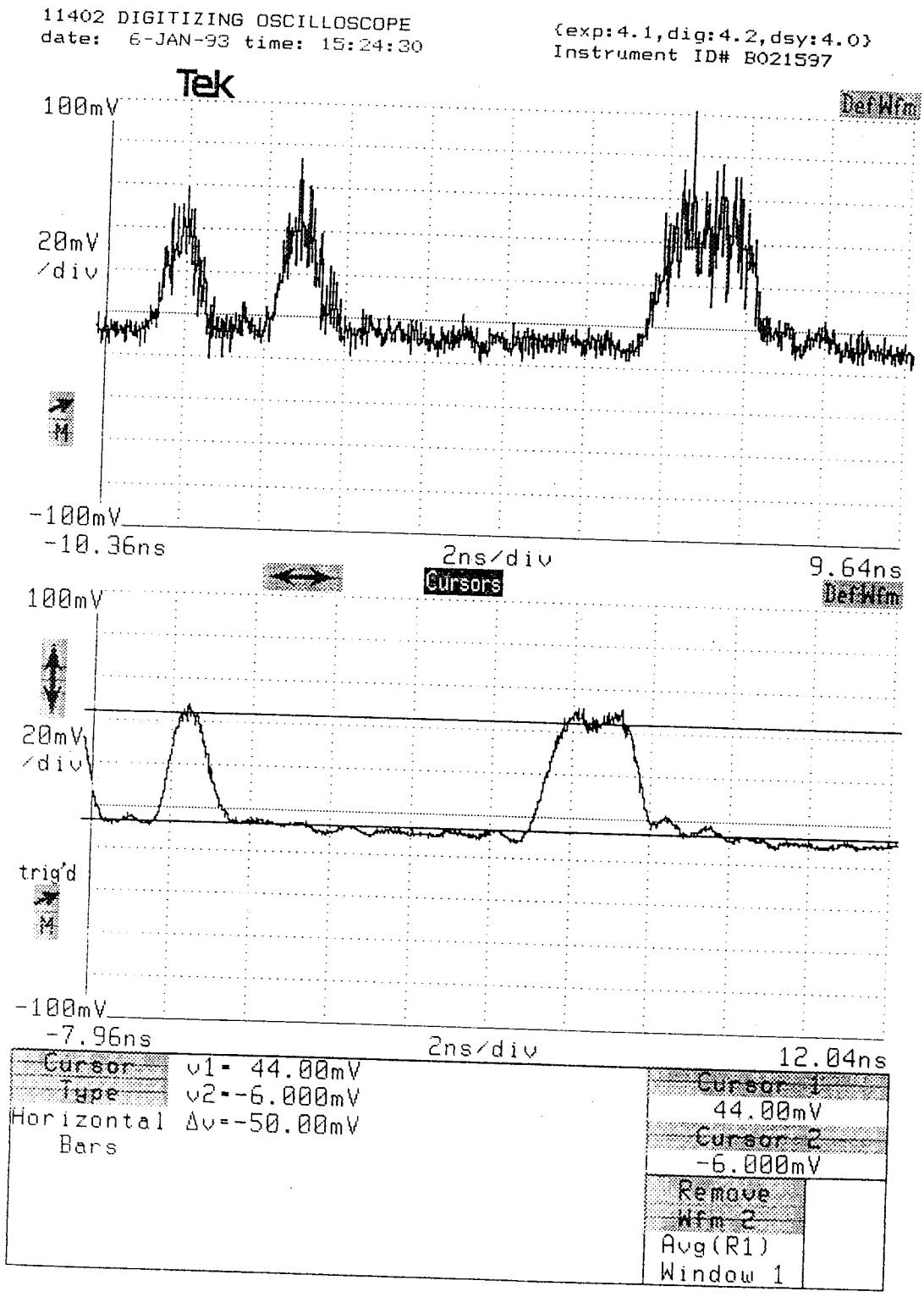

Figure 3. The waveform of the APD preamplifier after a MiniCircuit ZFL-1000LN amplifier under 6.5 nW average input optical signal. The trace in the lower graticule is the averaged waveform.

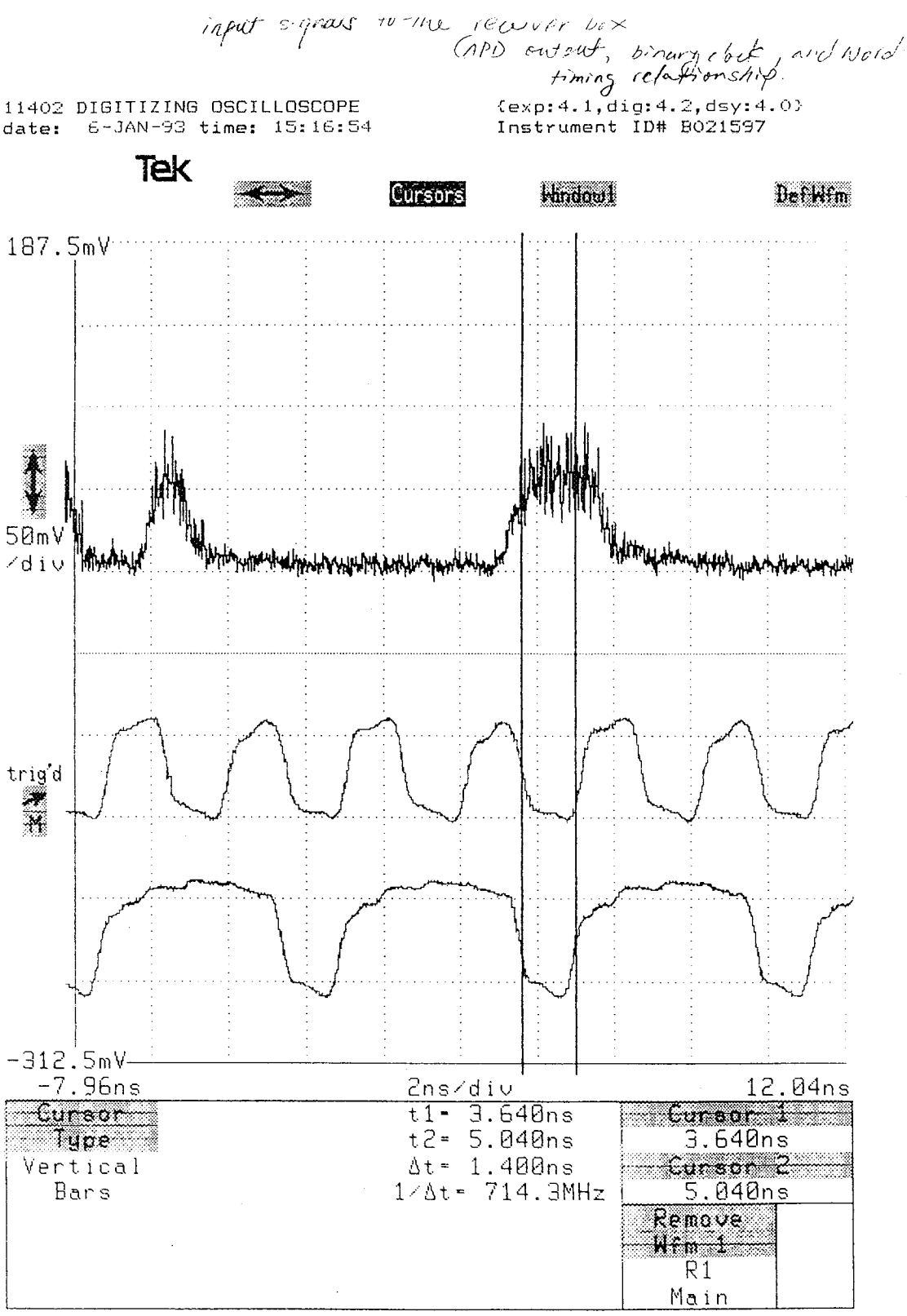

Figure 4. Timing relationship between the received QPPM signal, the binary data clock, and the QPPM word sync at the input of the QPPM receiver box.

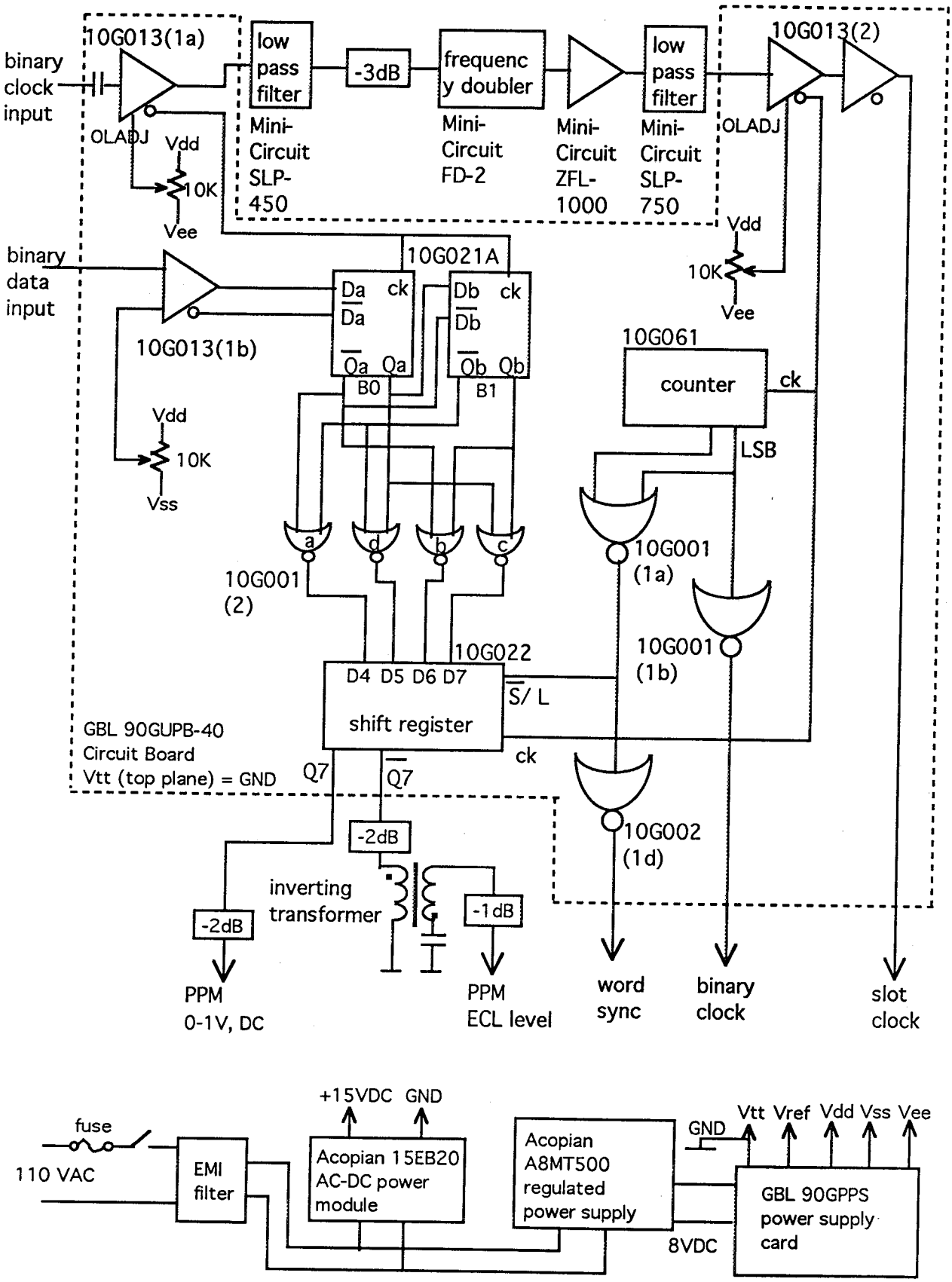

Figure 5. Circuit diagram of the 325 Mbps QPPM encoder

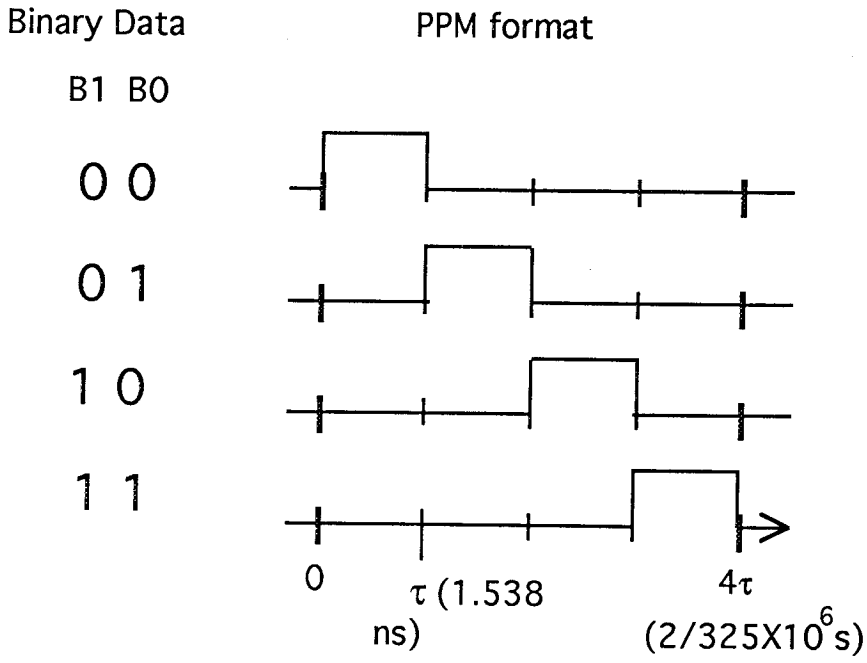

Figure 6. QPPM encoding format

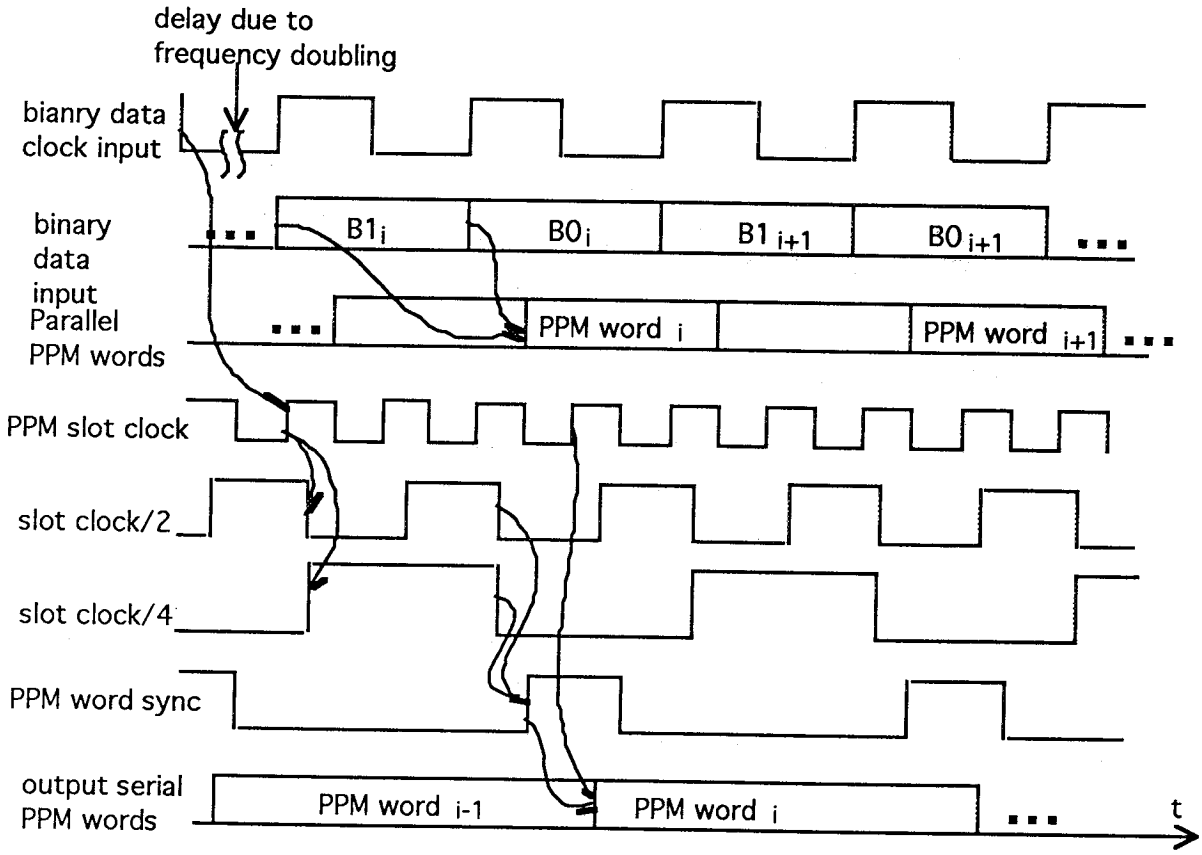

Figure 7. QPPM Encoder timing diagram

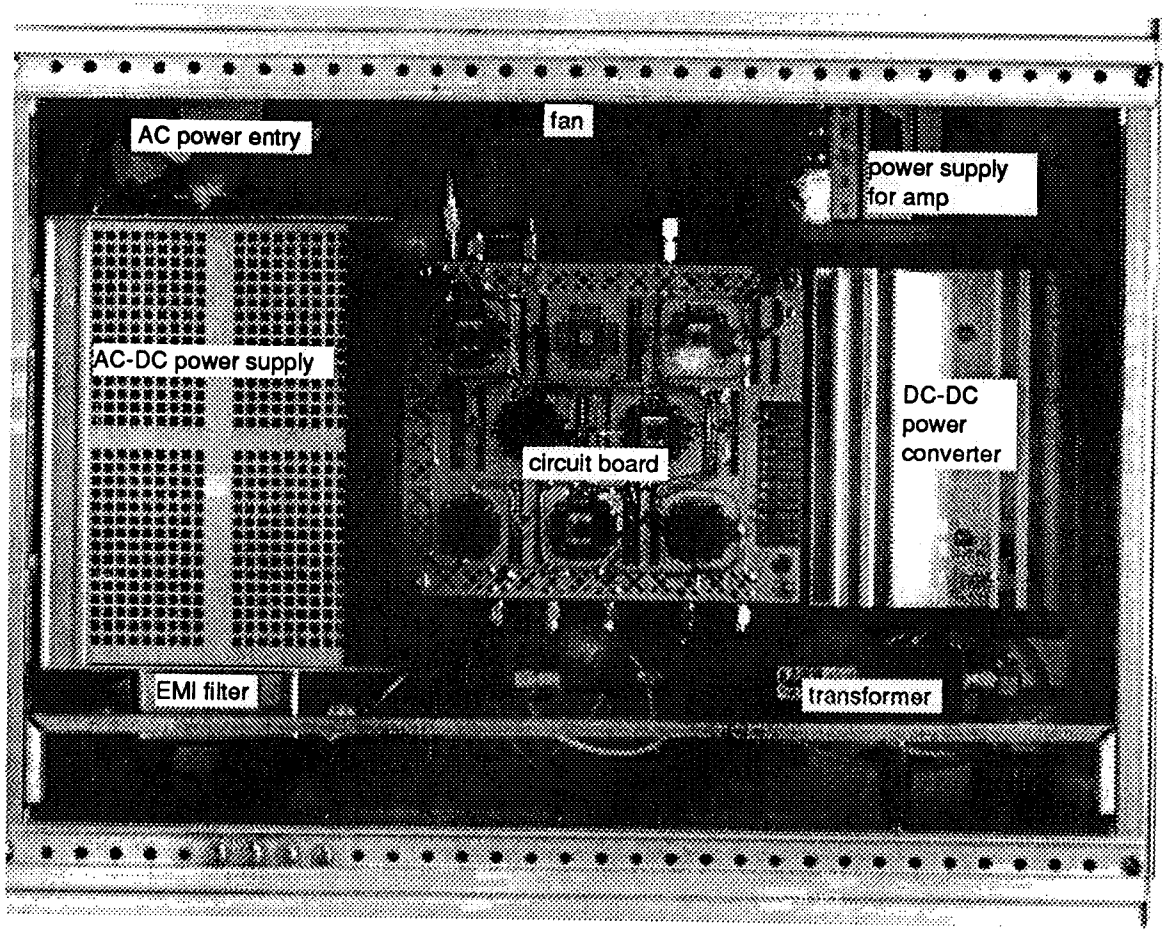

Front Panel, Signal Inputs and Outputs

Figure 8. Top view of the 325 Mbps QPPM encoder.

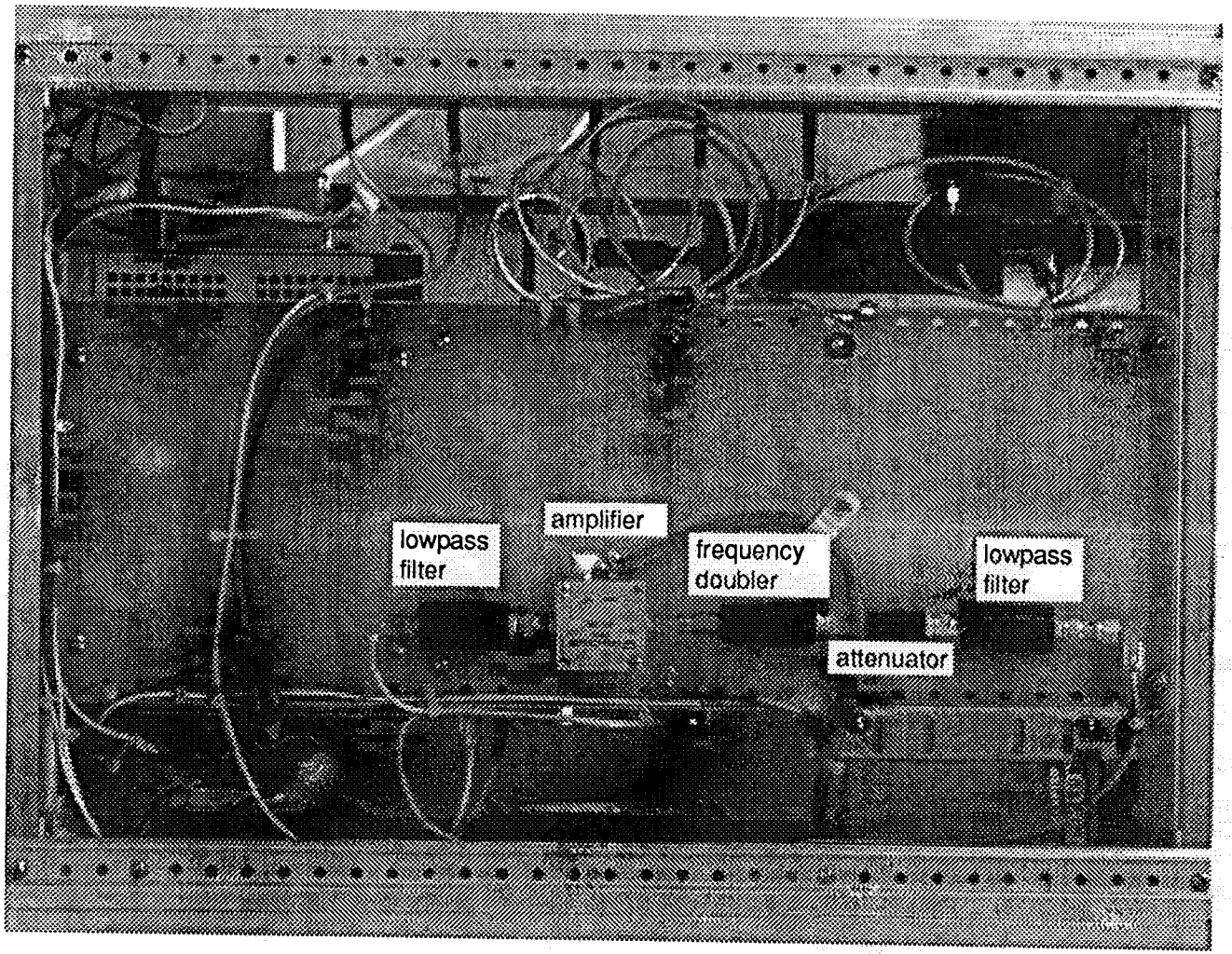

Figure 9. Bottom view of the 325 Mbps QPPM encoder.

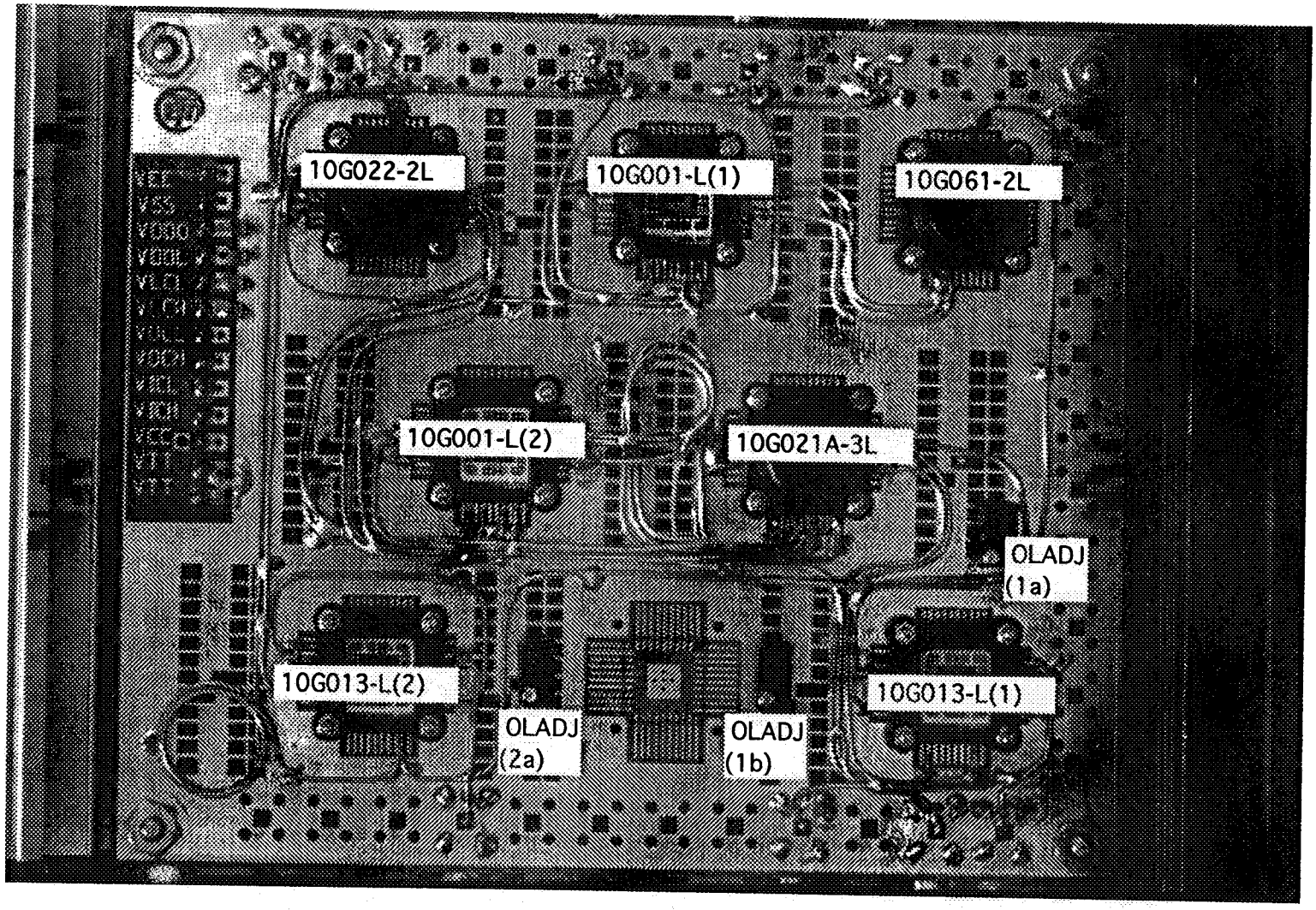

Figure 10. Top view of the 325 Mbps QPPM encoder circuit board

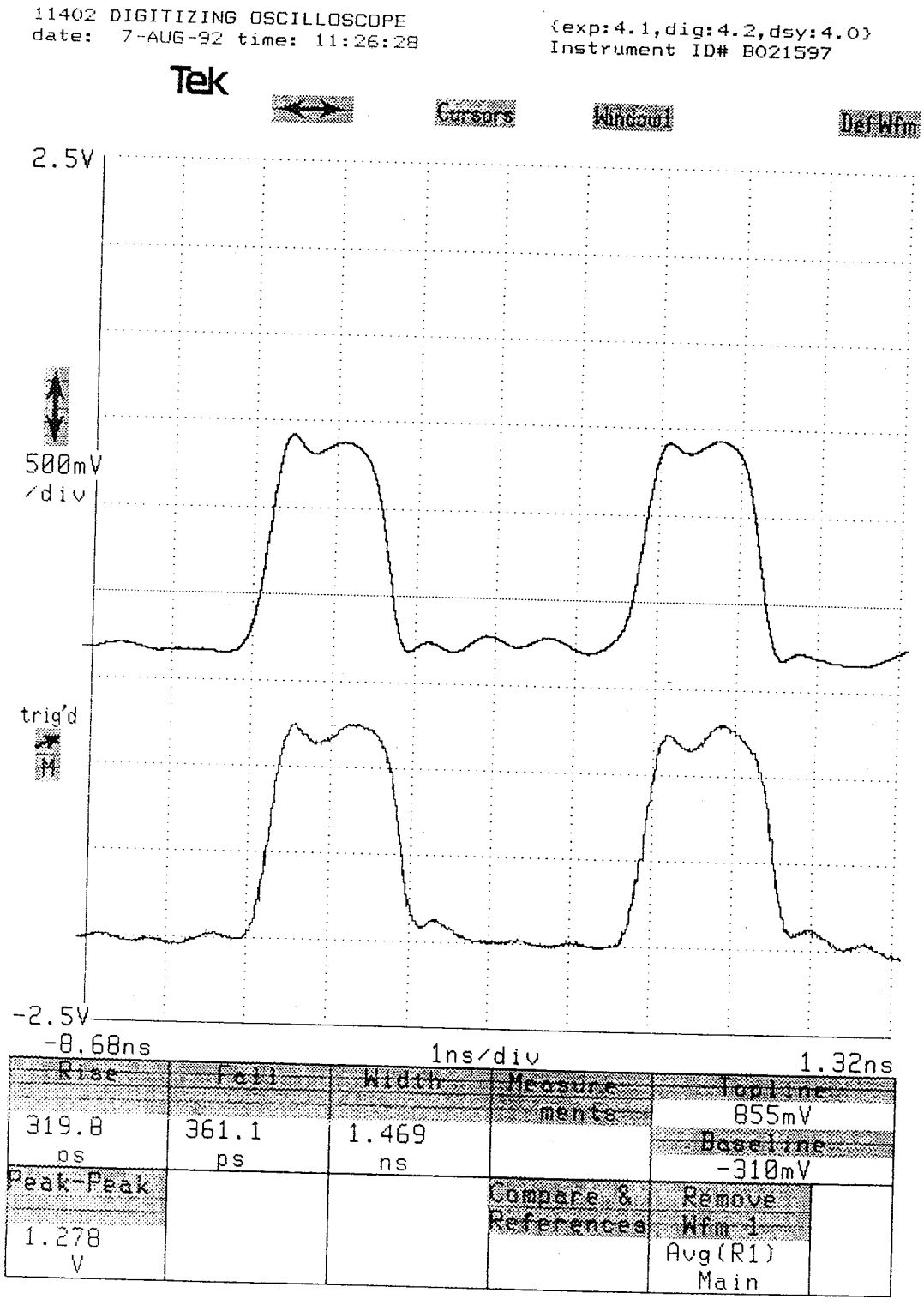

Figure 11. QPPM pulse shapes of the QPPM encoder outputs. The top trace is from the ECL level output terminal and the lower trace is from the 0-1 V output terminal.

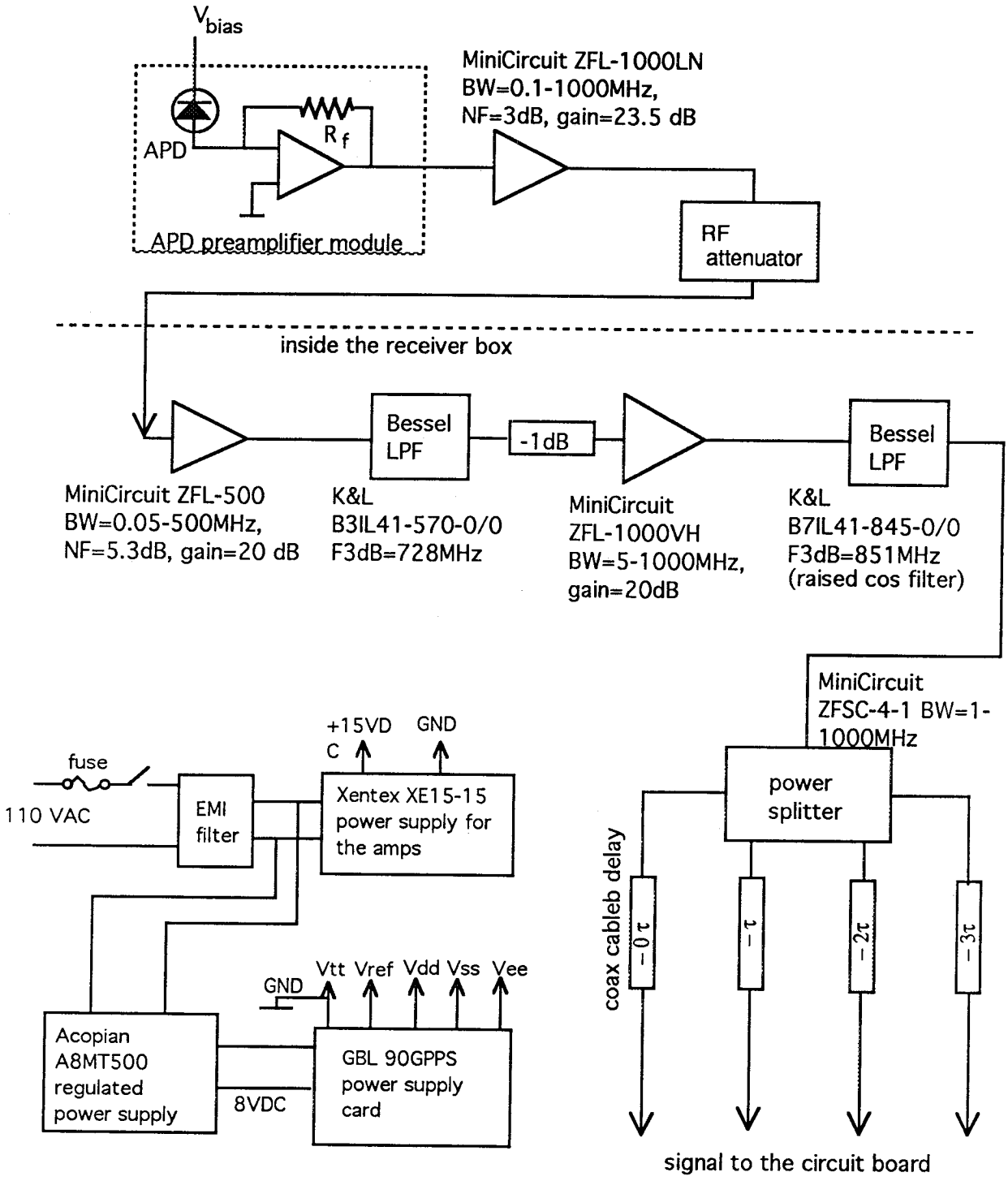

Figure 12 Circuit diagram of the 325 Mbps QPPM receiver (a)
Analog signal amplification and filtering

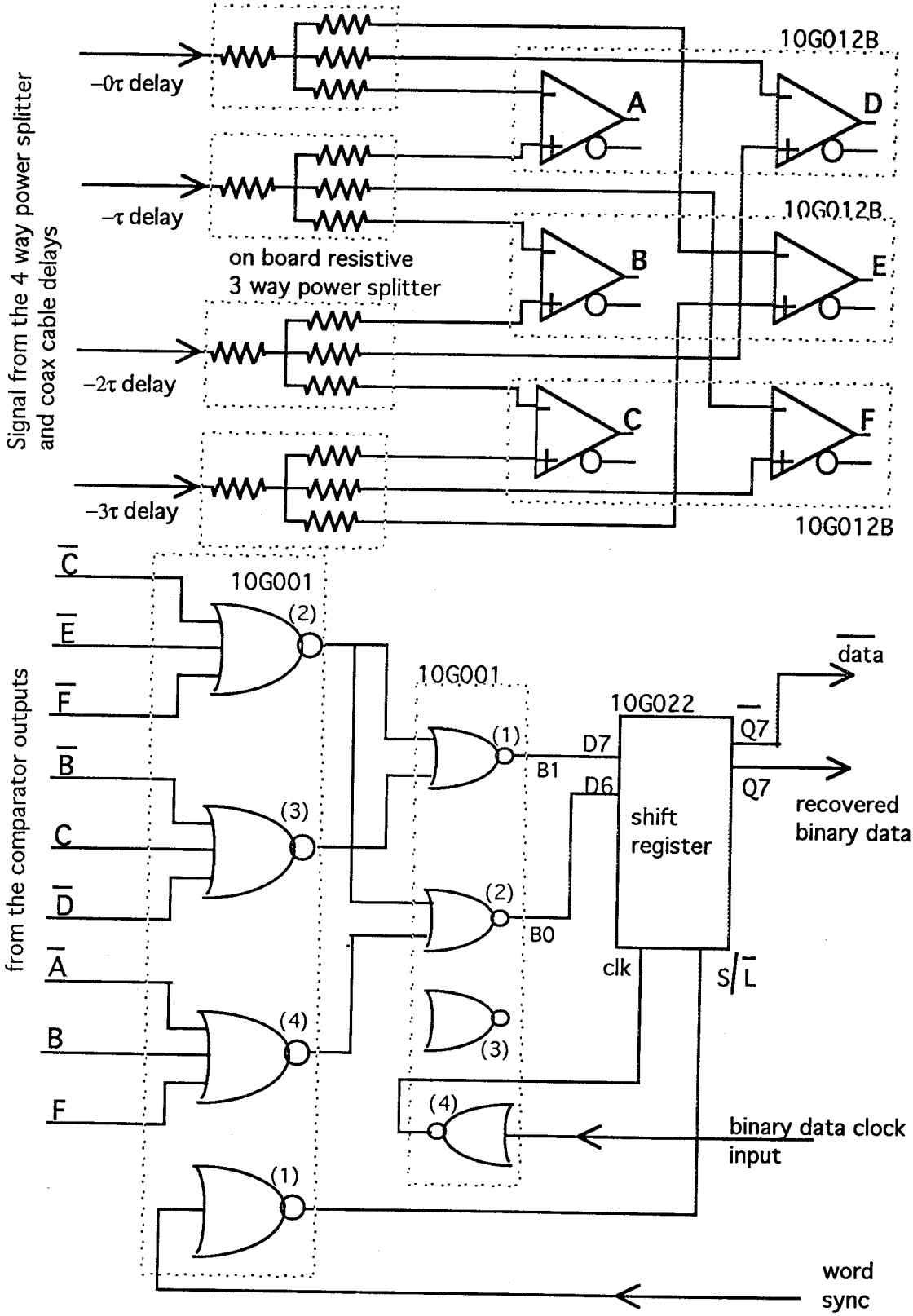

Figure 13. Circuit diagram of the 325 Mbps QPPM receiver (b) The circuit board

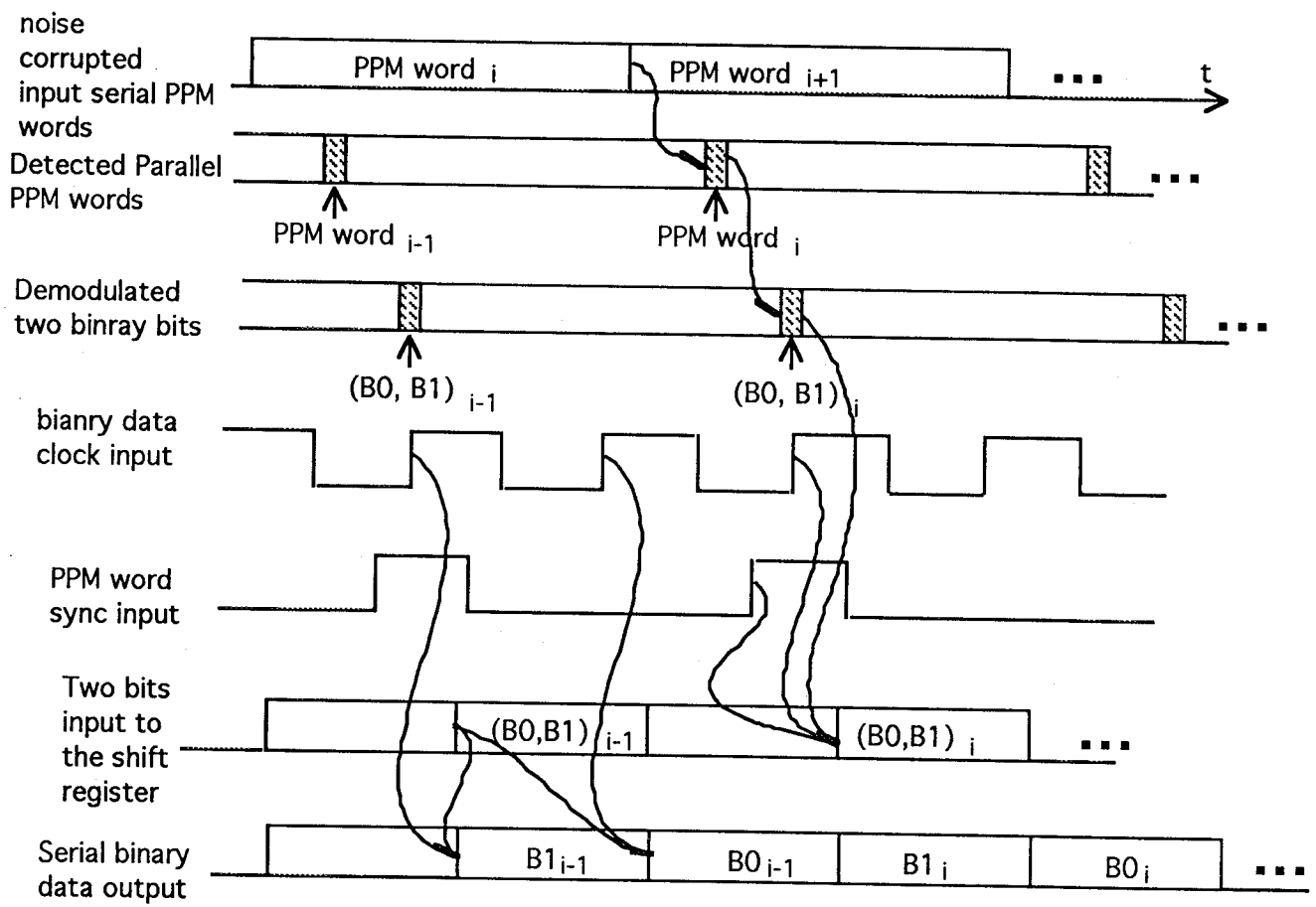

Figure 14. 325 Mbps QPPM receiver timing diagram

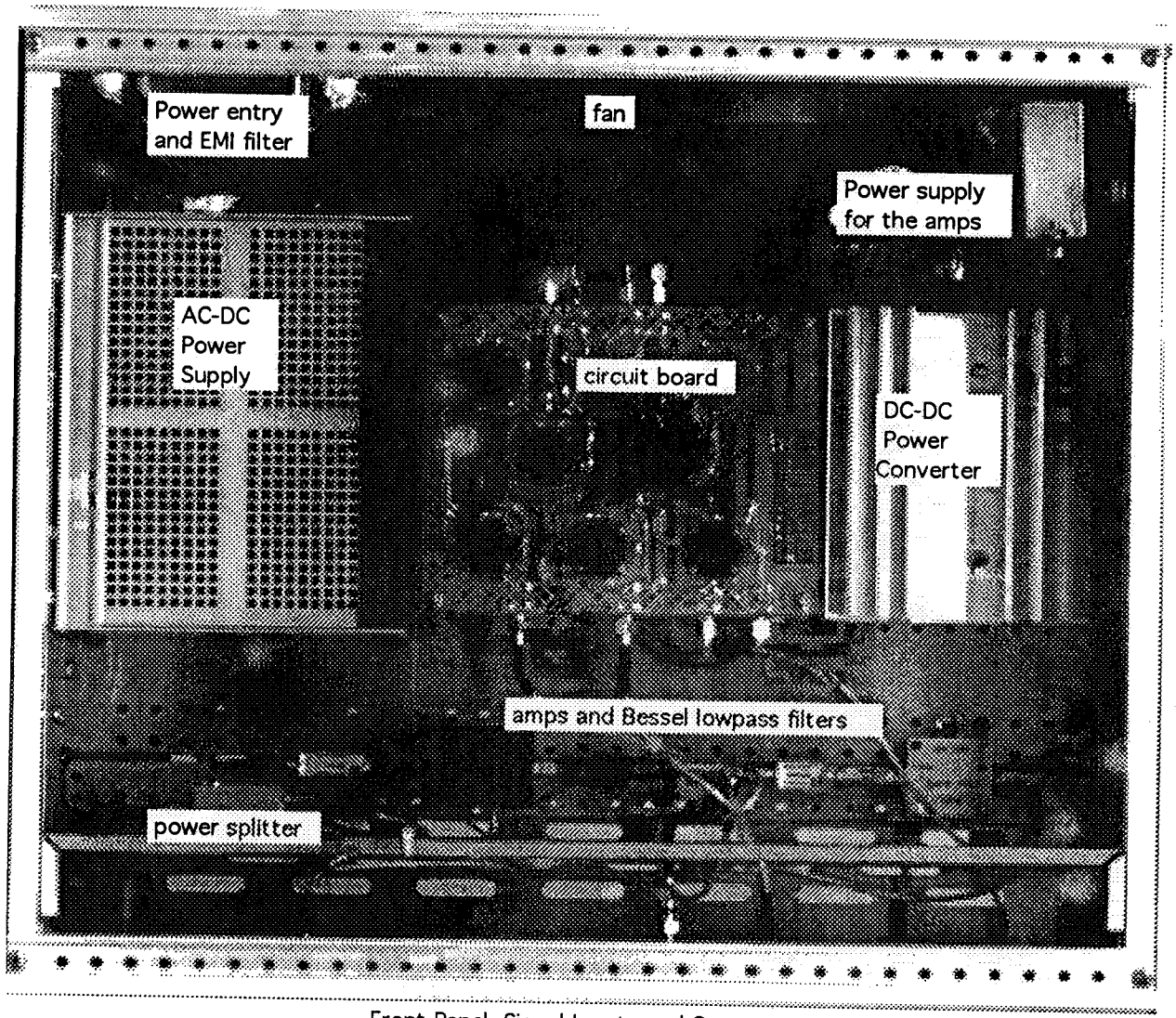

Figure 15. Top view of the 325 Mbps QPPM receiver

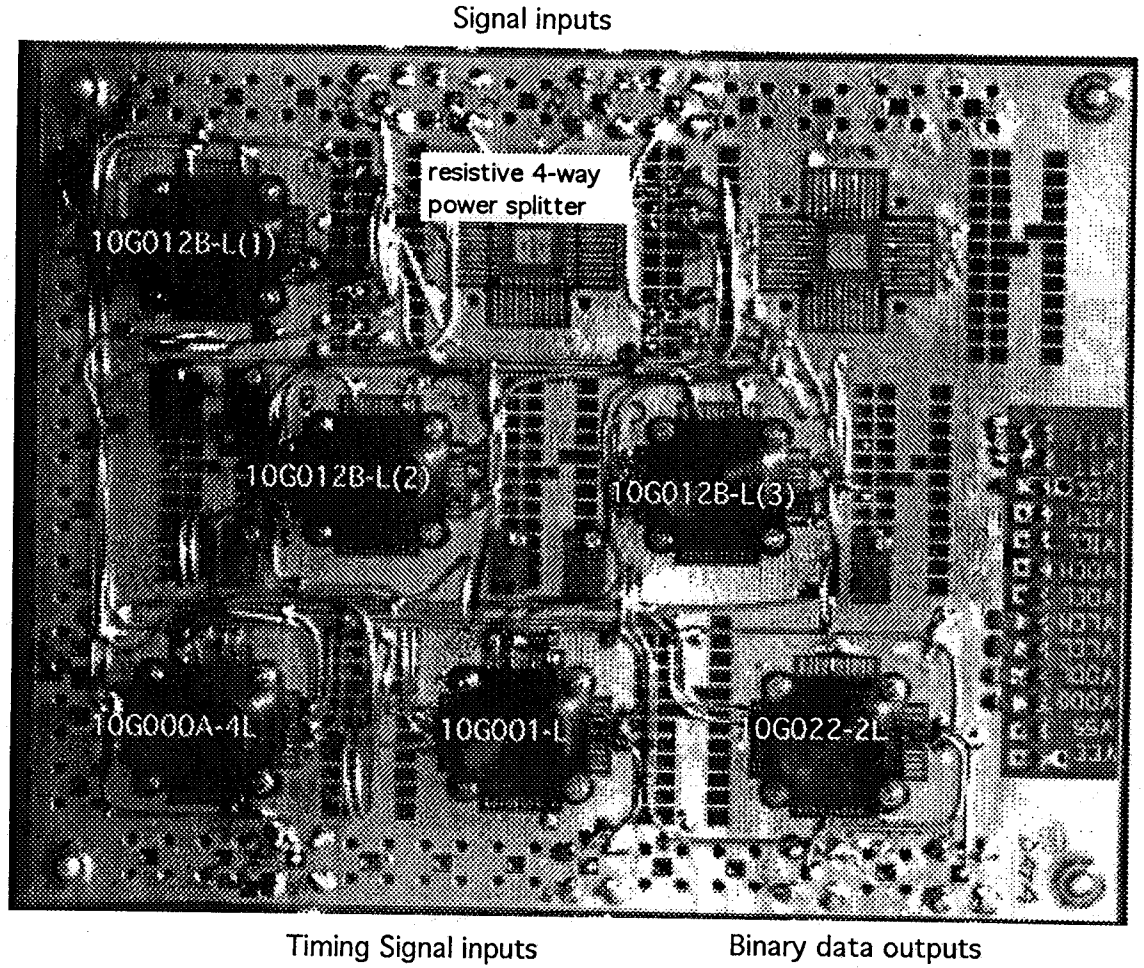

Figure 16. Top view of the 325 Mbps QPPM receiver circcuit board

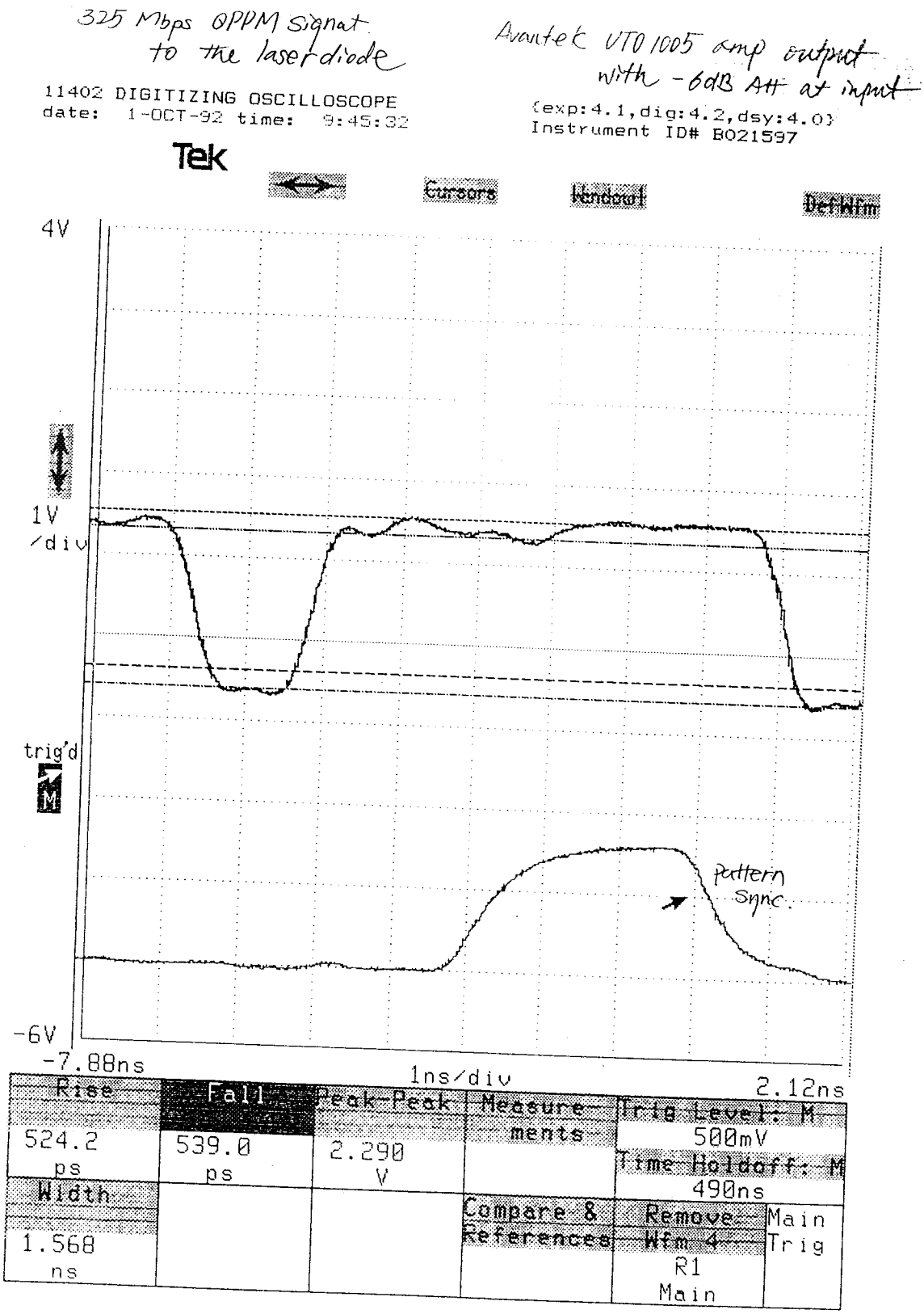

Figure 17. Pulse shape of the laser diode driving signal (the input to the bias tee).

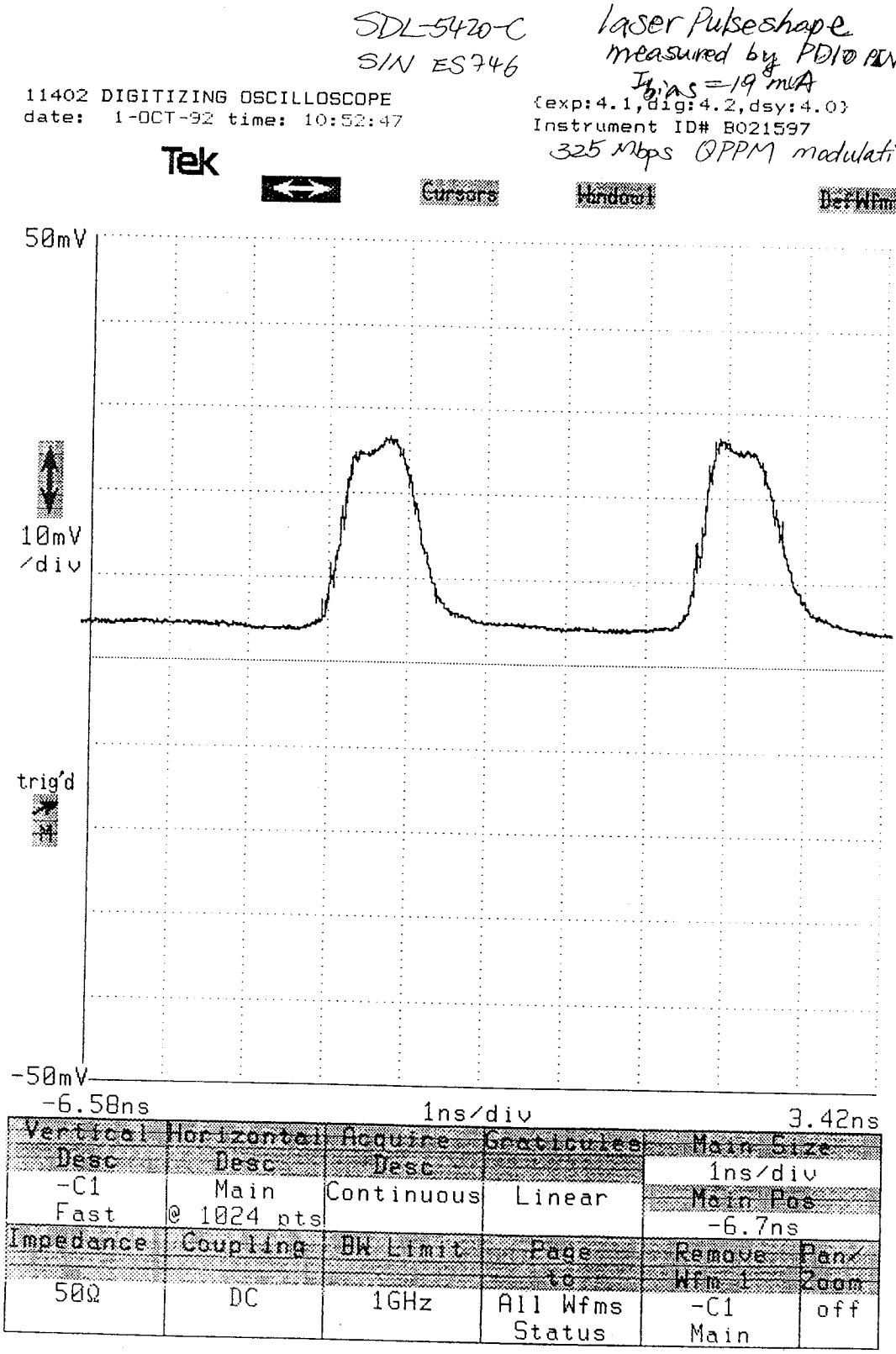

Figure 18. Laser diode output pulse shape measured with a high speed photodiode (OE-PD10).

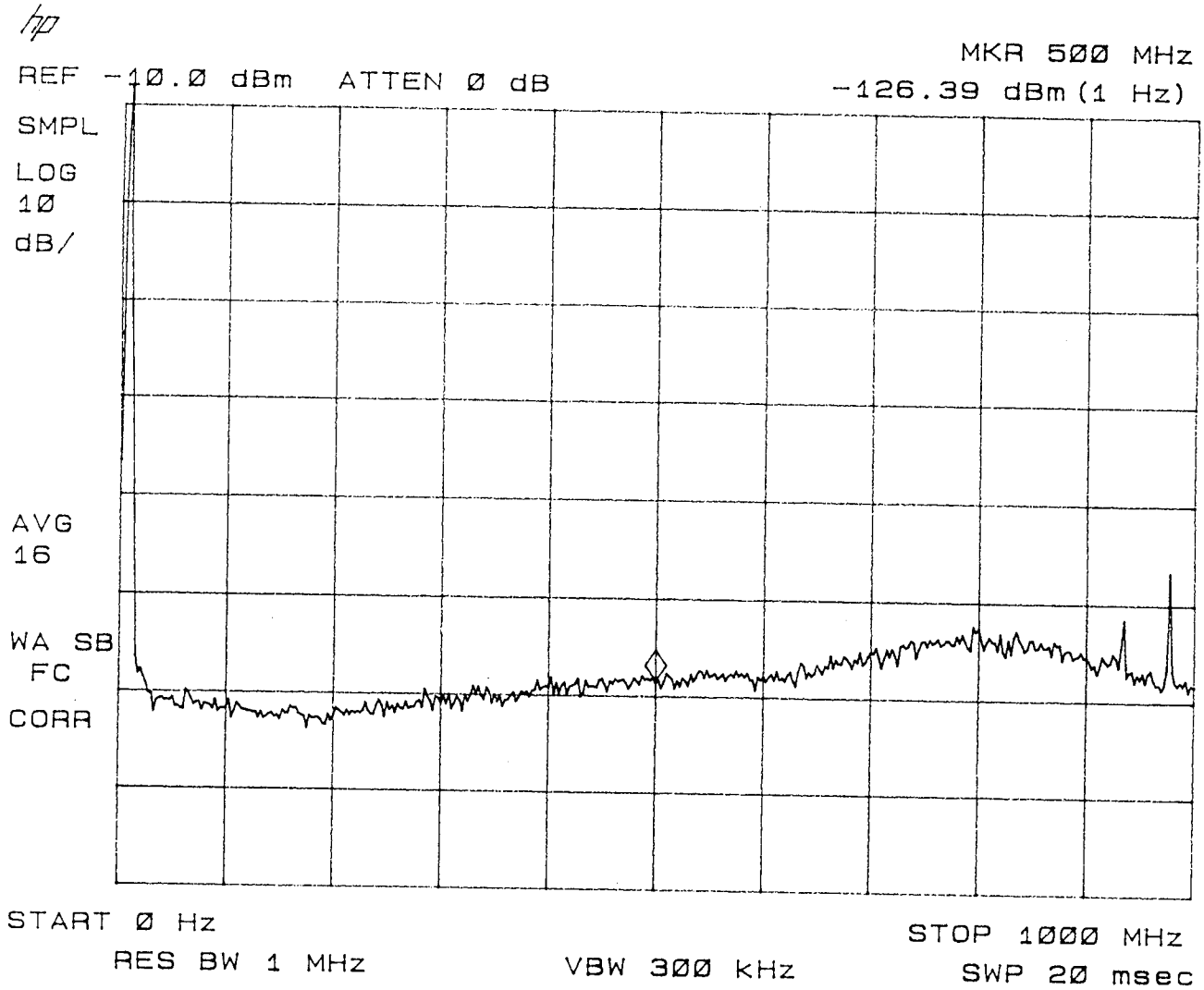

Figure 19. Noise power spectrum of the APD preamplifier. A 23.5 dB amplifier was used before the spectrum analyzer.

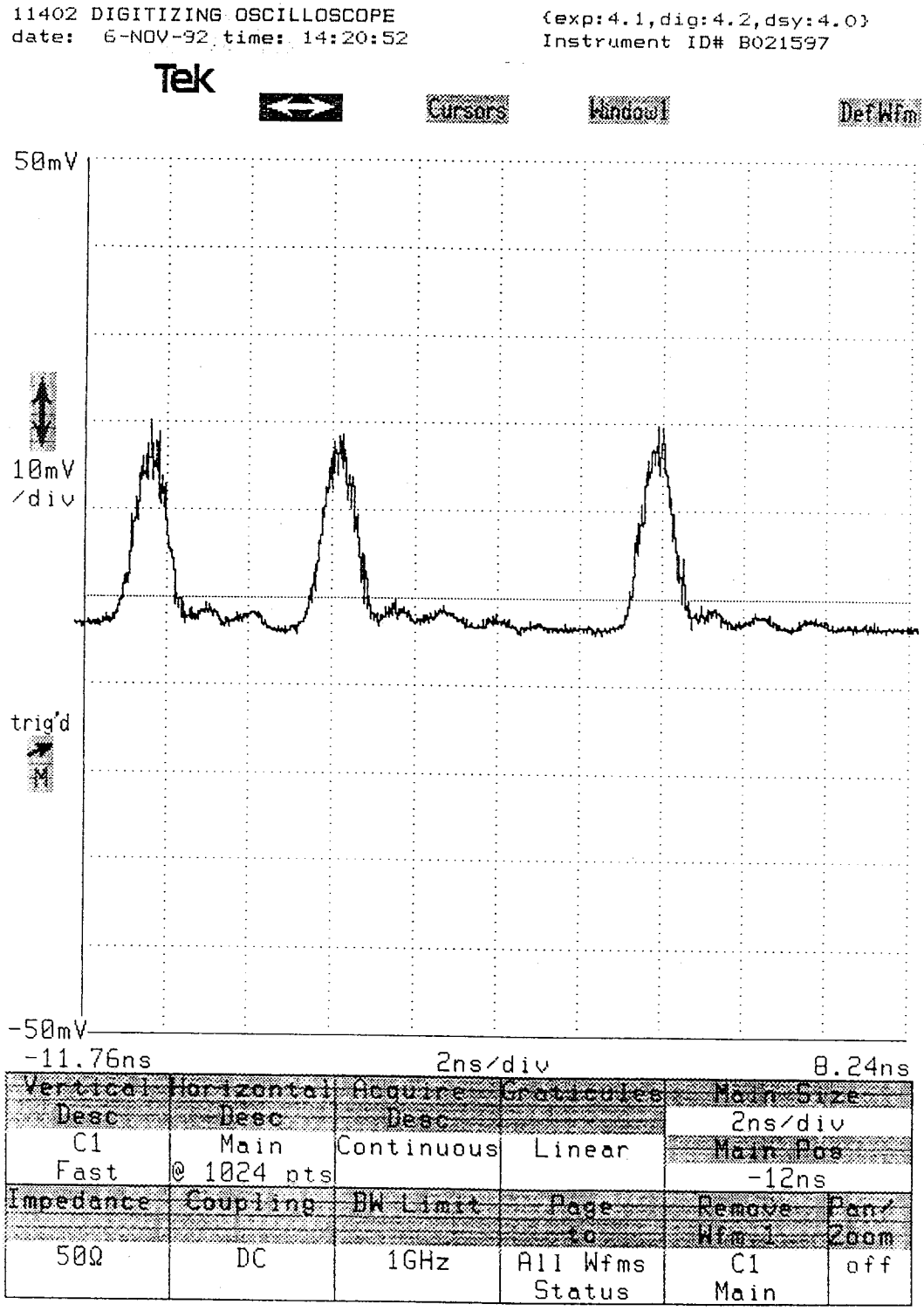

Figure 20. QPPM signal output from the APD preamplifier under 50 nW average input optical signal power and a relatively low average APD gain.

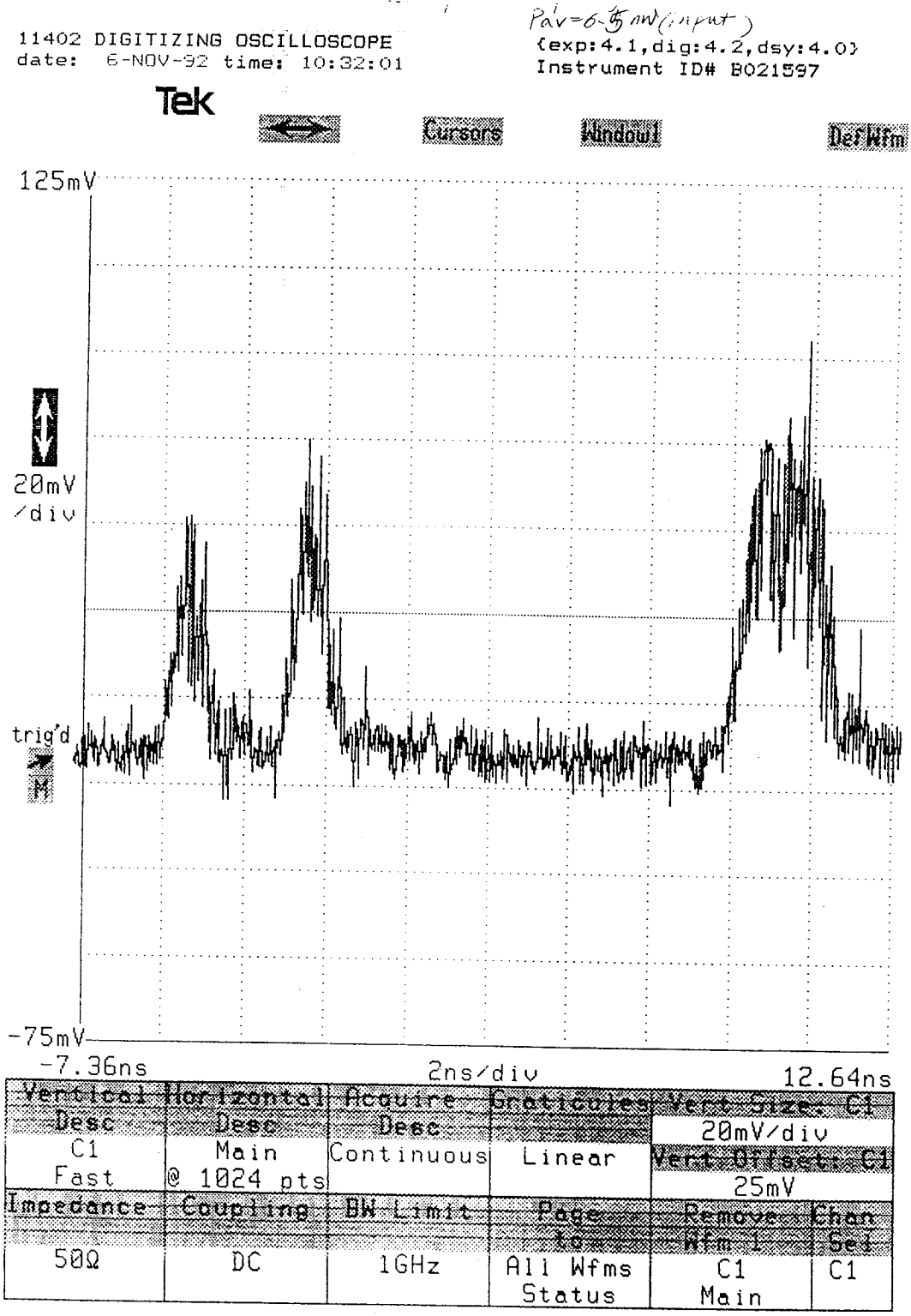

Figure 21. QPPM signal output from the APD preamplifier under 6.5 nW (84 photons/bit) average input optical signal power. A 23.5 dB gain amplifier (MiniCircuit ZFL-1000LN) was used before the oscilloscope.

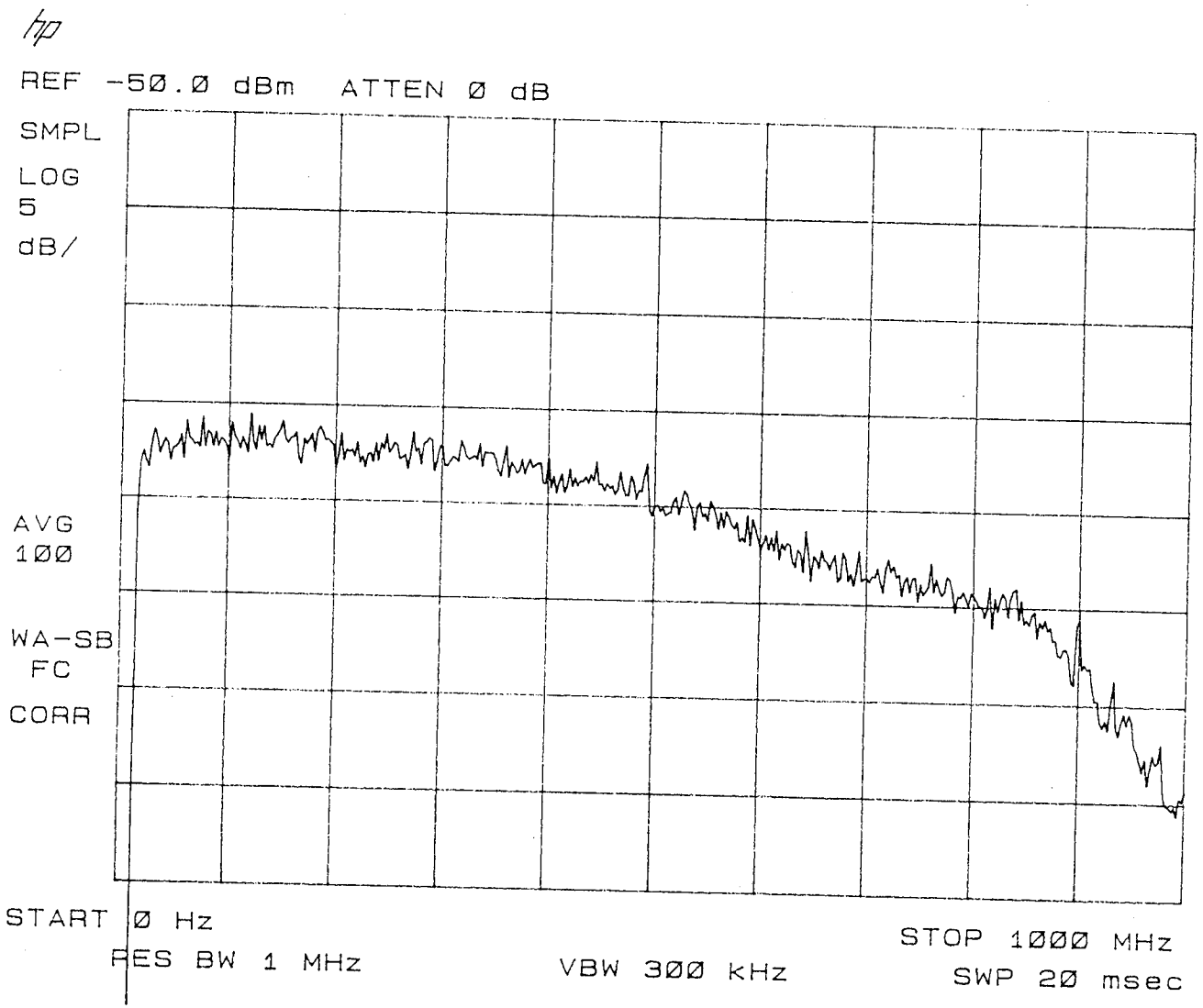

Figure 22. Frequency response of the raised cosine filter used in the QPPM receiver.

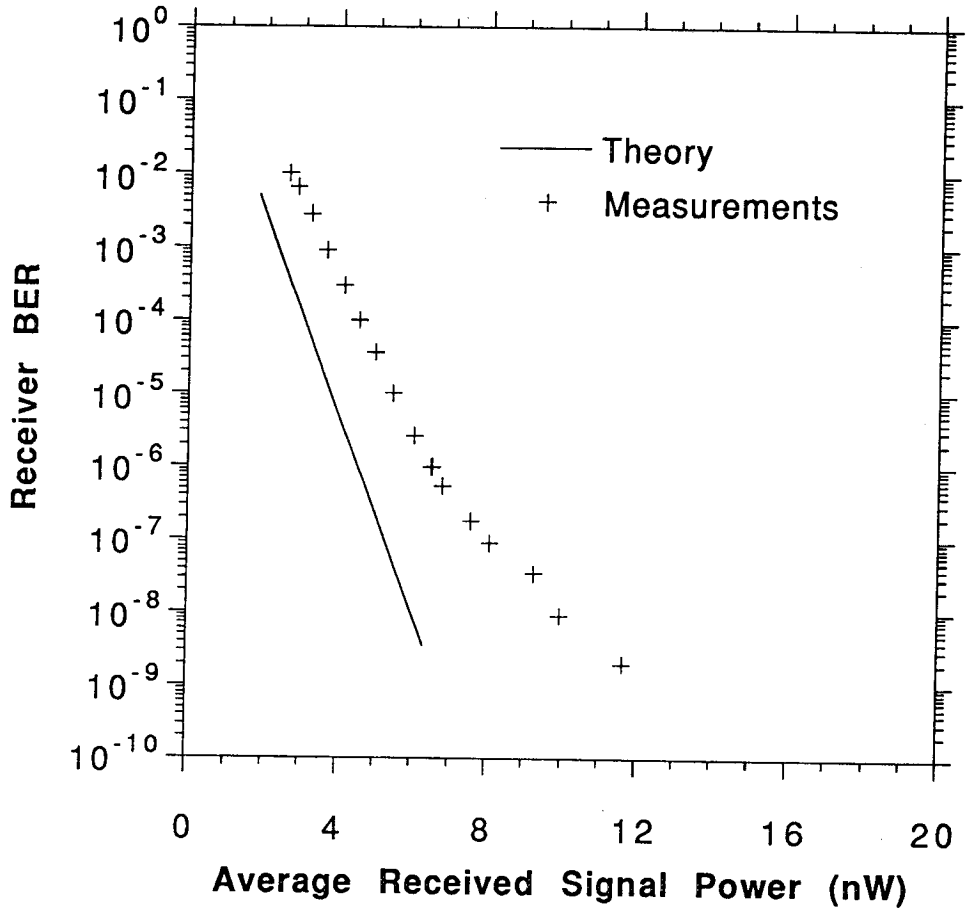

Figure 23. Receiver BER vs. average received optical signal power using the EG&G *Slik* APD and the Anadigics ATA12000 transimpedance preamplifier.

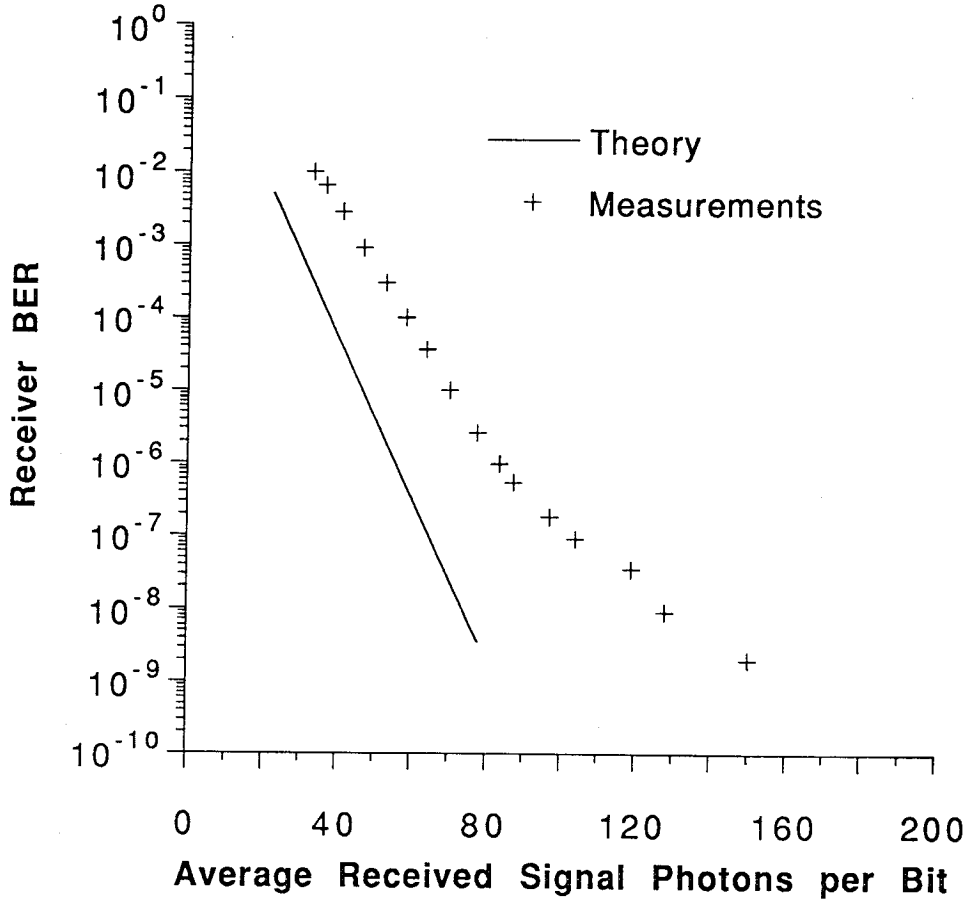

Figure 24. Receiver BER vs. average received signal photons per bit using the EG&G *Slik* APD and the Anadigics ATA12000 transimpedance preamplifier.

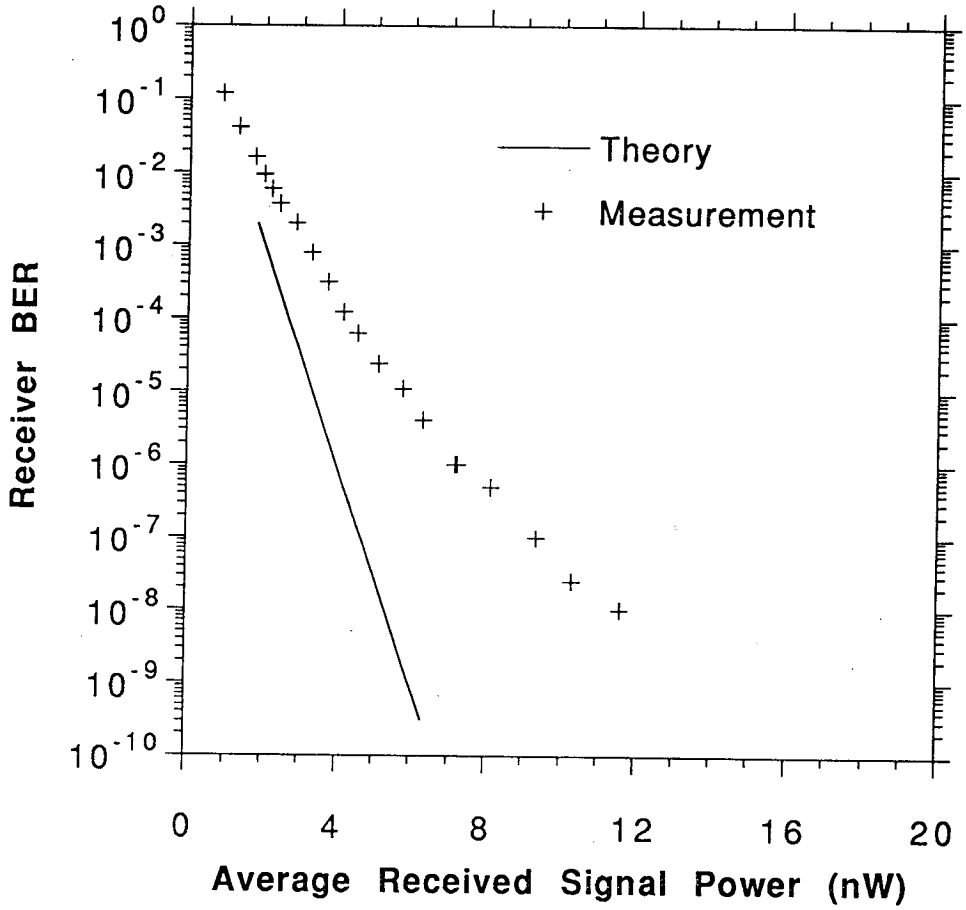

Figure 25. Receiver BER vs. average received optical signal power using the EG&G *Slik* APD and the GigaBit Logic 16G072-10X transimpedance preamplifier.

Table 1. Receiver BER vs Received Optical Signal Power, Theoretical Calculations and Measurement Data.

Ph/bit (incident)	Average received power (nW)	Calculated BER Anadigic preamp	Calculated BER GigaBit logic preamp	Average received power (nW) measurement	Incident ph/bit measurement	Rcvr BER measurement Anadigic preamp	Average received power (nW) measurement	Incident ph/bit measurement	Rcvr BER measurement GigaBit Logic preamp
22.22	1.80	5.04e-03	1.96e-03	2.60	33.0	1.00e-02	0.87	11.0	1.20e-01
24.44	1.98	2.87e-03	1.04e-03	2.83	36.4	6.60e-03	1.30	17.0	4.20e-02
26.67	2.16	1.63e-03	5.53e-04	3.20	41.1	2.80e-03	1.74	22.0	1.60e-02
28.89	2.34	9.25e-04	2.94e-04	3.63	46.6	9.10e-04	1.96	25.0	9.40e-03
31.11	2.52	5.25e-04	1.57e-04	4.11	52.8	3.00e-04	2.17	28.0	5.90e-03
33.33	2.70	2.98e-04	8.34e-05	4.53	58.2	1.00e-04	2.39	31.0	3.70e-03
35.56	2.88	1.69e-04	4.44e-05	4.96	63.7	3.60e-05	2.83	36.0	2.00e-03
37.78	3.06	9.57e-05	2.37e-05	5.44	70.0	1.00e-05	3.26	42.0	7.90e-04
40.00	3.24	5.42e-05	1.26e-05	6.03	77.5	2.60e-06	3.70	47.0	3.10e-04
42.22	3.42	3.07e-05	6.75e-06	6.49	83.4	9.80e-07	4.13	53.0	1.20e-04
44.44	3.60	1.74e-05	3.61e-06	6.50	83.5	9.90e-07	4.52	58.0	6.10e-05
46.67	3.78	9.86e-06	1.93e-06	6.79	87.3	5.40e-07	5.09	65.0	2.40e-05
48.89	3.96	5.59e-06	1.03e-06	7.55	97.0	1.80e-07	5.74	74.0	1.10e-05
51.11	4.14	3.17e-06	5.52e-07	8.07	104.0	9.00e-08	6.30	81.0	4.10e-06
53.33	4.32	1.79e-06	2.95e-07	9.26	119.0	3.50e-08	7.17	92.0	1.00e-06
55.56	4.50	1.02e-06	1.58e-07	9.95	128.0	9.00e-09	7.22	92.0	1.00e-06
57.78	4.69	5.76e-07	8.48e-08	11.66	150.0	2.00e-09	8.13	104.0	5.00e-07
60.00	4.87	3.27e-07	4.54e-08				9.35	120.0	1.00e-07
62.22	5.05	1.85e-07	2.44e-08				10.30	132.0	2.50e-08
64.44	5.23	1.05e-07	1.31e-08				11.60	150.0	1.00e-08
66.67	5.41	5.96e-08	7.01e-09						
68.89	5.59	3.38e-08	3.76e-09						
71.11	5.77	1.92e-08	2.02e-09						
73.33	5.95	1.09e-08	1.09e-09						
75.56	6.13	6.16e-09	5.83e-10						
77.78	6.31	3.50e-09	3.13e-10						

Test Results of the 325 Mbps QPPM High Speed Data Transmission GaAs ASICs

Xiaoli Sun

Department of Electrical and Computer Engineering
The Johns Hopkins University
Baltimore, Maryland, 21218-2686
(410)516-8186/(301)286-0773

August 1993

SUMMARY

The test results are presented of the 325 Mbps quaternary pulse position modulation (QPPM) GaAs application specific integrated circuits (ASIC) developed by Galaxy Microsystems Inc. All the three ASIC chips tested were functional though they reached only 70% the specified operating speed. Two design flaws were found in the QPPM timing recovery circuits. The inputs to the phase detector for the QPPM slot timing recovery were incorrect. The QPPM word boundary detection circuit did not have any memory and averaging mechanism to smooth out false alarms in the detection of back-to-back QPPM pulse pairs. Reliable synchronization between the transmitter and the receiver could not be established. As a result, the receiver bit error rate (BER) as a function of the input signal power could not be determined. The phase detector for the QPPM slot timing recovery was found to have insufficient gain. The track-and-hold circuits in the QPPM detection circuit were shown to have a clock leakage of 28 dB.

1. Introduction

Galaxy Microsystems Incorporated developed three GaAs ASIC chips for the electronics subsystem of NASA's high speed free space optical communication project. Those ASIC chips were designed to encode binary data into QPPM format to drive the laser transmitter, and detect and demodulate the received signal from the photodetector back to binary data at 325 Mbps single channel data rate. The chips were manufactured using the GaAs integrated circuit technology by the custom foundry service of TriQuint Semiconductor.

There are three chips made. Chip 1 was designed to encode either 1.3 Gbps or 650 Mbps binary data into four or two QPPM signals at 325 Mbps. The chip contains a 1-to-2 or 1-to-4 demultiplexer, four QPPM encoders, and a 8-to-1 or two 4-to-1 and/or a 2-to-1 multiplexer. The multiplexers serve to recombine binary bits from four 325 Mbps QPPM receivers into a single 1.3 Gbps or two 650 Mbps binary data streams. The 2-to-1 multiplexer is to convert every two parallel bits output from a QPPM receiver into a serial data stream. Chip 1 also contains a 511 bit pseudo noise (PN) sequence generator for test purposes.

Chip 2 contains a one channel QPPM detection and demodulation circuit and the timing recovery circuit. Maximum likelihood (ML) QPPM detection is performed using four track-and-hold circuit cells and six comparators. The QPPM slot timing recovery circuit consists of a phase detector and an external loop filter and voltage controlled crystal oscillator (VCXO). The QPPM word timing recovery circuit consists of a divided by 4 counter and a back-to-back QPPM word pair detector.

Chip 3 is similar to Chip 2 but has a sequential ML QPPM detector which uses only three track-and-hold circuits and three comparators. In addition to the main circuit, Chip 3 also contains a phase detector cell, two slightly different track-and-hold circuit cells, and a source follower cell with all their input and output terminals bound out for the measurement of the characteristics of those cells.

Three chips from one of each were tested in the lab of the Photonics Branch, NASA Goddard Space Flight Center. The chips were mounted on a TriQuint ETF-MLC68/40 test fixture which supplied all DC voltages with bypass capacitors and 50 ohm transmission lines and terminations for all the high speed signals. All the three chips being tested were operational and free of defects. However, they only operated up to a clock speed which was about 70% of the design goal. Two design flaws were found in the QPPM slot and word timing recovery circuits. The synchronization of the QPPM receiver could not be established for the input signal and noise levels which we interested. Therefore, the receiver bit error rate (BER) versus the input optical signal power could not be determined.

The detailed description of the chips can be found in the report by Galaxy [1].

2. Test Results of Chip 1

2.1. Test Setup

Figure 1 shows the test setup. All the DC voltage supplies were given according to the manufacturer's specification. Input pins, either the high speed signal ports or the logic controls, were terminated through 50 ohm resistors to V_{tt} (-2V) at the chip sit. All the logic controls signals, therefore, had logic level "0" when unconnected. Logic "1" control signals were obtained by connecting the -1 volts DC power supply to the control terminals. Output pins were left unterminated at the chip sites but terminated at the input ports of the measurement instrument. Since the high speed signal from the chip require 50 ohm to V_{tt} termination while the oscilloscope had 50 ohm to ground termination, two inverting transformers (Picosecond Pulse Lab, Model 5100) had to be used between the output ports of the chip and the input terminals of the oscilloscope. The transformers had a primary to secondary turn ratio of 1:1 and were modified to have their primary

terminated to V_{tt}. The transformers had a pulse rise time of 20 ps and was shown to cause little distortions in the output signal waveforms.

The quiescent DC current drawn by the chip from V_{ee} was about 200 mA, which corresponded to a quiescent power dissipation of 1.4 Watts. This was very close to the estimated power dissipation of 1.38 Watts, given in Galaxy's report.

An Anritsu ME522A BER tester was used as a programmable binary data source. The 511 bit PN code generator on the chip could not be used because it did not provide a synchronization bit for the oscilloscope to trigger on.

2.2. Demultiplexer and QPPM Encoder under Double Channel Operation

The demultiplexer and the QPPM encoder under Double Channel operation mode split and then encode every other two bits into Channels 1 and 3. The outputs of Channels 2 and 4 duplicate those of Channels 1 and 3, but with one clock period delay. The QPPM slot clock frequency is the same as the input clock for the binary data because the data rate for each QPPM channel is half the input data rate and the QPPM slot clock frequency of each channel is twice the corresponding binary data rate.

The output waveforms from the four QPPM channels were measured for all zero, all 1, and a 16 bit word binary sequence input at 100 Mbps. The output QPPM signal from all the four QPPM channel were all correct according to the design with QPPM pulse in the first, second, third, and fourth slot for binary data 00, 01, 10, and 11 (least significant bit first), respectively. Channels 1 through 4 gave the QPPM signals for every other two bits of the source binary data. Channels 2 and 4 had one bit delay with respect to Channels 1 and 2. The QPPM outputs were further tested and found to be correct for two more randomly picked 16 bit words.

However, the QPPM outputs became abnormal as the source binary data rate was increased to above 550 Mbps (275 Mbps for each QPPM channel). Some QPPM channels started to output no pulses for some QPPM word periods and some QPPM channels had no output at all even for all zero binary data input at 570 Mbps (280 Mbps per QPPM channel).

Figure 2 shows the waveforms of the four QPPM channel outputs in response to the 16 bit binary sequence "0100101101010110" at a data rate of 250 Mbps per channel. The horizontal scale was set to one QPPM word period per division. Figure 3 is the same as Figure 2 but at 280 Mbps per channel data rate. There was missing pulses on two of the traces in Figure 2, which means some of the QPPM word periods contained no pulse at all.

The pulse shapes of the QPPM outputs were measured at 560 Mbps source binary data rate. Figure 4 shows a picture of a typical QPPM pulseshape measured with a sampling oscilloscope (Tektronic 7104 with 7T11A sampling sweep unit and 7S11 sampling unit). The rise and fall times were about 500 ps and the peak-to-peak pulse amplitude was about 800 mV.

Figure 5 shows the output waveforms of the four QPPM channel for all zero binary data input at 500 Mbps. The timing offsets between the four waveforms were mostly caused by the unequal signal path lengths of the test fixture.

2.3. Single and Four Channel Operations

Single channel operation was to encode the input binary data into a single channel QPPM signal output. This operation mode was not tested since it was the same as the Double Channel operation but with the input binary data repeated every bit.

Four channel operation was to divide the input binary data into four QPPM channels. This operation mode was tested with 32 bit binary

data sequence at 500 Mbps. The data rate of each QPPM channel was one fourth the input binary data rate, or 125 Mbps. The waveforms of the four QPPM outputs were all correct and corresponding to the input data pattern.

2.4. The Multiplexer

The multiplexer was designed to recombine the binary bits from four identical and parallel QPPM receivers into one bit stream at four times the data rate of each QPPM channel. It simply functioned as a 8-to-1 or two 4-to-1 multiplexers with a latch for every two input bits. It also had one 2-to-1 multiplexing output for the first two input bits.

The 4-to-1 and the 2-to-1 multiplexer outputs were tested successfully under different combinations of all constant (static) input bits. The maximum data rates at the 4-to-1 and 2-to-1 multiplexer outputs were found to be greater than 700 Mbps and 350 Mbps, respectively, which exceeded the design goal of 650 Mbps and 325 Mbps. We then replaced one of the static input with a randomly picked 16 bit binary sequence, "0100101101010110" and set the input data rate to 162.5 Mbps. Figure 6 shows the 16 bit binary data sequence and the clock signal for the latch. Both of the 4-to-1 and the 2-to-1 multiplexer outputs responded correctly to the input data, as shown in Figure 7. The input bit pattern was set to: 16 bit sequence " at Bit 1 input, static "1" at Bit 2 and Bit 3 inputs, and static "0" at Bit 4 input. The 4-to-1 multiplexer output Bits 1 through 4 and the 2-to-1 multiplexer output Bits 1 and 2.

We could not test the multiplexer with all dynamic input data at Bits 1 through 8 inputs because we did not have a multichannel data generator. We could not test the 8-to-1 multiplexing output because we could not obtain both the $\times 4$ and $\times 8$ clocks required by the chip to perform this function.

3. Test Results of Chip 2

3.1. Chip 2 Circuit Design

Chip 2 consists of a clock divider, a phase detector, a QPPM word boundary detector, a ML QPPM detector, and a 2-to-1 multiplexer. The phase detector was to be used in the phase lock loop (PLL) for the QPPM slot timing recovery. The loop filter and the voltage controlled crystal oscillator (VCXO) of the PLL were external to the chip. The 2-to-1 multiplexer was to combine the 2 binary bits output from the ML QPPM detector into a serial binary data stream.

Two design flaws were found during the study of the schematic circuit diagram of the chip. One was in the phase detector and the other was in the QPPM word boundary detector.

The phase detector used is a standard double balanced analog mixer and the inputs should have consisted of the QPPM slot clock and the nonlinear filtered QPPM signal. The nonlinear filtering is necessary to generate a spectrum line at the QPPM slot clock frequency [2]. However, the two inputs to the phase detector in Chip 2 were the QPPM signal itself and the slot clock divided by 2. The phase detector under this configuration could not possibly detect any phase error according to the well known theory [2,3]. Furthermore, the spectrum of the nonlinear processed QPPM signal only contain discrete components at the slot clock and its harmonics but not subharmonics, such as slot clock divided by 2.

The QPPM word boundary detector in Chip 2 did not have any averaging, or "flywheel", mechanism to smooth out false alarms in the detection of the back-to-back QPPM pulse pairs. Each detection of a back-to-back pulse pair reset the QPPM word boundary. Therefore, any false detection would cause catastrophic bit error, due to a wrong word boundary timing, until a correct detection of a back-to-back QPPM pulse pair. It has been shown that the false alarm rate of back-to-back pulse pair detection was two to three orders of magnitude higher than the BER of the ML QPPM detector with nearly perfect timing recovery.

In practice, the timing recovery circuits of a well designed QPPM receiver should be near perfect and have little impact on the overall receiver BER.

The QPPM slot clock phase detector could be bypassed by supplying a synchronous clock directly to the chip. However, the QPPM word boundary detector could not be bypassed since it was internal to the chip. Therefore, we could not measure the actual receiver BER as a function of the input signal power without being overwhelmed by false alarms in the QPPM word boundary detection. However, we did test the logic functions of the chip under infinite input signal to noise ratio (SNR).

3.2 Test Setup

Figure 8 shows a block diagram of the test setup. The clock source to the chip was from either a 1.3 GHz VCXO (Vectron 283Y1581) or a frequency synthesizer (HP8660D) at twice the QPPM slot clock frequency. The frequency synthesizer was used to test the chip at different data rate other than 325 Mbps. The QPPM slot clock output from the chip was then used to clock the signal generator (Anritsu ME522A BERT transmitter) which was programmed to generate QPPM signal. The inverting transformer converted 50 ohm to V_{tt} (-2V) termination required by the chip to 50 ohm to ground required by the Anritsu ME522A data generator. The QPPM data was fed to Chip 2 for detection and demodulation. The bias Tee was used to provide a proper DC offset to the signal as required by the chip. The input signal to noise ratio was effectively infinite since no noise was injected. The output waveforms of the binary data and timing signals were measured with an oscilloscope. The HP54123A oscilloscope had an 18 GHz bandwidth and was used whenever HP54111D (400 MHz bandwidth) could not be used.

The quiescent DC current drawn by the chip was about 320 mA from V_{ee} (-5.2 V) and 100 mA from V_{cc} (5 V), which corresponded to a

quiescent power dissipation of 2.16 Watts. This was very close to the estimated power dissipation of 2.158 Watts given in Galaxy's report.

3.3. The Clock Generator

The clock generator was designed to buffer and divided the input clock by 2 and 4 to generate the QPPM slot clock and the binary data clock. It was tested successfully using the 1.3 GHz VCXO as the input. Figure 9 shows the waveforms of the buffered 1.3 GHz clock (lower trace) and the divided by 2 clock (upper trace). Figure 10 shows the output waveforms of the divided by 2 and 4 clocks. The output rise and fall times were about 500 ps.

3.4. The QPPM Detection Circuit

Abnormal data outputs were observed from the ML QPPM detector at 1.3 GHz input clock frequency. The 2-to-1 multiplexer output also did not correspond to the inputs. The HP8660D frequency synthesizer was then used as the clock source to vary the input clock frequency.

The data outputs appeared to be correct as the clock frequency was lowered to 980 MHz (245 Mbps binary data rate). Figure 11 shows the output waveforms of the QPPM detector in response to an input QPPM data patters "10, 11, 00, 01". There were three data outputs, two parallel binary data bits (top two traces) and the multiplexed serial bits (the 3rd trace) which had three QPPM slot time delay. The QPPM data input to the chip was also shown in Figure 11 (bottom trace). Figure 12 shows the binary data clock, the QPPM word boundary signal, the latch signal for the multiplexer input, and one of the parallel binary bits output from the chip under the same input data as in Figure 11.

The data outputs appeared to have glitches or "ghosts" as the clock frequency increased to above 990 MHz (495 MHz slot clock rate or

247.5 Mbps binary data rate). Figure 13 shows the same waveforms as in Figure 11 but at 990 MHz clock frequency.

4. Test Results of Chip 3

4.1. Test Setup

The test setup for Chip 3 was same as that for Chip 2 because they were the same except for the addition individual circuit cells.

The quiescent DC current drawn by the chip was about 370 mA from V_{ee} (-5.2 V) and 170 mA from V_{cc} (5 V), which corresponded to a quiescent power dissipation of 2.77 Watts. This was very close to the estimated power dissipation of 2.681 Watts given in Galaxy's report.

The operation of the chip at 125 Mbps per channel were tested successfully. The word boundary detection circuit and the ML QPPM detection circuit functioned according to the design. We did not test the chip at different clock frequencies because this part of the circuit was similar to Chip 2. We concentrated ourselves on the testing of the individual cells on Chip 3.

4.2. The Clock Generator

The clock generator on Chip 3 was exactly the same as the one on Chip 2. It functioned according to the design up to the full speed. The input signal used was generated by the a 1.3 GHz VCXO which had a rise and fall time of less than 250 ps from 10% to 90% and a peak-to-peak amplitude of 1.0 volts. The rise time of the divided by two clock was 200 ps from 20 to 80% and 360 ps from 10 to 90%. The fall time was about 250 ps from 20 to 80% and 450 ps from 10 to 90%. The peak-to-peak amplitude was about 780 mV (ECL level signal).

As the input clock frequency was lowered to below 300 MHz, the divided by two output had an uneven pulse spacing and the divided by

four output had a duty cycle much smaller than 50%, as shown in Figure 14. The circuit also oscillated at about 880 MHz (440 MHz at the divided by two output) when there was no input.

4.3. The Phase Detector

The phase detector on the chip was actually a double balanced analog mixer. It was tested with an 125 MHz clock (500 MHz at the input of the clock generator) as the local oscillator and an 8 QPPM word sequence as the data input. The local oscillator and the data input were synchronous and the phase difference could be adjusted by changing the length of the coax cable. High impedance probes of the oscilloscope were used in order not to overload the circuit.

However, only noises were observed at the output of the phase detector, as shown in Figure 15. The DC component hardly varied with the phase difference between the two input signals. Ordinary double balanced analog mixers should form the product of the two input signals with a relatively high gain [5]. For square wave local oscillator clock input, the output should be equal to the input signal with its polarity switched at the transitions of the local oscillator clock. The voltage swing of the output is usually close to 1 volts and the DC component of the phase detector output should correspond to the phase difference between the two input signals.

4.4. The Source Follower and the Comparator

The source follower worked well with a gain of about 0.5 and good linearity. Figure 16 shows the waveforms of the input and output under a 325 Mbps QPPM input signal. The timing offset and the vertical scale of one of the waveforms was adjusted so that the two overlaid on each other. The pulse shapes are shown almost identical.

The comparator also performed well with an input signal dynamic range of at least 16 dB (0.16-1.0 V_{p-p}). Figures 17, 18, and 19 show the source follower outputs and the comparator outputs under 1.0, 0.16 (-16dB), and 0.080 (-22dB) volts peak-to-peak input signals. The DC offset of the input signal was adjusted very close to the threshold level of the comparator.

4.5. The Track-and-Hold Circuit

Figure 20 shows the DC response of TAH 1, TAH 2, and the source follower. The relationship between the input and the outputs was linear for input from 0.5 to 2.5 volts.

The input signal was then changed to a 8 word QPPM sequence at 325 Mbps. The oscilloscope used was a HP54123A (21GHz BW) with -6dB attenuators at the input ports. Figures 21 and 22 shows the output waveforms of the two track-and-hold (TAH) circuits along with the source follower outputs for a 0.71 V_{p-p} input signal. Figures 23 and 24 compare the waveforms of the input data and the track-and-hold output. TAH 1 had a slightly larger gain than TAH 2. They both tracked and held at high speed without interference from the previous sample. The gain was about 0.4. The ringings on the TAH outputs were 15-20% the pulse amplitude.

Figures 25 and 26 shows the waveforms of the TAH outputs when the input signal level was attenuated by -10dB. The noise level due to ringings on the TAH outputs were about the same as those shown in Figures 21 and 22. The deterioration of the output SNR was evident.

Figure 27 shows the TAH outputs with no input signal. It is shown that the ringings had the same frequency as the sampling clock (650 MHz) and therefore were actually the clock leakage. This was even more evident when we lower the sampling clock frequency to 200 MHz, as shown in Figure 28. TAH 1 had a higher level clock leakage than TAH 2. The peak-to-peak values of the ringings were about 40 mV after

considering the -6dB attenuator at the oscilloscope input. Since the input clock amplitude was 1.0 V_{p-p}, the clock leakage was about 0.04 or -28 dB. If the maximum input signal level was 1 V_{p-p}, the maximum TAH signal output would be 400 mV. The TAH output SNR would be limited to no greater than 20 dB.

If one operates the TAH with a ±6dB input signal dynamic range as required to accommodate the random photodetector gain fluctuation, the nominal SNR at the TAH output would be only 7 dB just due to the clock leakage. The SNR required to achieve an receiver BER of 10^{-6} should be about 15 dB.

References

[1] "High Speed Digital Data Transmission," Final report on Contract NAS5-31484, prepared for NASA Goddard Space Flight Center, Engineering Procurement Office, Code 287, Greenbelt, MD 20771, by Galaxy Microsystems, Inc., 8140 N. MoPac Expressway, Building 3, Suite 115, Austin, Texas 78759, telephone number (512) 794-9694, Feb. 1993 (Draft).

[2] F. M. Davidson and X. Sun, "Slot Clock Recovery in Optical PPM Communication Systems with Avalanche Photodiode Photodetectors," *IEEE Trans. Commun.*, Vol. 37, No. 11, pp. 1164-1172. Nov. 1989.

[3] W. R. Bennett, "Statistics of Regenerative Digital Transmission," *Bell Syst. Tech. J.*, Vol. 37, pp. 1501-1542, Nov. 1958.

[4] X. Sun and F. M. Davidson, "Word Timing Recovery in Direct Detection Optical PPM Communication Systems with Avalanche Photodiodes Using a Phase Lock Loop." IEEE Trans. Commun., Vol. 38, No. 5, pp. 666-673, May 1990.

[5] H. Stark, F. B. Tuteur, and J. B. Anderson, *Modern Electrical Communications—Analog, Digital, and Optical Systems*, 2nd Ed., Prentice Hall, Englewood Cliffs, NJ, 1988, pp. 233-244.

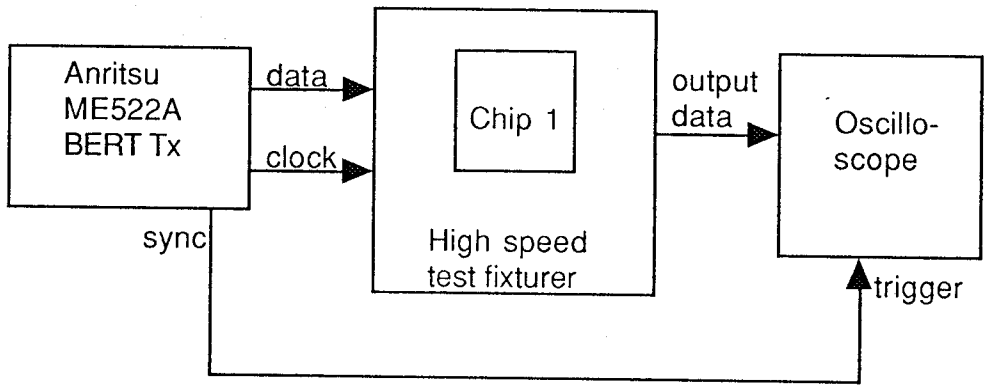

Figure 1. Chip 1 test setup.

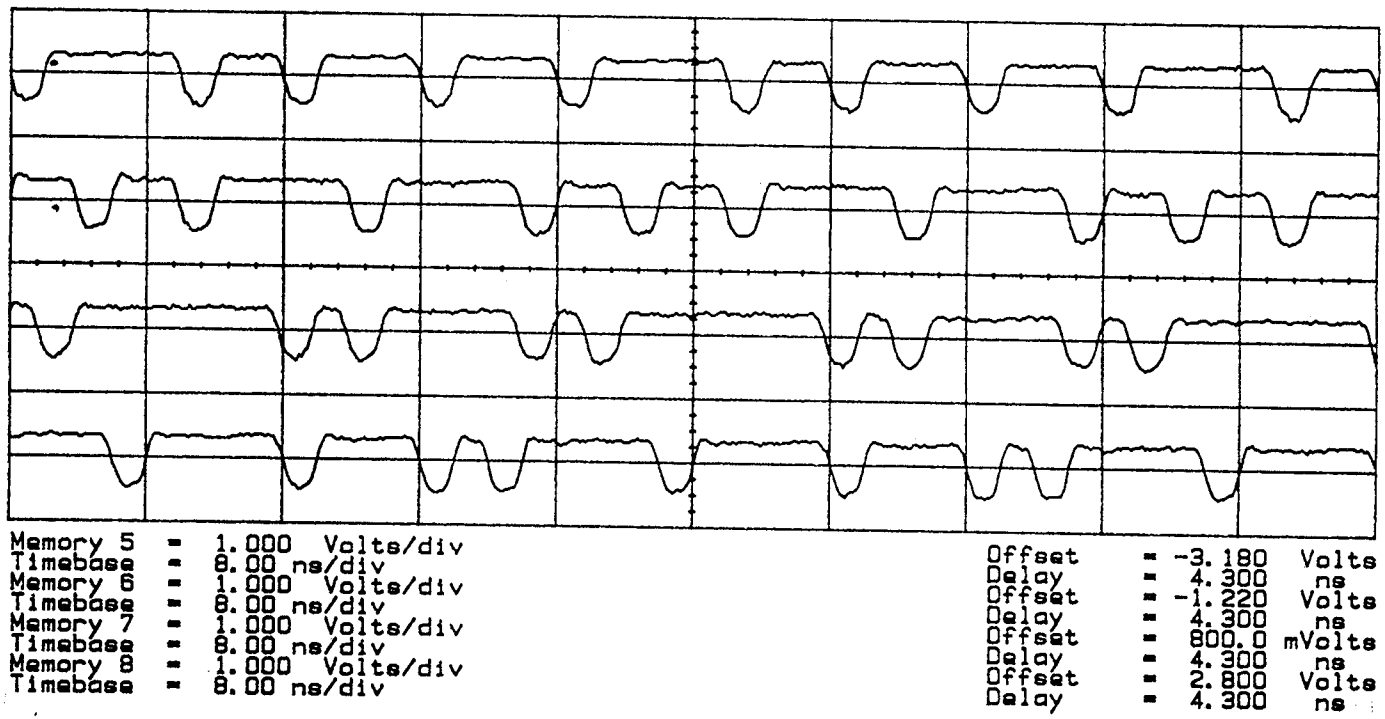

Figure 2. Waveforms of Channels 1, 2, 3, and 4, from top down, QPPM signal outputs at 250 Mbps per channel and double channel operation. The horizontal scale is one QPPM word interval per division. All the waveforms were inverted in polarity due to the use of inverting transformer. The input binary data pattern was "0100101101010110".

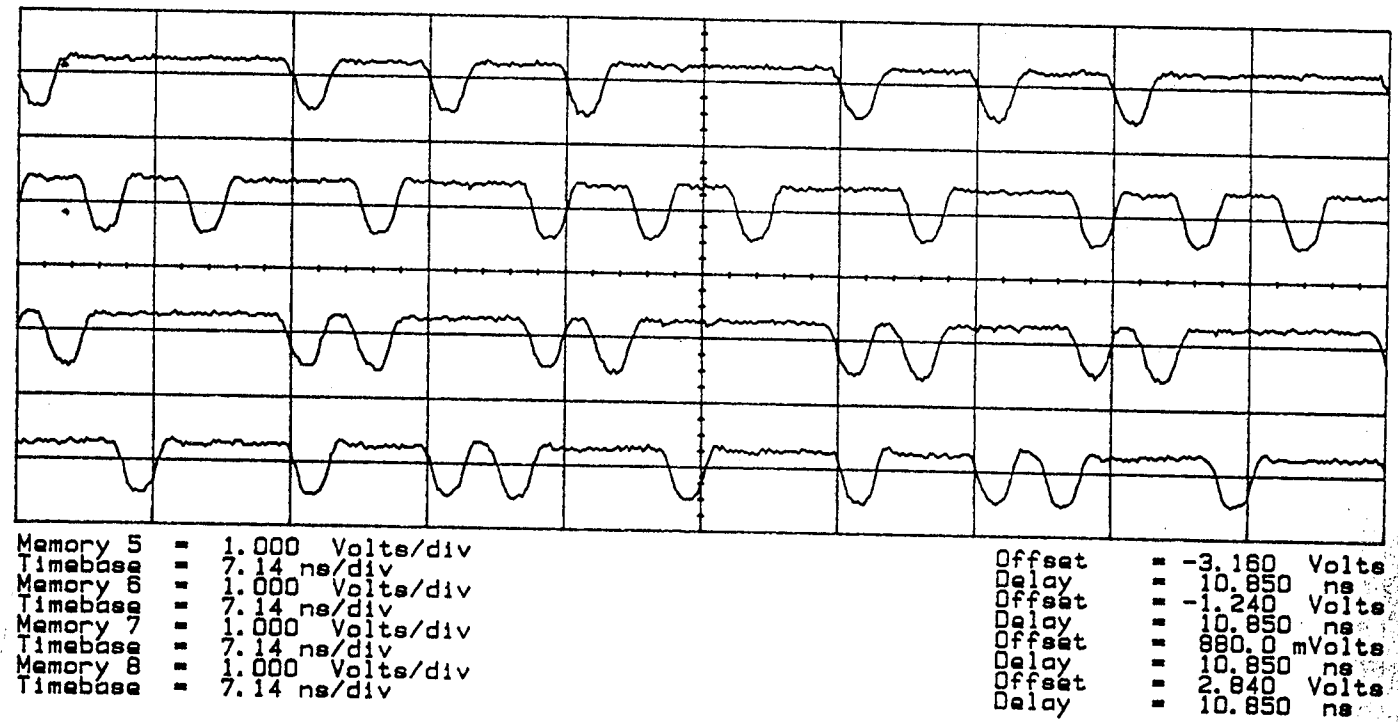

Figure 3. Same as Figure 2 but at 280 Mbps per QPPM channel. The top trace, the Channel 1 output, is no longer legitimate QPPM signal since two of the QPPM intervals contain no pulses at all.

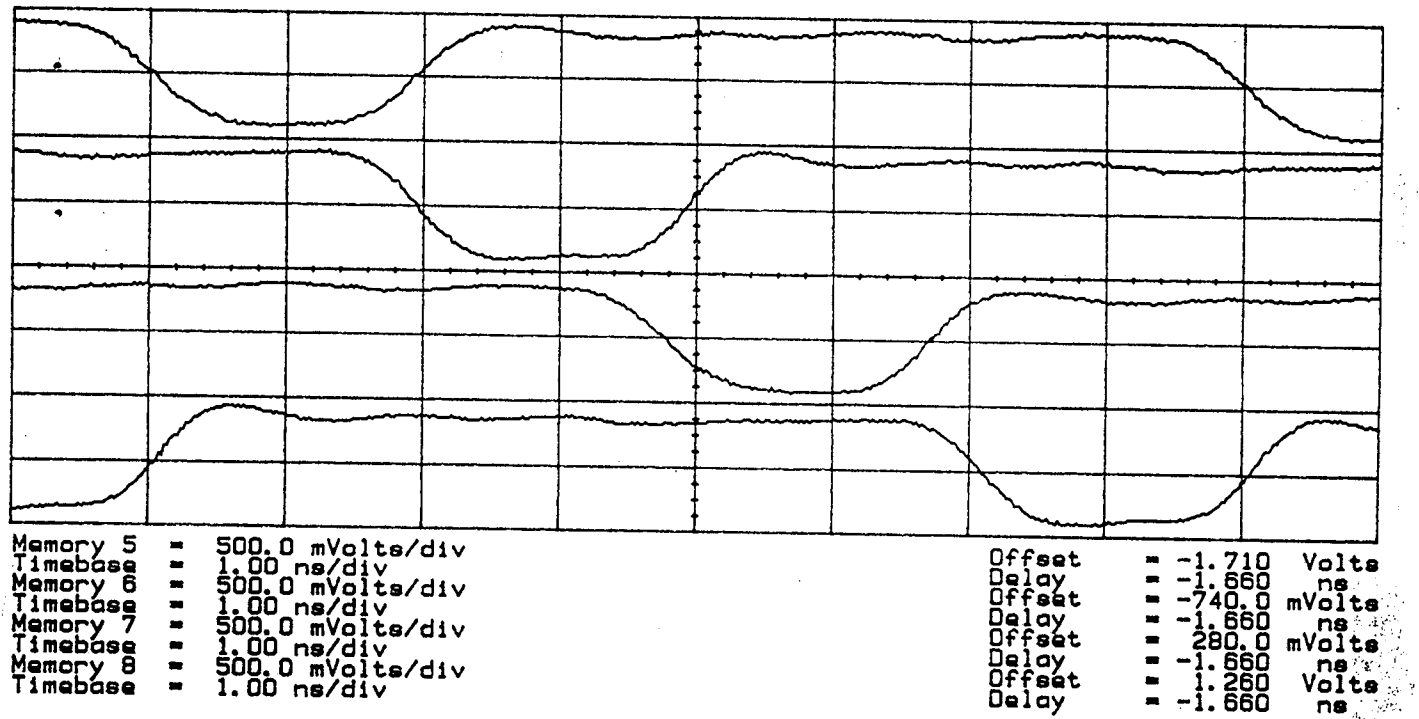

Figure 4. Waveforms of QPPM Channels 1 through 4 outputs under all zero binary data at input at 250 Mbps per channel (QPPM slot rate 500 MHz).

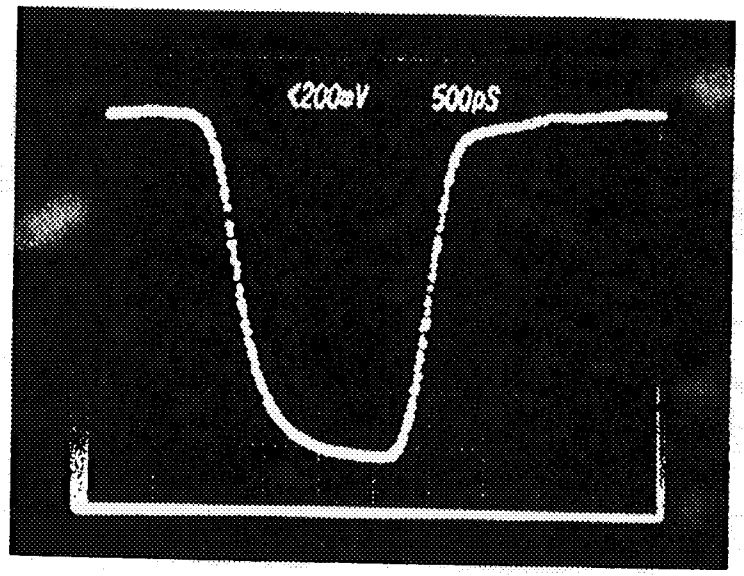

Figure 5. Typical pulse shape of the output QPPM signal at 280 Mbps per channel. The oscilloscope used was a TEK7104 with 7T11A sampling sweep unit and 7S11 sampling unit.

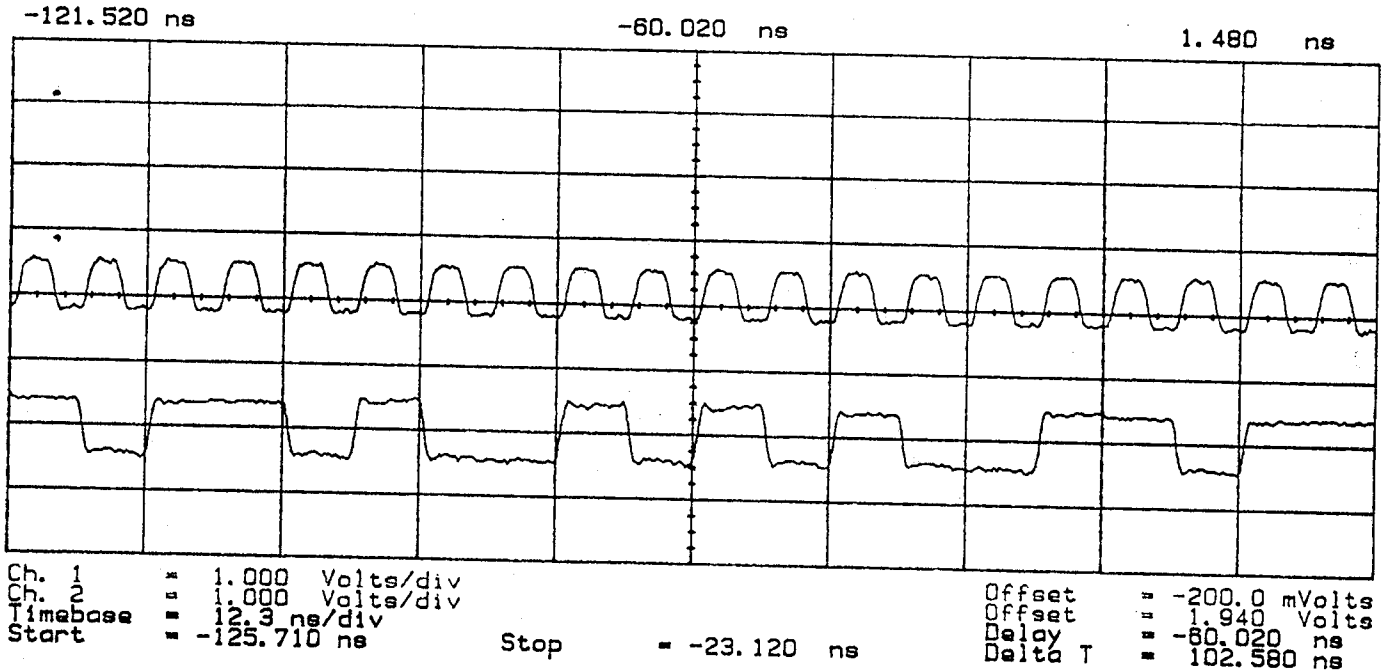

Figure 6. Waveforms of the 162.5 Mbps binary data (lower trace) and the latch clock (upper trace) at Bit 1 input of the multiplexer.

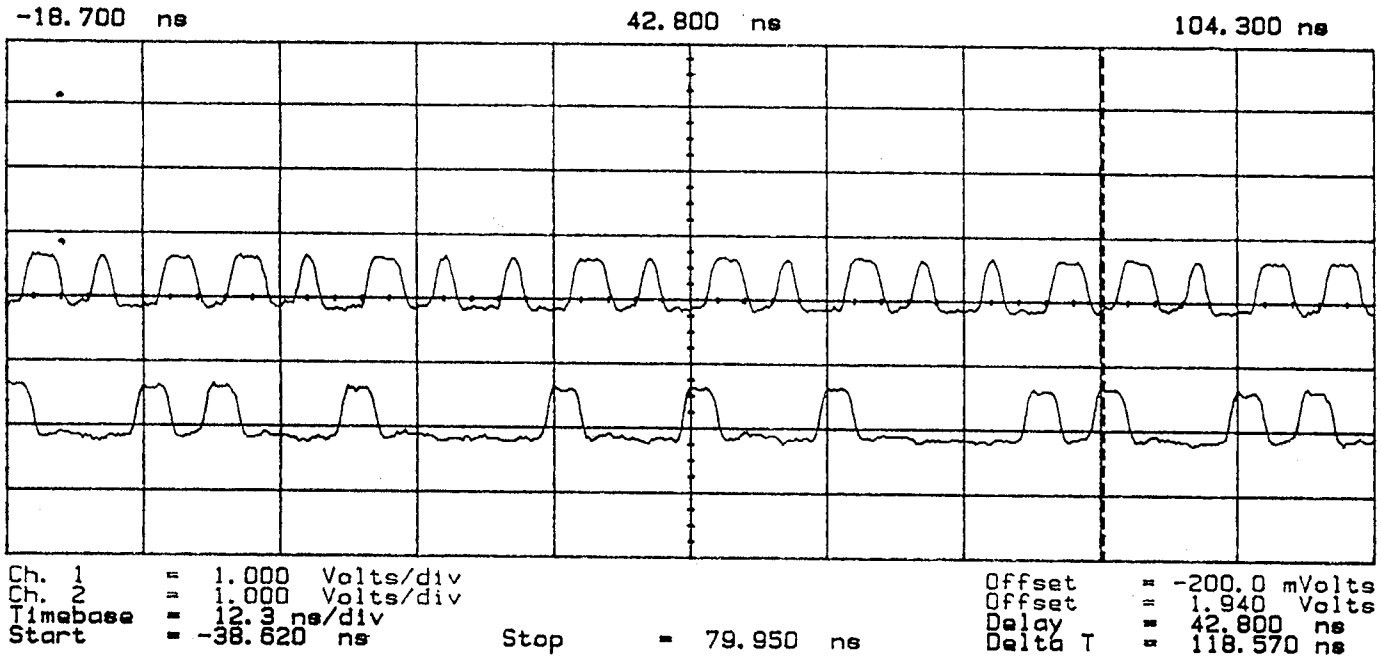

Figure 7. Outputs of the 4-to-1 multiplexer (upper trace) and 2-to-1 (lower trace) multiplexer. The input bits pattern was binary sequence shown in Figure 6 at Bit 1, static high at Bits 2 and 3, and static low at Bit 4, at 162.5 Mbps input data rate. The 4-to-1 multiplexer output consisted of Bit 1, Bit 2, Bit 3, and Bit 4, with Bit 1 come first. The 2-to-1 multiplexer output consisted of Bit 1 and Bit 2, with Bit 1 come first.

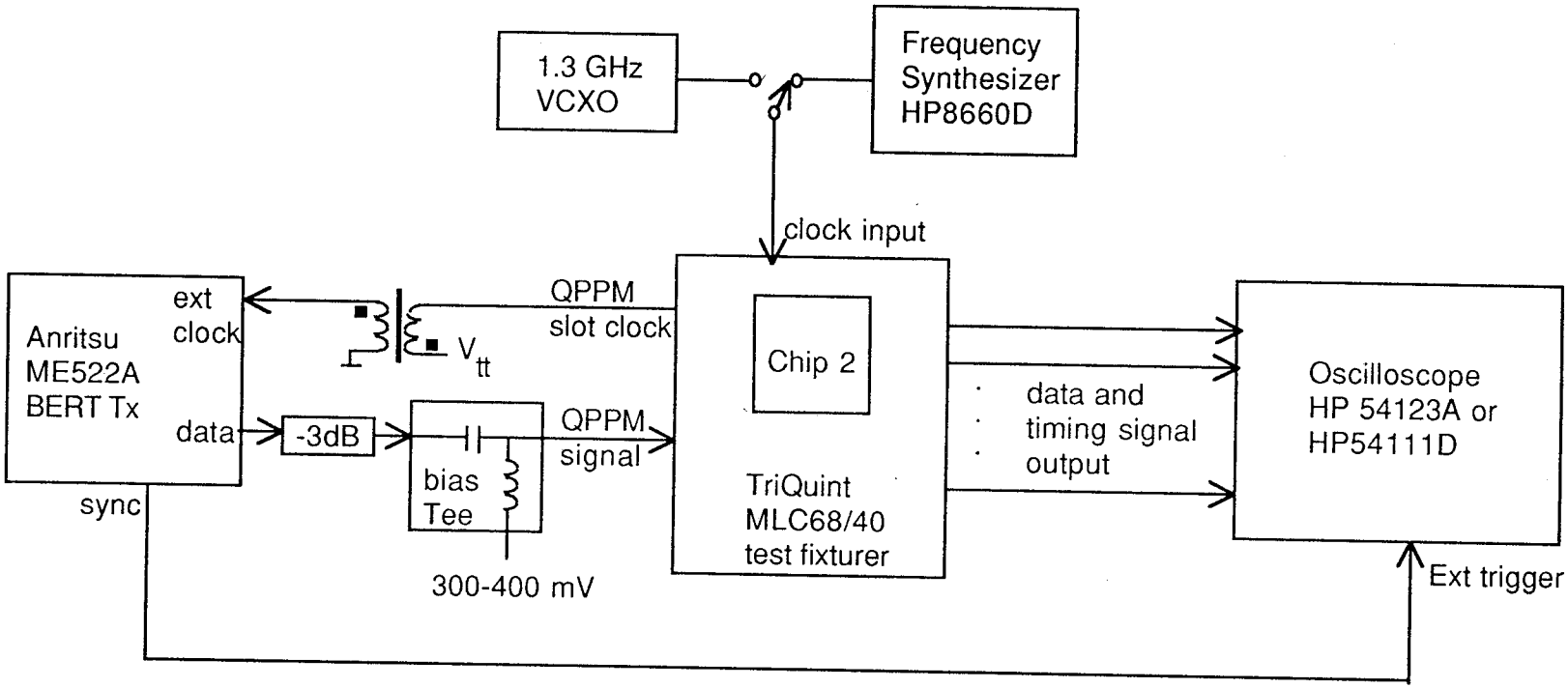

Figure 8. Chip 2 test setup.

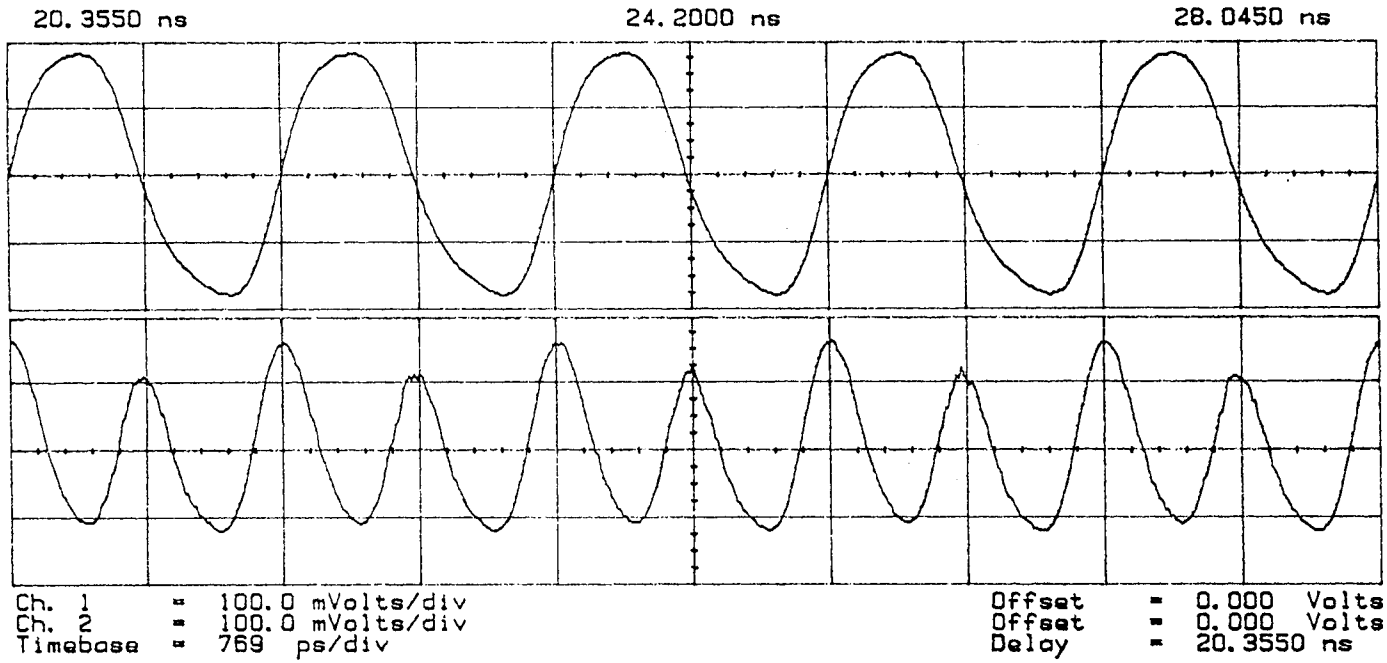

Figure 9. Chip 2 clock generator output waveforms under 1.3 GHz input clock. The bottom trace was the buffered input clock at 1.3 GHz and the top trace was the divided by 2 clock which was to be used as the QPPM slot clock (650 MHz).

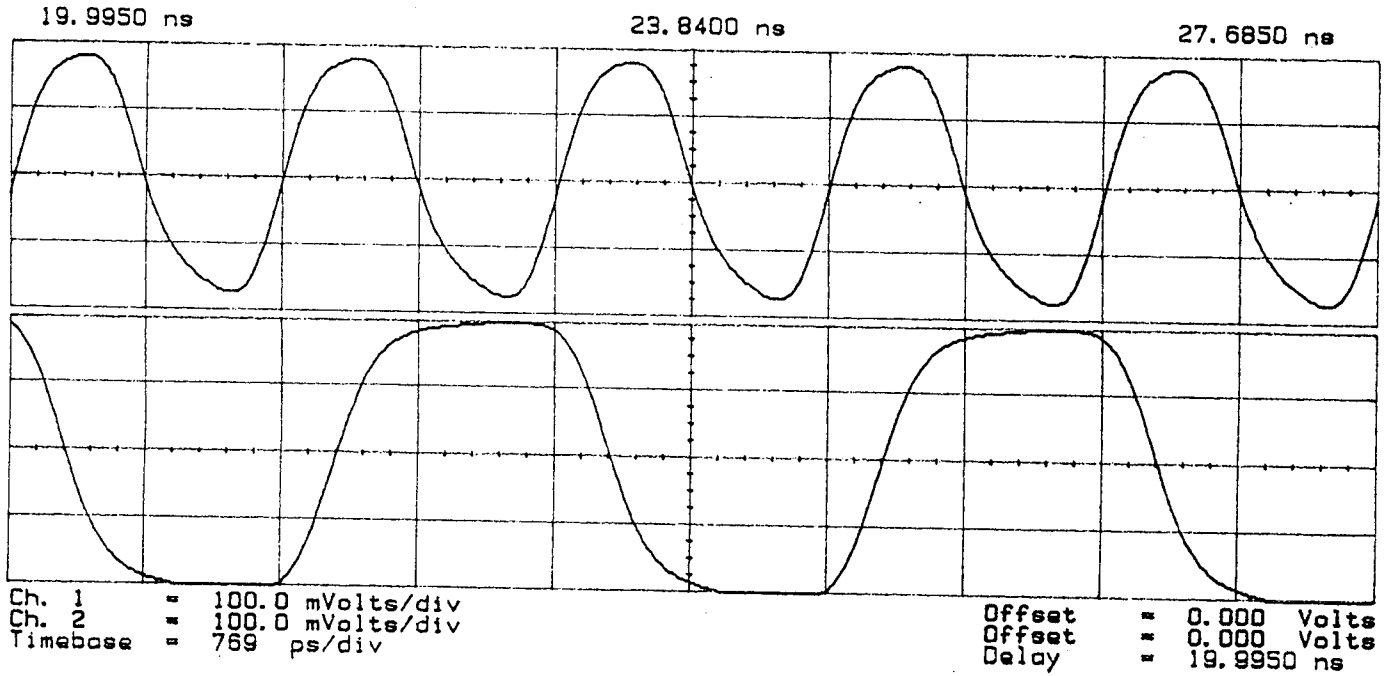

Figure 10. Chip 2 clock generator output waveforms. The top trace was the divided by 2 clock to be used as QPPM slot clock (650 MHz) and the bottom trace was the divided by 4 clock to be used as binary data clock (325 Mbps).

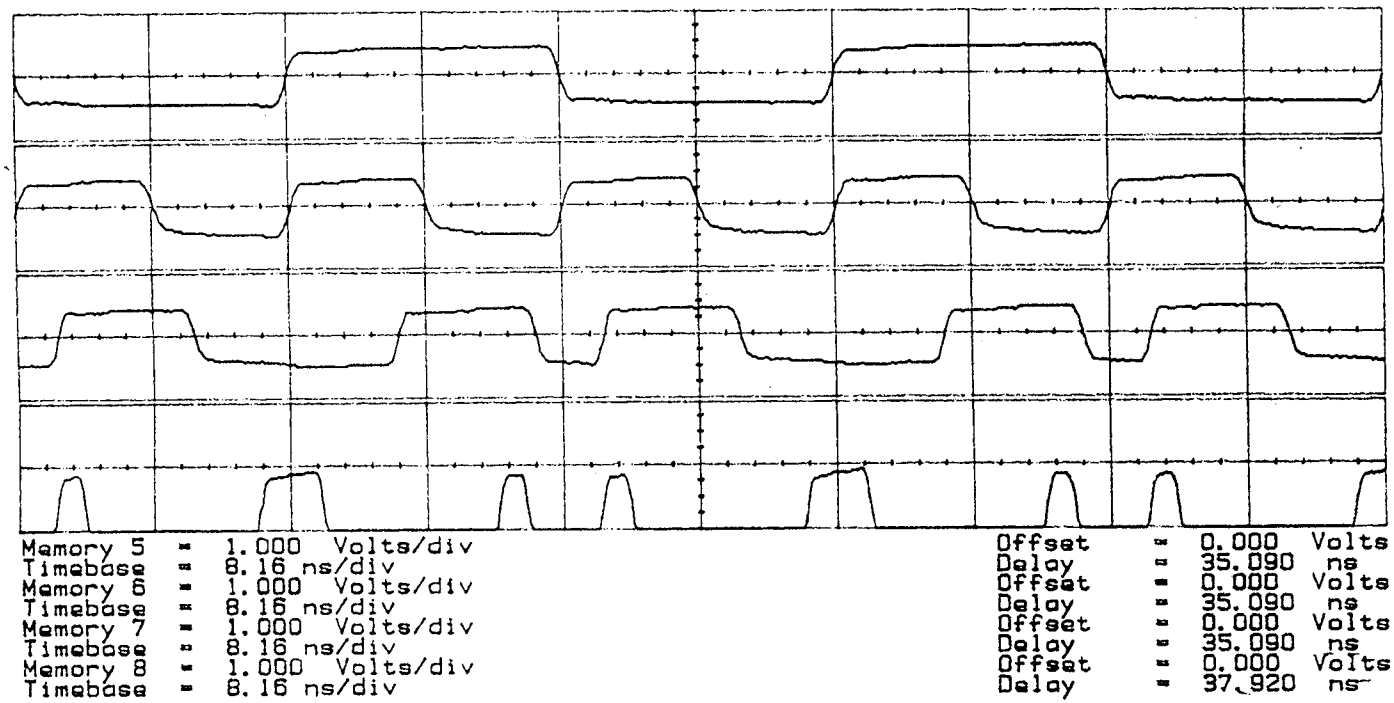

Figure 11. The regenerated binary data by the QPPM detector in response to an input QPPM data patters "10, 11, 00, 01," at 245 Mbps (input clock frequency 980 MHz). The top two traces were the two parallel binary data bits and the third trace was the multiplexed serial bit output which had three QPPM slot time delay. The bottom trace was the QPPM data input to the chip.

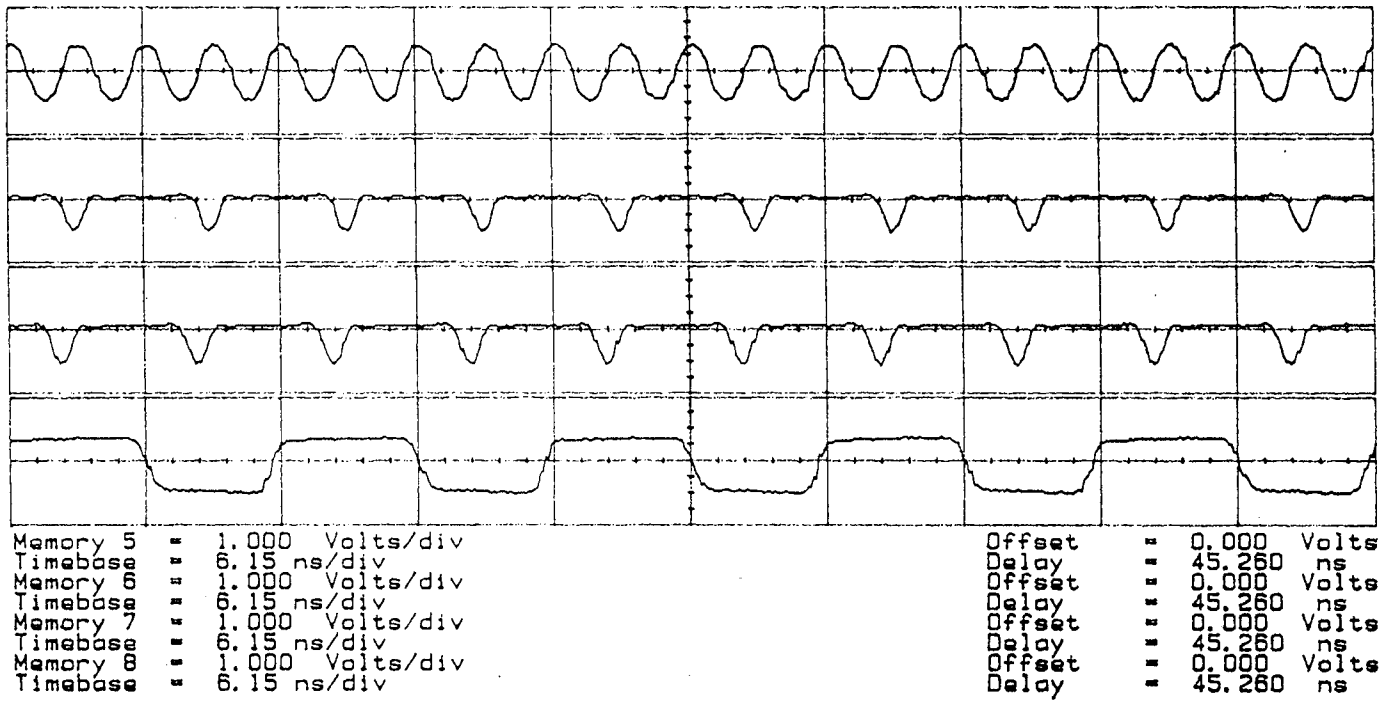

Figure 12. The binary data clock, the QPPM word boundary signal, the latch signal for the multiplexer input, and one of the parallel binary bits output from Chip 2 under the same input data and clock rate as in Figure 11.

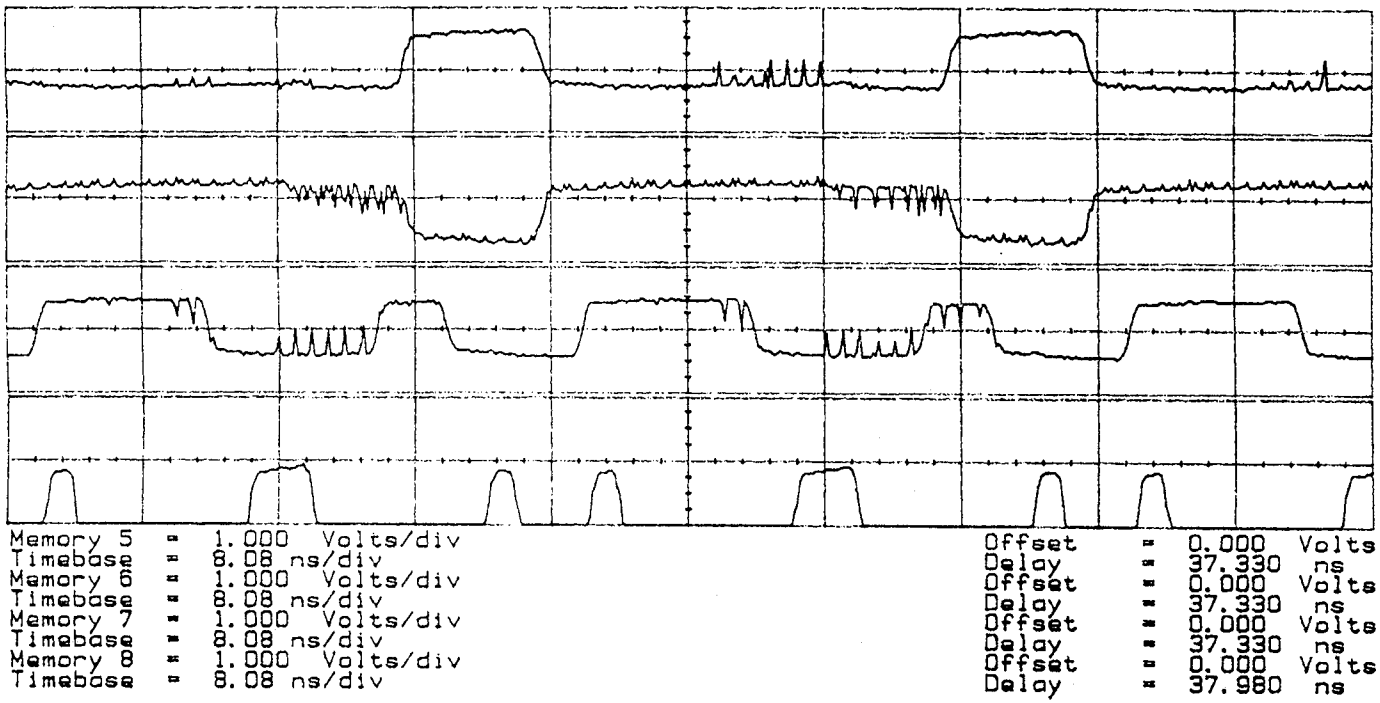

Figure 13. Same as Figure 11 but at 990 MHz input clock frequency which corresponded to a slot clock frequency of 495 MHz and a binary data rate of 247.5 Mbps. The glitches on the waveforms were abnormal and believed to result from insufficient time margins for the signals between various parts of the circuit on the chip.

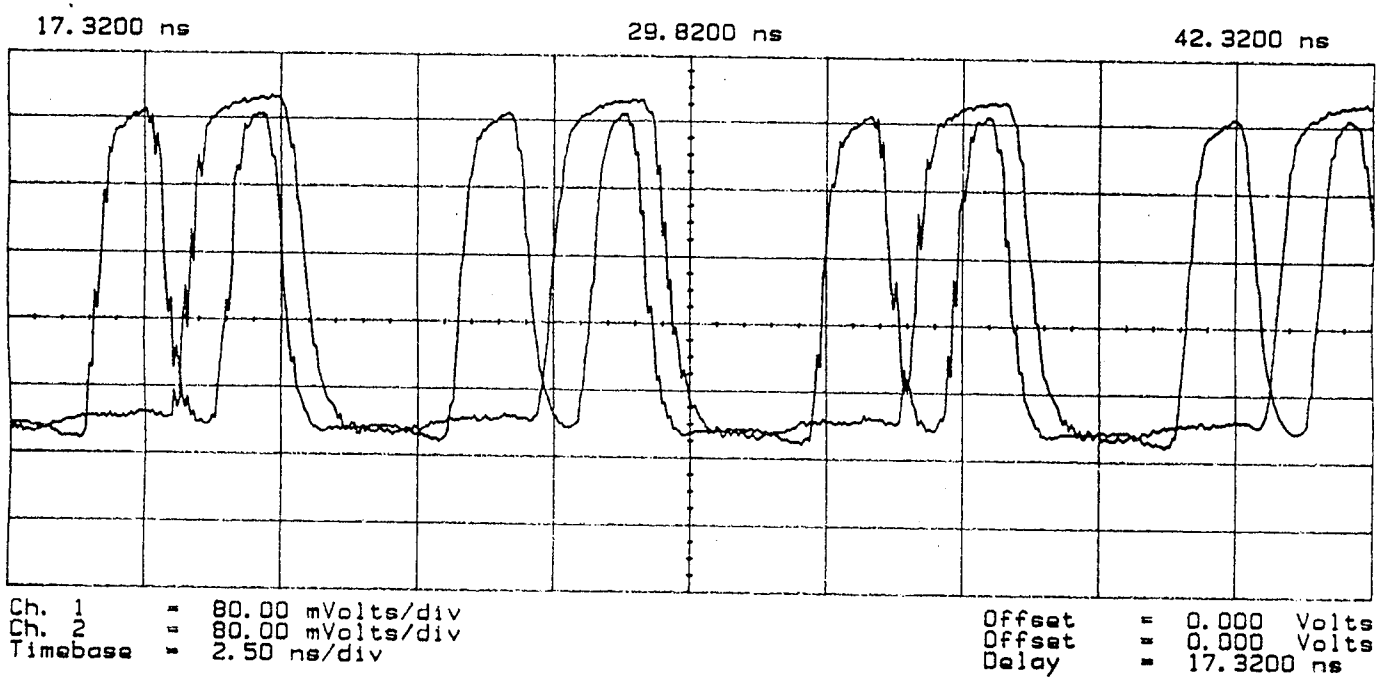

Figure 14. The clock generator outputs at an input clock frequency of 300 MHz. The trace with single pulses at 125 MHz and less than 50% duty cycle is the divided by four clock. The trace with repetitive twin pulses is the abnormal divided by two clock.

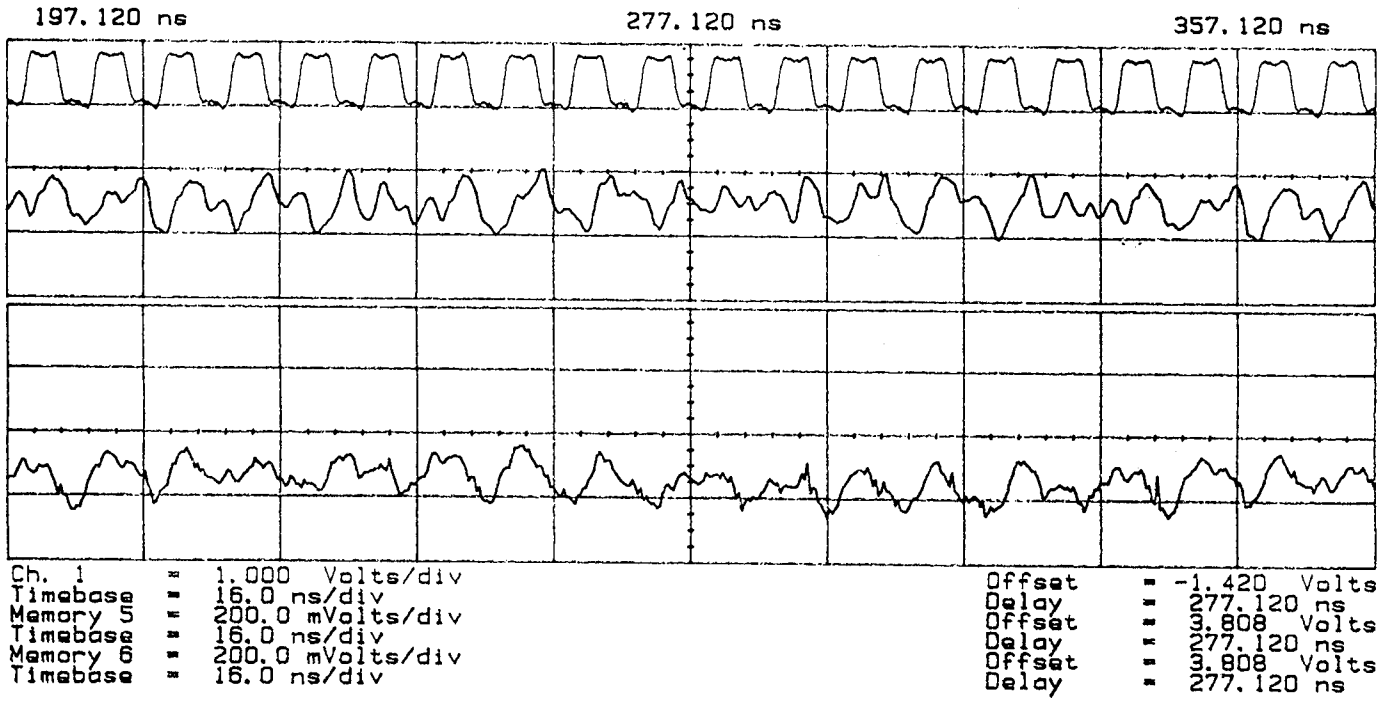

Figure 15 Phase detector outputs along with the divided by four clock at an input slot clock frequency of 500 MHz. The data input was a 8 word QPPM sequence. The input impedance of the oscilloscope was 1 MΩ.

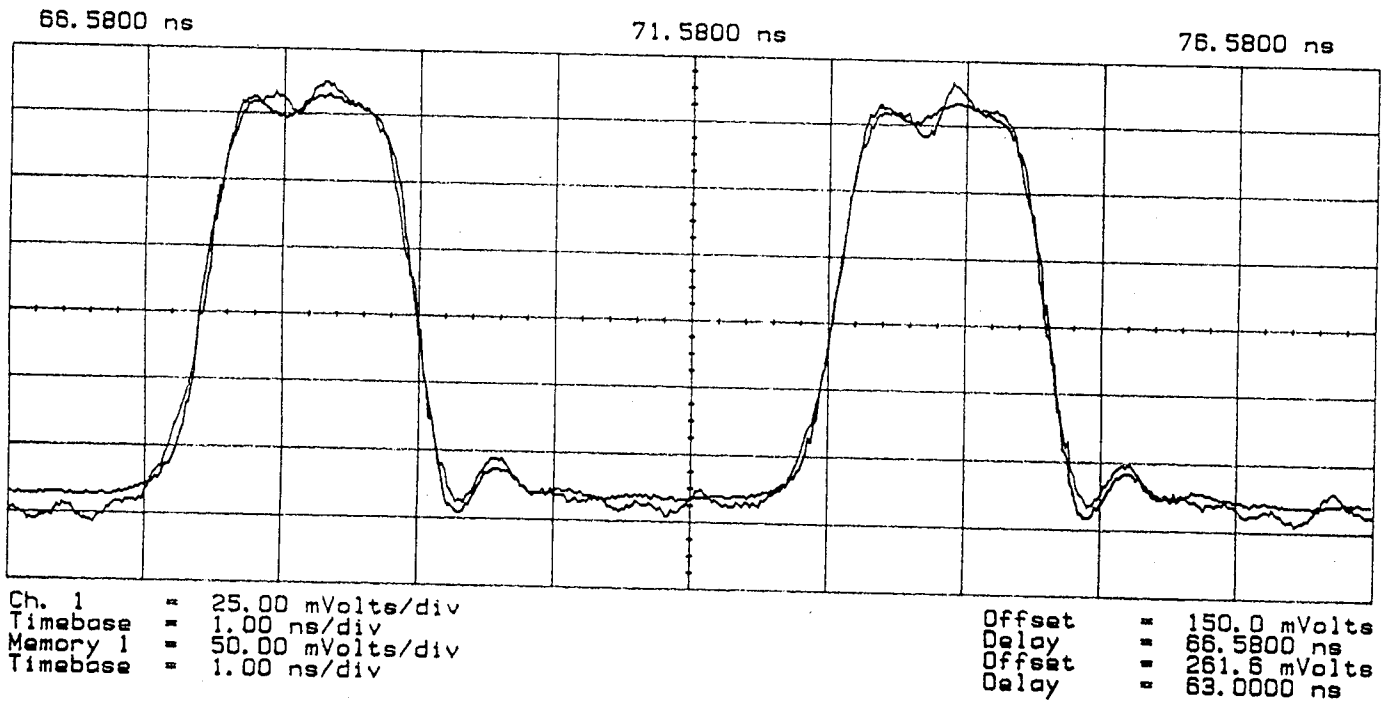

Figure 16. The waveforms of the input and the output of the source follower. Both the signals were attenuated by -6dB before entering the oscilloscope. The waveform with higher amplitude was the input. The timing offset and the vertical scale of one of the waveforms was adjusted so that the two overlaid on each other.

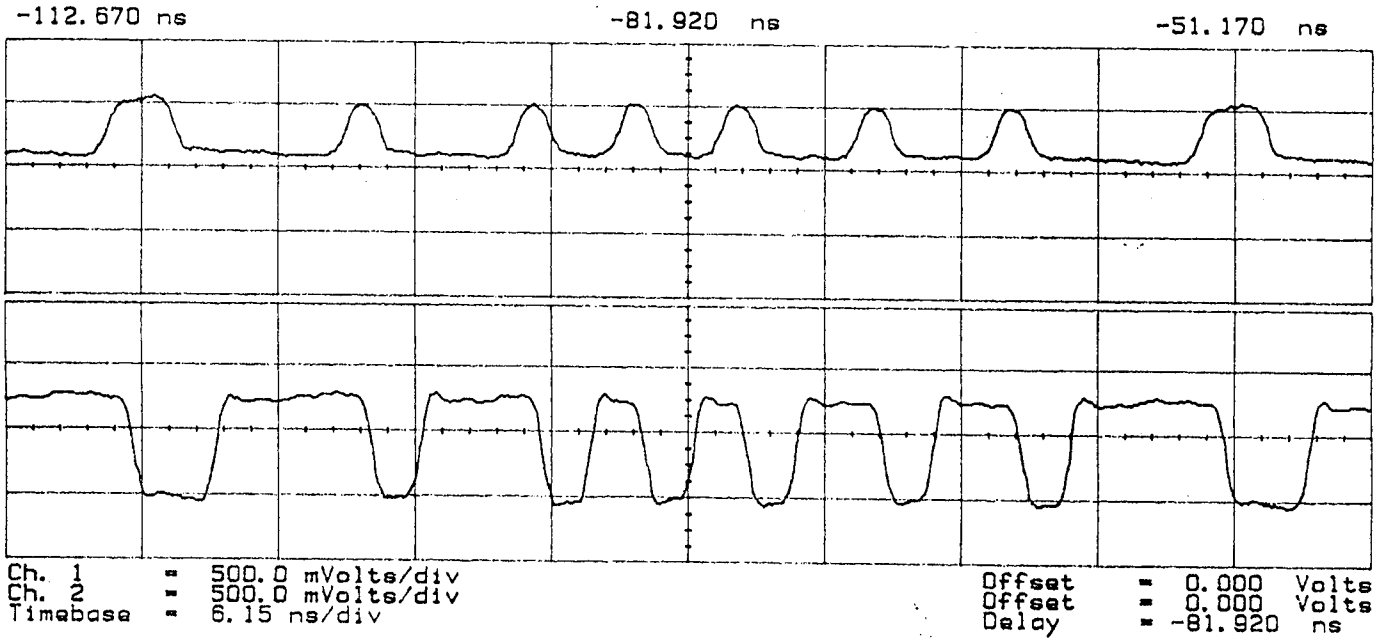

Figure 17. The source follower output waveform (top trace) and the comparator output waveform (lower trace). The input signal was a 8 word 325 Mbps QPPM sequence with an 1 V_{p-p} amplitude and a DC offset of 420 mV.

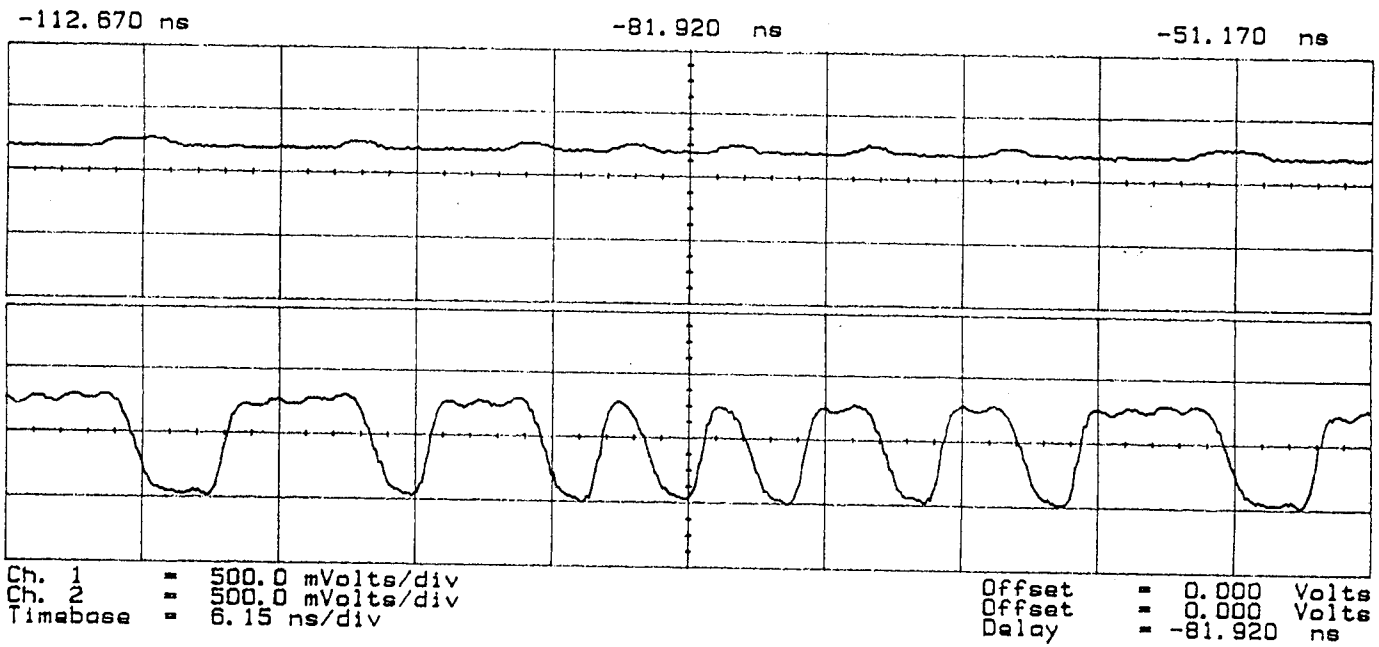

Figure 18. Same as Figure 17 but the input signal was attenuated by -16 dB.

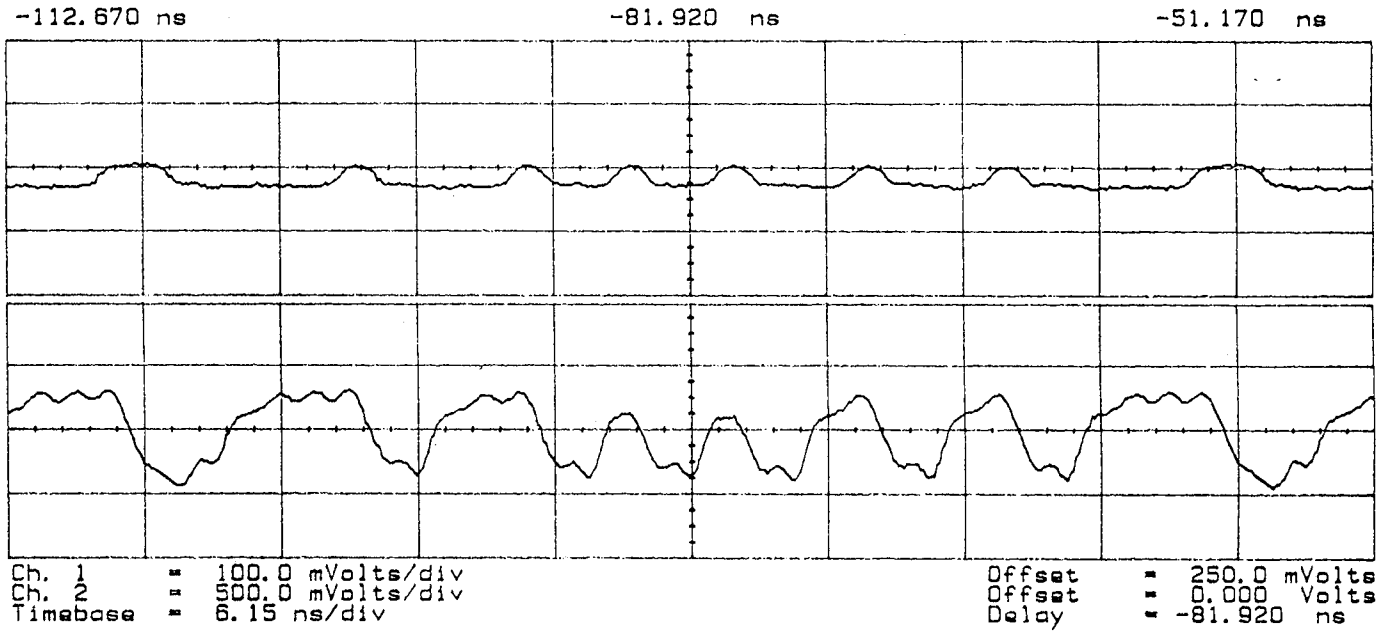

Figure 19. Same as Figure 17 but the input signal was attenuated by -22 dB.

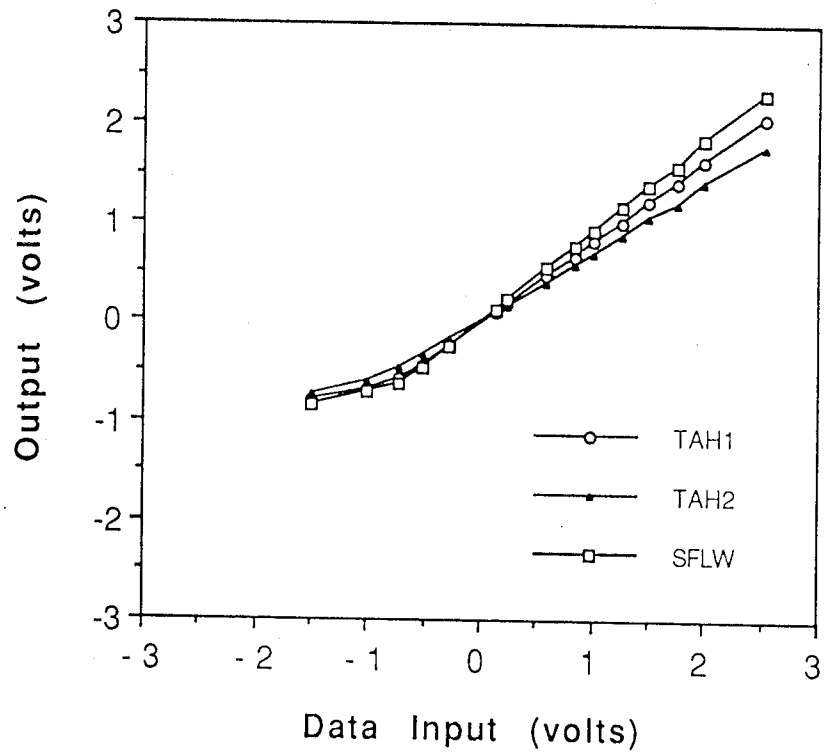

Figure 20. DC response of TAH 1, TAH 2, and the source follower.

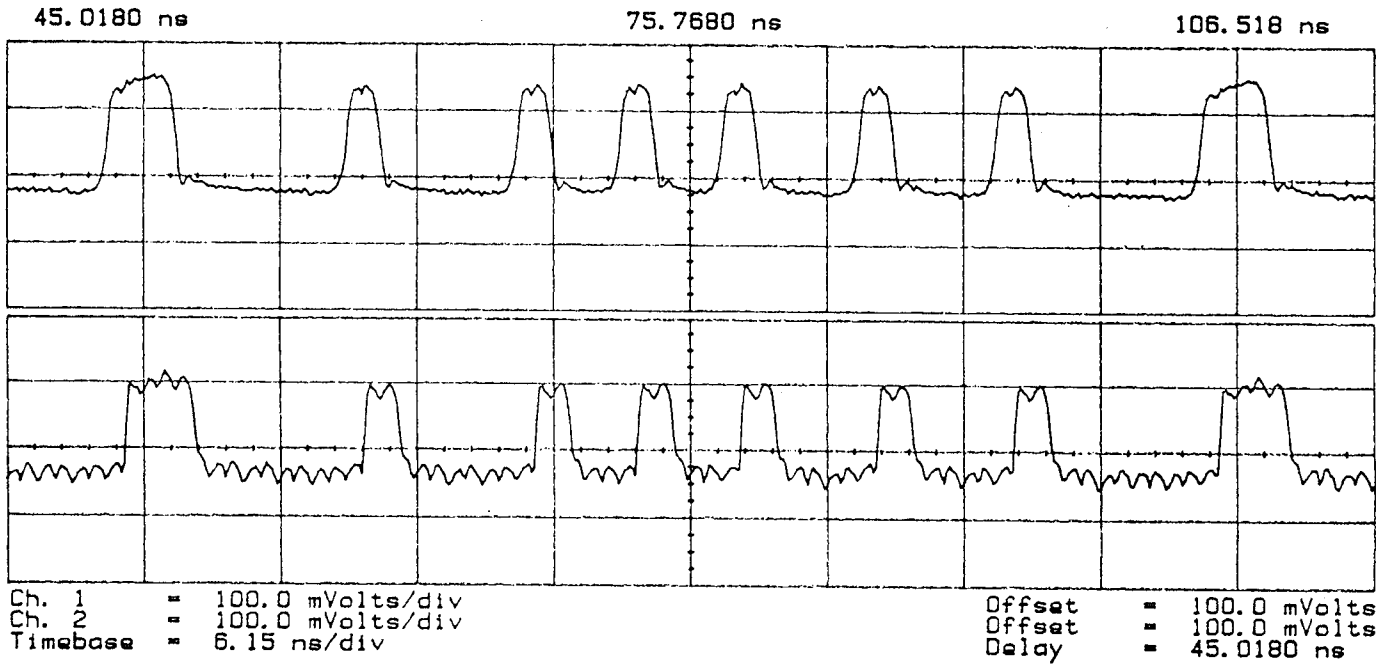

Figure 21. Waveforms of the source follower output (top trace) and the TAH 1 output (lower trace). The input signal was a 8 word 325 Mbps QPPM sequence with an amplitude of 0.71 V_{p-p}. Both the output signals were attenuated by -6dB before entering the oscilloscope.

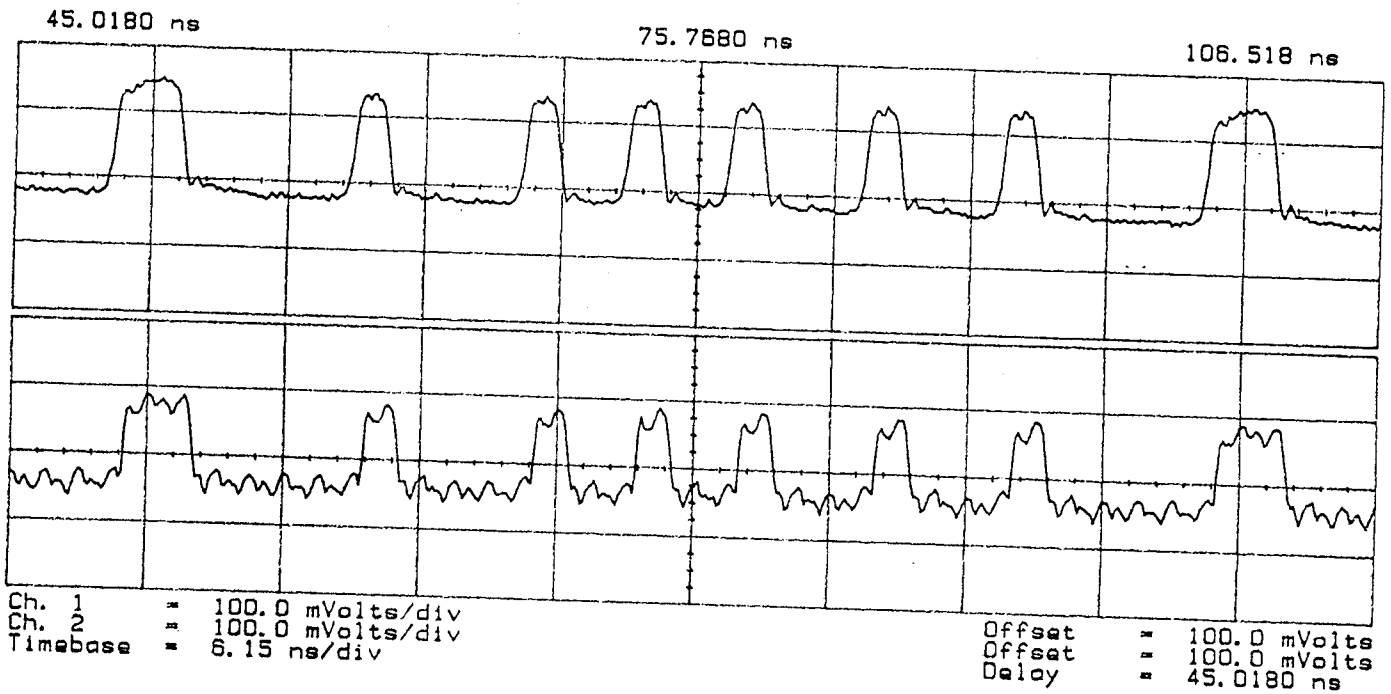

Figure 22. Waveforms of the source follower output (top trace) and the TAH 2 output (lower trace). The input signal was a 8 word 325 Mbps QPPM sequence with an 0.71 V_{p-p} amplitude. Both the output signals were attenuated by -6dB before entering the oscilloscope.

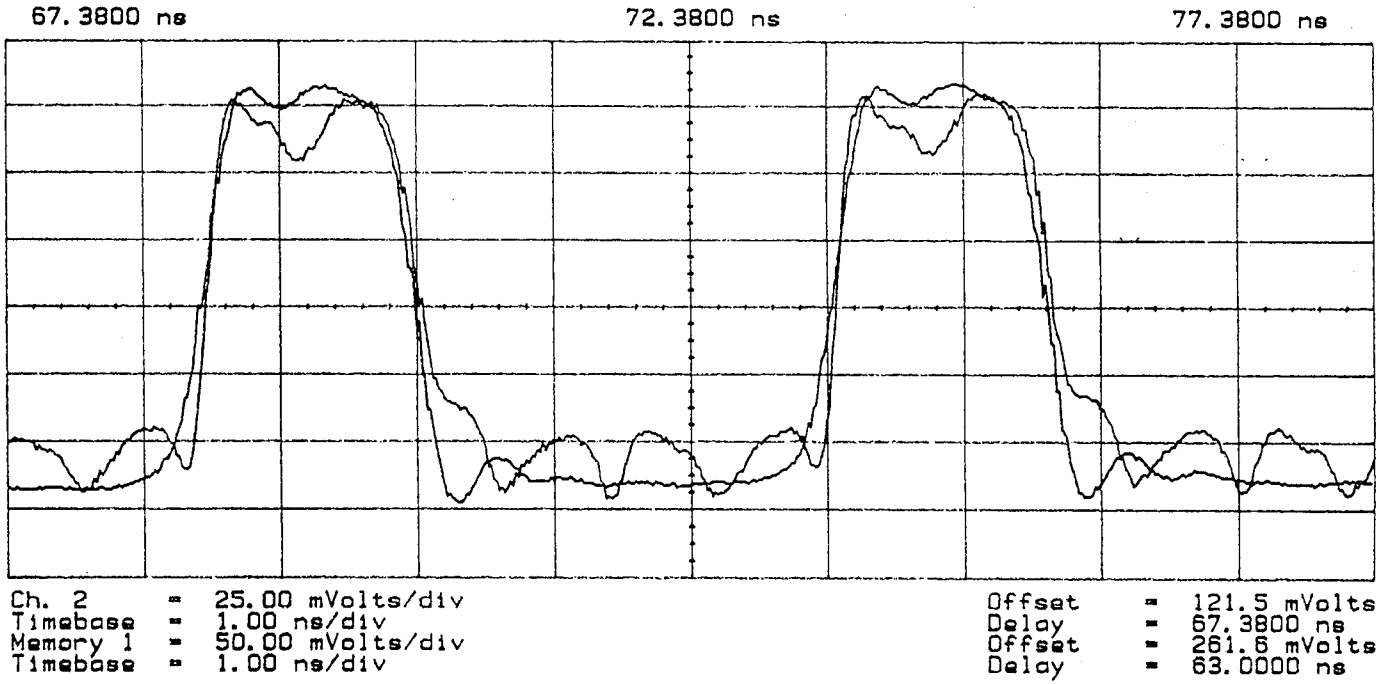

Figure 23. Same as Figure 20 but with different horizontal and vertical scales.

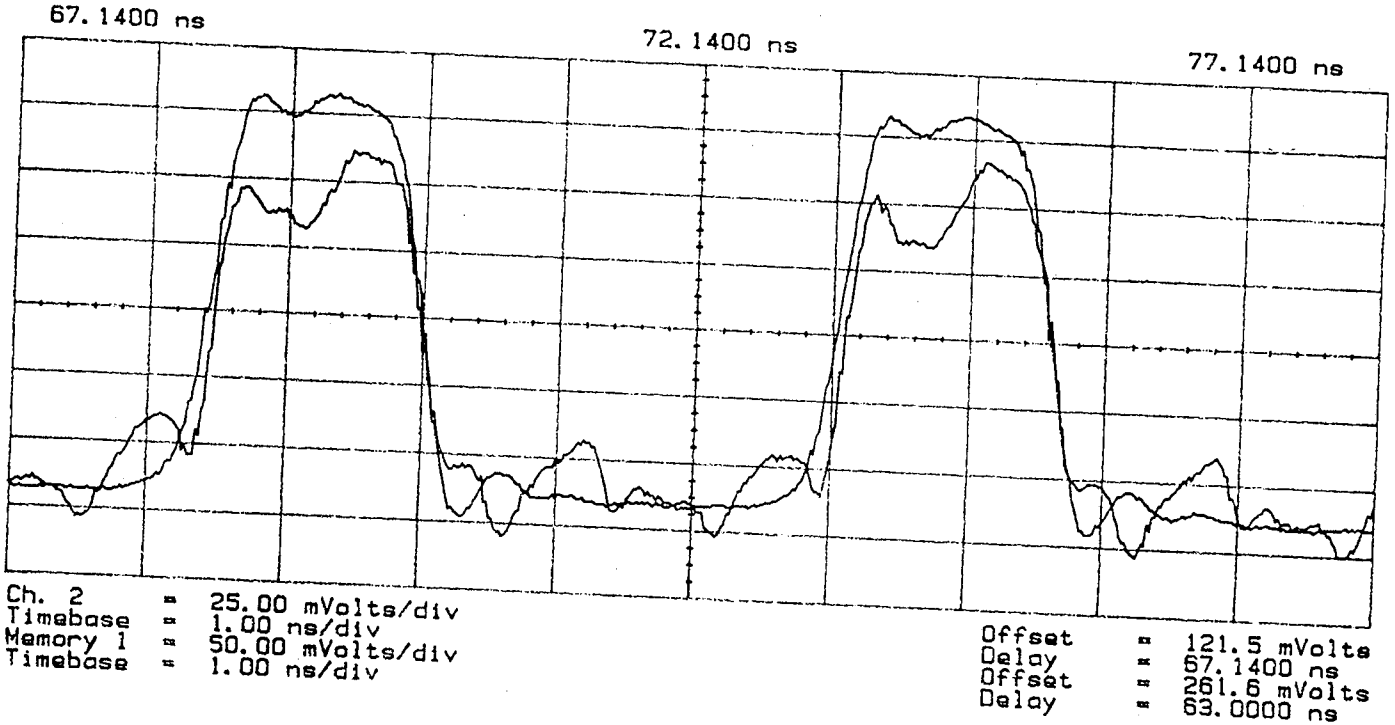

Figure 24. Same as Figure 21 but with different horizontal and vertical scales.

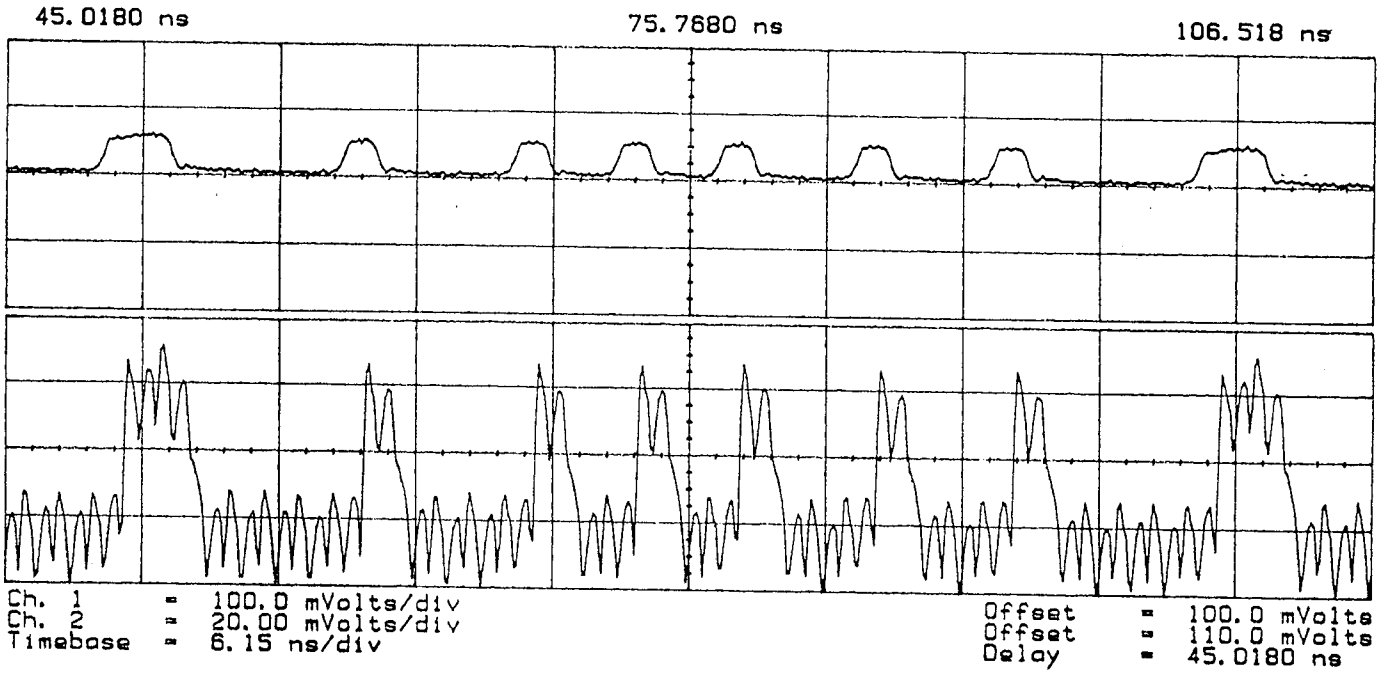

Figure 25. Waveforms of the source follower output (top trace) and the TAH 1 output (lower trace). The input signal was a 8 word 325 Mbps QPPM sequence with an amplitude of 0.22 V_{p-p} (-10 dB compared with Figure 21). Both the output signals were attenuated by -6dB before entering the oscilloscope.

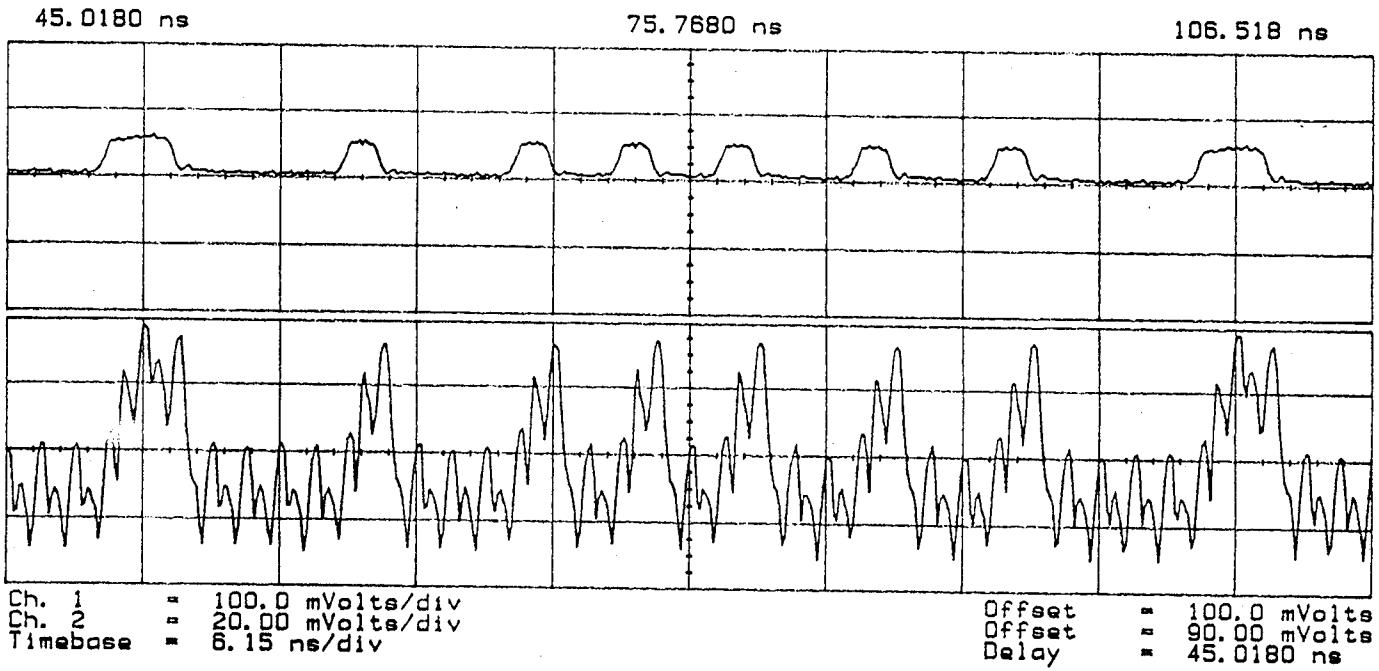

Figure 26. Waveforms of the source follower output (top trace) and the TAH 2 output (lower trace). The input signal was a 8 word 325 Mbps QPPM sequence with an amplitude of 0.22 V_{p-p} (-10 dB compared with Figure 22). Both the output signals were attenuated by -6dB before entering the oscilloscope.

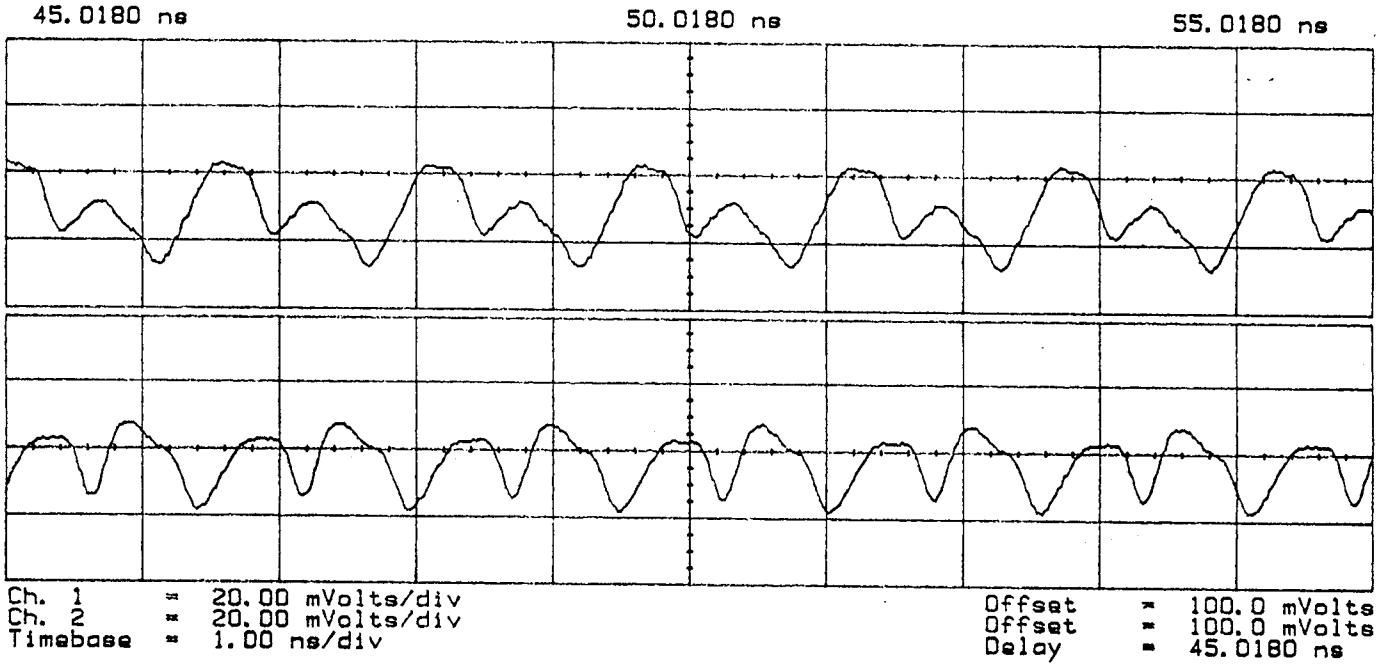

Figure 27. TAH 1 (top trace) and TAH 2 (lower trace) output waveforms when there was no input signal. The frequency of the ringings corresponded to the sampling clock (650 MHz).

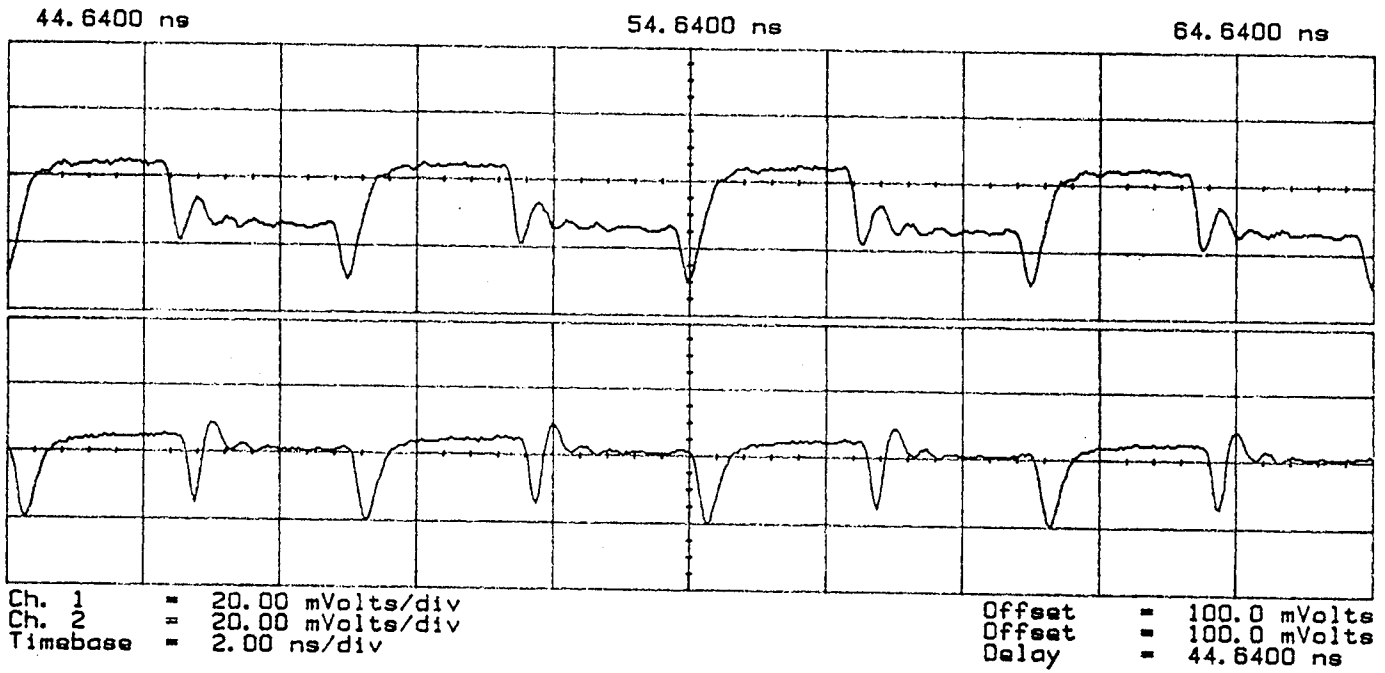

Figure 28. Same as Figure 27 but the sampling clock was changed to 200 MHz. The correspondence between the ringings and the sampling clock was more evident.

Receiver Performance Analysis of BPPM Optical Communication Systems Using 1.3 μm Wavelength Transmitter and InGaAs PIN Photodiodes

Xiaoli Sun

Department of Electrical and Computer Engineering
The Johns Hopkins University
Baltimore, MD 21218

March 1993

Binary pulse position modulation (BPPM, or Manchester) signal format is to transmit every information bit into a BPPM pulse positioned in one of the two time slot. The width of each BPPM pulse is one half the bit interval. A BPPM receiver has to have twice the bandwidth as compared to a conventional non-return-to-zero (NRZ) on-off-keyed (OOK) receiver at the same source binary data rate. The major advantage of BPPM is constant signal duty cycle independent of the data patterns being sent.

1. Maximum Likelihood Detection

The optimal receiver structure for a BPPM optical communication system is the maximum likelihood (ML) detection which requires integrating the photodetector output over each BPPM time slot and comparing them to find the largest. The integration in practice is realized by sampling the output of a matched filter at the end of each BPPM slot time. A comparator is then used to determine the slot which contains the largest signal.

We first define x_1 and x_0 as the signal output from the matched filter in terms of number of electrons. We further assume that x_1 and x_0 follow Gaussian distributions with means and variances $\bar{x}_1$, $\bar{x}_0$, σ_1^2, and σ_0^2, respectively. The receiver bit error rate (BER) can be written as

$$BER = \mathrm{Prob}(x_1 \le x_0) = \int_{-\infty}^{\infty}\int_{x_1}^{\infty} \frac{1}{\sqrt{2\pi}} e^{-\frac{(x_1-\bar{x}_1)^2}{2\sigma_1^2}} \cdot \frac{1}{\sqrt{2\pi}} e^{-\frac{(x_0-\bar{x}_0)^2}{2\sigma_0^2}} dx_0 dx_1 . \quad (1)$$

Let $u = \frac{x_0 - \overline{x_0}}{\sqrt{2}\sigma_0}$ and $z = \frac{x_1 - \overline{x_1}}{\sqrt{2}\sigma_1}$,

$$BER = \int_{-\infty}^{\infty} \frac{1}{\sqrt{\pi}} e^{-z^2} \int_{\frac{\sigma_1}{\sigma_0} z + \frac{\overline{x_1} - \overline{x_0}}{\sqrt{2}\sigma_0}}^{\infty} \frac{1}{\sqrt{\pi}} e^{-u^2} du\, dz. \tag{2}$$

The standard complimentary error function is defined as

$$\begin{aligned} &erfc(x) = 1 - erf(x) \\ &erf(x) = \int_0^x \frac{2}{\sqrt{\pi}} e^{-v^2} dv, \quad erf(\infty) = 1 \\ &erfc(x) = 1 - \int_0^x \frac{2}{\sqrt{\pi}} e^{-v^2} dv = 1 - \left[erf(\infty) - \int_x^{\infty} \frac{2}{\sqrt{\pi}} e^{-v^2} dv \right] \\ &erfc(x) = \int_x^{\infty} \frac{2}{\sqrt{\pi}} e^{-v^2} dv \end{aligned} \tag{3}$$

Substituting (3) into (2)

$$BER = \frac{1}{2\sqrt{\pi}} \int_{-\infty}^{\infty} e^{-z^2} erfc\left(\frac{\sigma_1}{\sigma_0} z + \frac{\overline{x_1} - \overline{x_0}}{\sqrt{2}\sigma_0}\right) dz. \tag{4}$$

The second term of the argument of the complimentary error function in (4) is often defined as the square root of the signal to noise ratio (SNR), i.e.

$$SNR = \left(\frac{\overline{x_1} - \overline{x_0}}{\sigma_0}\right)^2. \tag{5}$$

2. Threshold Crossing Detection

A simpler detection scheme for BPPM signal is to first integrate the received signal over each BPPM time slot and then compare them against a preset threshold.

Similar to equation (1), the receiver BER for a given threshold level, x_{th}, can be written as

$$BER = 1 - \text{Prob}(x_1 \geq x_{th})\,\text{Prob}(x_0 \leq x_{th})$$

$$= 1 - \int_{x_{th}}^{\infty} \frac{1}{\sqrt{2\pi}} e^{-\frac{(x_1 - \overline{x_1})^2}{2\sigma_1^2}} dx_1 \int_{-\infty}^{x_{th}} \frac{1}{\sqrt{2\pi}} e^{-\frac{(x_0 - \overline{x_0})^2}{2\sigma_0^2}} dx_0 \,. \qquad (6)$$

Let $u = \frac{x_0 - \overline{x_0}}{\sqrt{2}\sigma_0}$ and $z = \frac{x_1 - \overline{x_1}}{\sqrt{2}\sigma_1}$,

$$BER = 1 - \int_{\frac{x_{th} - \overline{x_1}}{\sqrt{2}\sigma_1}}^{\infty} \frac{1}{\sqrt{\pi}} e^{-z^2} dz \int_{-\infty}^{\frac{x_{th} - \overline{x_0}}{\sqrt{2}\sigma_0}} \frac{1}{\sqrt{\pi}} e^{-u^2} du \qquad (7)$$

Substituting the complimentary error function (3) into (7)

$$BER = 1 - \frac{1}{2} erfc\left(\frac{x_{th} - \overline{x_1}}{\sqrt{2}\sigma_1}\right) \frac{1}{2} erfc\left(-\frac{x_{th} - \overline{x_0}}{\sqrt{2}\sigma_0}\right). \qquad (8)$$

There should an optimal threshold level which gives the minimum receiver BER. The optimal threshold value can be obtained by taking the derivative of (7) with respect to x_{th} , equating it to zero, and solving the equation for x_{th} . However, no explicit solution could be found, even with the powerful software called Mathematica, because x_{th} appears both in the exponent and the limits of integrals in the equation to be solved.

In practice, the threshold is often set to one half the pulse amplitude. One can simply AC couple the input signal and tie the threshold level of the threshold comparator to ground. The BPPM signal has a constant duty cycle of 50% and the average DC level is always equal to one half of the pulse amplitude. Under this condition,

$$x_{th} = \frac{\overline{x_1} + \overline{x_0}}{2} \qquad (9)$$

and

$$BER = 1 - \frac{1}{2} erfc\left(-\frac{\overline{x_1} - \overline{x_0}}{2\sqrt{2}\sigma_1}\right) . \qquad (10)$$

3. Calculation of the Means and the Variances of the Signal

The means of the signal are given by

$$\overline{x_0} = \overline{n_b} + \frac{\overline{n_s}}{\alpha_{ext}} + \frac{I_d \tau}{q}$$

$$\overline{x_1} = \overline{n_b} + \overline{n_s}\left(1 - \frac{1}{\alpha_{ext}}\right) + \frac{I_d \tau}{q}$$

where

$\overline{n_b}$ = average number of background radiation photons per slot,

$\overline{n_s}$ = average number of signal photons per pulse,

α_{ext} = Transmitter on-off extinction ratio,

I_d = photodetector dark current,

τ = BPPM slot time, equal to one half bit interval,

q = electron charge.

The average numbers of signal and background radiation photons per pulse are given by

$$\overline{n_s} = \frac{\eta P_{1pk} \tau}{hf} = \frac{2\eta P_{1av} \tau}{hf} \qquad (11)$$

$$\overline{n_b} = \frac{\eta P_b \tau}{hf}$$

where

η is the photodetector quantum efficiency,

P_{1pk} and P_{1av} are the peak and average optical signal power and $P_{1pk} = 2P_{1av}$,

P_b is the background radiation power,

$hf = hc/\lambda$ is the photon energy with c the speed of light,

λ is the transmitter wavelength.

The variances of the signal are given by

$$\sigma_0^2 = \overline{n_b} + \frac{\overline{n_s}}{\alpha_{ext}} + \frac{I_d \tau}{q} + \frac{2KT_e \tau}{Rq^2}$$

$$\sigma_1^2 = \overline{n_b} + \overline{n_s}\left(1 - \frac{1}{\alpha_{ext}}\right) + \frac{I_d \tau}{q} + \frac{2KT_e \tau}{Rq^2} \qquad (12)$$

where K is Boltzmann constant,
T_e is the equivalent noise temperature,
R is the photodetector load resistance (transimpedance)

The last term in (12) represents the amplifier thermal noise assuming it is white noise. The preamplifier is usually the dominant circuit noise source. Transimpedance preamplifier noise is often given by its spectral current noise density, $(d\langle i_n^2\rangle/df)^{1/2}$, in $A/Hz^{1/2}$, which is related to the equivalent noise temperature, T_e, and transimpedance, R, by

$$\frac{d\langle i_n^2\rangle}{df} = \frac{4KT_e}{R}. \qquad (13)$$

4. Numerical Calculation of Receiver BER vs. Input Signal Power

A computer program is written in "C" language to evaluate equation (4) and (10). The complimentary error function is from the standard math library from the C compiler. The numerical integration subroutine is copied from the famous book *Numerical Recipes in C*. A list of the program is attached along with two sets of calculation results at 1 Mbps and 20 Mbps, assuming a typical InGaAs PIN photodiode and a typical preamplifier are used in the receiver.

1 Mbps BPPM Receiver Performance

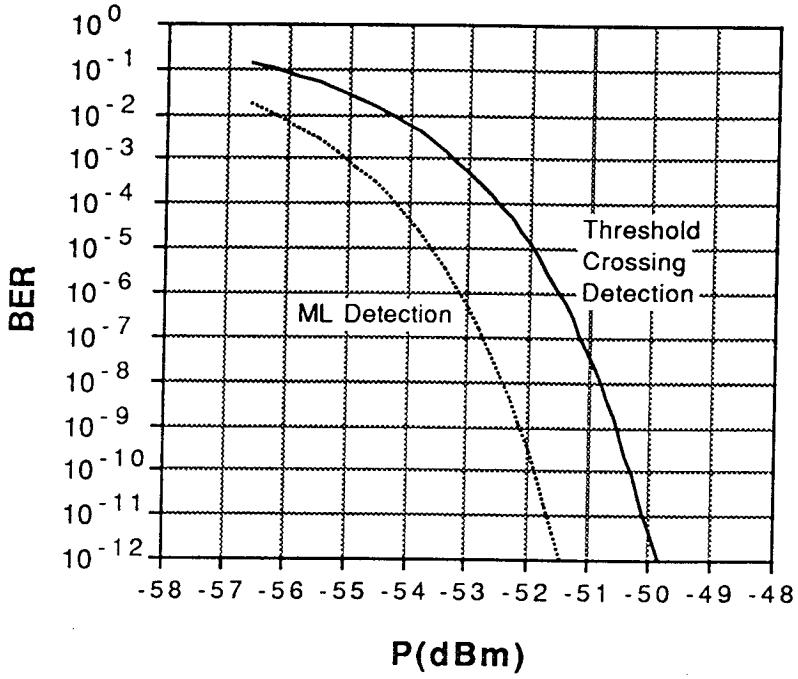

20 Mbps BPPM Receiver Performance

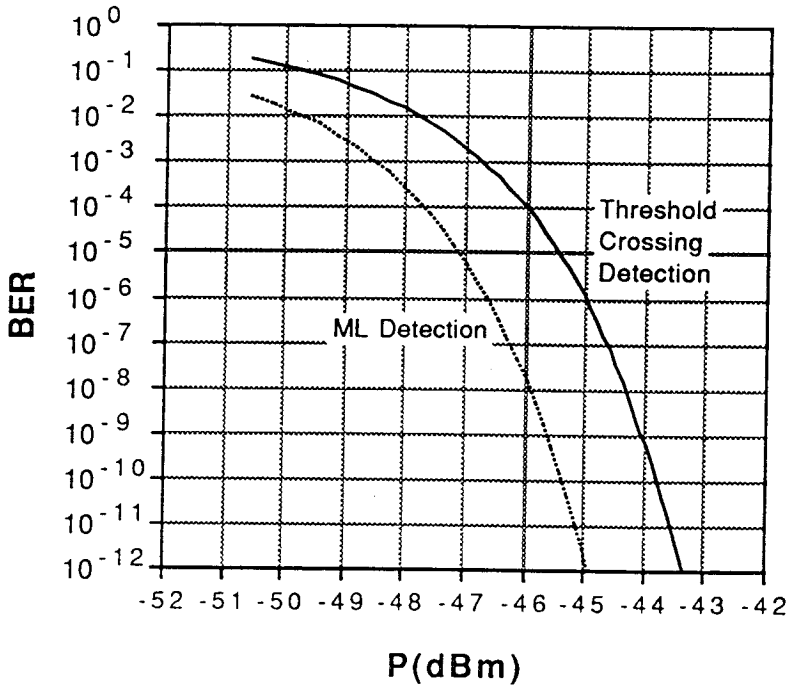

```
/* This program computes the receiver BER of a BPPM receiver using a PIN */


/* Standard I/O device and math library */

#include <stdio.h>
#include <math.h>


/* Constants */

#define ECHARGE 1.6e-19 /* electron charge */
#define Kb 1.38e-23 /* Boltsmann constant */
#define PI 3.14159
#define A -10.0 /* Lower limit of the integral */
#define B 10.0  /* upper limit of the integral */


/* The subroutines */

float qtrap(), trapzd() ;


/* Global variables, parameters in the integrand */

static double s10, u0 ;


/* The integrand */

float pr(u)
double u ;
  {
        return exp( -u*u ) * erfc( s10*u + u0 ) ;
  }


/* The main program */

main()
{

/* Declaration of variables */

double ns, mns ; /* ns=lambdapeak*tau, mns=index */
double nsstart, dns, npts ; /* start and increment of ns, npts= # pts */
double Drt; /* source binary data rate */
float Ppk, Pav ; /* pk and ave signal power */
double BERML, BERTC;  /* BER, ML detection and threshold crossing detection */
float wvlngth, hf, eta ;    /* wavelength, photon energy, Qefficiency */
double In;    /* Preamplifier noise current in pA/rtHz  */
double eratio, nb, Id, T, Te, Rf ; /* extinction ratio, background cts/slot */
                        /* PPM slot time, noise temp. load resistance */
double nss, nbb, vx1, vx0 ; /* effective signal and background counts */
                                /* variances when 1 and 0 is transmitted */
FILE *results, *fopen(); /* the result file */


/* Ask for system parameters */

printf("ns from ?  \n" );
scanf("%lf", &nsstart );
printf("increment of ns = ?  \n" );
scanf("%lf", &dns );
printf("# of points = ?  \n" );
scanf("%lf", &npts );
```

```
printf("laser extinction ratio = ? \n" );
scanf("%lf", &eratio );
printf("background noise photons per slot = ? \n" );
scanf("%lf", &nb );
printf("Source Data Rate in Mbps = ? \n" );
scanf("%lf", &Drt );
printf("\n" );

/* Open the file to contain the results */

results=fopen("BER.d", "w");


/* Other system parameters */

wvlngth=1300;
eta=0.70;
Id=20.0e-9;
In=1.0e-12;
Rf=28000.0;
Te=In*In*Rf/4/Kb;
T=1.0/Drt/2.0*1.0e-6;
hf=1242.0/wvlngth*ECHARGE;


/* Print out the parameters */

fprintf(results,"Performance of BPPM Receiver Using a PIN Photodiode \n");
fprintf(results,"\n");
fprintf(results,"System Parameters: \n");
fprintf(results,"Datarate=%3.0fMbps, Qefficy=%2.2f, Darkcurrent=%3.1e\n",
                                                    Drt, eta, Id   );
fprintf(results,"Preampnoisecurrent=%5.2e pA/sqrtHz\n", In);
fprintf(results,"Loadresistance=%5.0f, Noisetemp=%4.0fK\n", Rf, Te );
fprintf(results,"Backgroundcts=%6.1f, Extratio=%6.0f\n", nb, eratio );
fprintf(results,"Wavelength=%4.0fnm\n", wvlngth);
fprintf(results,"\n" );

printf(" ph/bit     Ppk(nW)     Pav(nW)    Pav(dBm) \
 SNR0(dB)   BERML      BERTC\n");
fprintf(results,"  ph/bit    Ppk(nW)     Pav(nW)    Pav(dBm) \
 SNR0(dB)   BERML      BERTC\n");


/* Start computing BER */

for( mns=0; mns<=npts-1; ++mns )
    {
        ns=nsstart+mns*dns;
        nss=ns*(1.0-1.0/eratio );
        nbb=nb+ns/eratio;

        vx1= nss + nbb + Id*T/ECHARGE + 2.0*Kb*Te*T/Rf/ECHARGE/ECHARGE;
        vx0= nbb + Id*T/ECHARGE + 2.0*Kb*Te*T/Rf/ECHARGE/ECHARGE;

        s10=sqrt( vx1/vx0 );
        u0= nss/sqrt(2.0*vx0);

        BERML= 1.0/2.0/sqrt(PI) * qtrap( pr, A, B );

        BERTC= 1.0 - erfc(-nss/2.0/sqrt(2.0*vx1))
                                * erfc(-nss/2.0/sqrt(2.0*vx0)) / 4.0 ;
        if(BERTC<=1.0e-20) mns=npts;

        Ppk= ns/T/eta*hf;
        Pav=Ppk/2.0;
```

```
        printf("%7.0f     %3.3e    %3.3e    %6.2f     %7.2f    %8.2e    %8.2e\n",
         ns, Ppk*1.0e9, Pav*1.0e9, 10*log10(Pav*1000),
                                10*log10(2.0*u0*u0), BERML, BERTC );
        fprintf(results,"%7.0f     %3.3e    %3.3e    %6.2f     %7.2f \
  %8.2e   %8.2e\n",
               ns, Ppk*1.0e9, Pav*1.0e9, 10*log10(Pav*1000),
                                10*log10(2.0*u0*u0), BERML, BERTC );
   }
fclose(results);
}
```

```
/* A numerical integration subroutine copied from Numerical Recipe */

#include <math.h>
#include <stdio.h>

#define EPS 1.0e-4
#define JMAX 20

float qtrap(func, a, b)
float a, b;
float (*func)();
{
        int j;
        float s, olds, trapzd();
        void nrerror();

        olds = -1.0e30;
        for( j=1; j<=JMAX; j++ )  {
                s=trapzd(func, a, b, j);
                if (fabs(s-olds) < EPS*fabs(olds)) return s;
                olds=s;
        }
        nrerror("Too many steps in routine QTRAP");
}

#undef EPS
#undef JMAX


void nrerror(error_text)
char error_text[];
{
        void exit();

        fprintf(stderr,"Numerical Recipes run-time error...\n");
        fprintf(stderr,"%s\n",error_text);
        fprintf(stderr,"...now exiting to system...\n");
        exit(1);
}
```

```
/* Subsubroutine for numerical integration subroutine   */
/* copied from Numerical Recipes"                       */

#define FUNC(x) ((*func)(x))

float trapzd(func,a,b,n)
float a, b;
float (*func)();        /*ANSI: float (*func)(float);*/
int n;
{
        float x,tnm,sum,del;
        static float s;
        static int it;
        int j;

        if ( n == 1 ) {
                it=1;
                return (s=0.5*(b-a)*(FUNC(a)+FUNC(b)));
        } else {
                tnm=it;
                del=(b-a)/tnm;
                x=a+0.5*del;
                for (sum=0.0,j=1;j<=it;j++,x+=del) sum += FUNC(x);
                it *= 2;
                s=0.5*(s+(b-a)*sum/tnm);
                return s;
        }
}
```

Performance of BPPM Receiver Using a PIN Photodiode

System Parameters:
Datarate= 1Mbps, Qefficy=0.70, Darkcurrent=2.0e-08
Preampnoisecurrent=1.00e-12 pA/sqrtHz
Loadresistance=28000, Noisetemp= 507K
Backgroundcts= 100.0, Extratio= 20
Wavelength=1300nm

ph/bit	Ppk(nW)	Pav(nW)	Pav(dBm)	SNR0(dB)	BERML	BERTC
10000	4.367e+00	2.184e+00	-56.61	9.63	1.61e-02	1.26e-01
11000	4.804e+00	2.402e+00	-56.19	10.46	9.23e-03	9.34e-02
12000	5.241e+00	2.620e+00	-55.82	11.21	5.08e-03	6.79e-02
13000	5.678e+00	2.839e+00	-55.47	11.91	2.68e-03	4.84e-02
14000	6.114e+00	3.057e+00	-55.15	12.55	1.36e-03	3.37e-02
15000	6.551e+00	3.276e+00	-54.85	13.15	6.57e-04	2.30e-02
16000	6.988e+00	3.494e+00	-54.57	13.71	3.05e-04	1.53e-02
17000	7.425e+00	3.712e+00	-54.30	14.24	1.36e-04	1.00e-02
18000	7.861e+00	3.931e+00	-54.06	14.73	5.78e-05	6.40e-03
19000	8.298e+00	4.149e+00	-53.82	15.20	2.36e-05	4.01e-03
20000	8.735e+00	4.367e+00	-53.60	15.65	9.21e-06	2.45e-03
21000	9.172e+00	4.586e+00	-53.39	16.07	3.44e-06	1.47e-03
22000	9.608e+00	4.804e+00	-53.18	16.48	1.23e-06	8.64e-04
23000	1.005e+01	5.023e+00	-52.99	16.86	4.21e-07	4.96e-04
24000	1.048e+01	5.241e+00	-52.81	17.23	1.38e-07	2.79e-04
25000	1.092e+01	5.459e+00	-52.63	17.59	4.32e-08	1.53e-04
26000	1.136e+01	5.678e+00	-52.46	17.93	1.29e-08	8.26e-05
27000	1.179e+01	5.896e+00	-52.29	18.26	3.71e-09	4.35e-05
28000	1.223e+01	6.114e+00	-52.14	18.57	1.02e-09	2.24e-05
29000	1.267e+01	6.333e+00	-51.98	18.88	2.66e-10	1.13e-05
30000	1.310e+01	6.551e+00	-51.84	19.17	6.68e-11	5.58e-06
31000	1.354e+01	6.770e+00	-51.69	19.46	1.60e-11	2.69e-06
32000	1.398e+01	6.988e+00	-51.56	19.73	3.67e-12	1.27e-06
33000	1.441e+01	7.206e+00	-51.42	20.00	8.04e-13	5.87e-07
34000	1.485e+01	7.425e+00	-51.29	20.26	1.68e-13	2.65e-07
35000	1.529e+01	7.643e+00	-51.17	20.51	3.38e-14	1.17e-07
36000	1.572e+01	7.861e+00	-51.04	20.75	6.47e-15	5.06e-08
37000	1.616e+01	8.080e+00	-50.93	20.99	1.18e-15	2.14e-08
38000	1.660e+01	8.298e+00	-50.81	21.22	2.07e-16	8.84e-09
39000	1.703e+01	8.517e+00	-50.70	21.45	3.47e-17	3.57e-09
40000	1.747e+01	8.735e+00	-50.59	21.67	5.55e-18	1.41e-09
41000	1.791e+01	8.953e+00	-50.48	21.88	8.50e-19	5.46e-10
42000	1.834e+01	9.172e+00	-50.38	22.09	1.24e-19	2.07e-10
43000	1.878e+01	9.390e+00	-50.27	22.30	1.74e-20	7.64e-11
44000	1.922e+01	9.608e+00	-50.17	22.50	2.32e-21	2.76e-11
45000	1.965e+01	9.827e+00	-50.08	22.69	2.96e-22	9.77e-12
46000	2.009e+01	1.005e+01	-49.98	22.88	3.62e-23	3.38e-12
47000	2.053e+01	1.026e+01	-49.89	23.07	4.22e-24	1.14e-12
48000	2.096e+01	1.048e+01	-49.80	23.25	4.71e-25	3.78e-13
49000	2.140e+01	1.070e+01	-49.71	23.43	5.02e-26	1.22e-13
50000	2.184e+01	1.092e+01	-49.62	23.61	5.12e-27	3.86e-14
51000	2.227e+01	1.114e+01	-49.53	23.78	4.99e-28	1.20e-14
52000	2.271e+01	1.136e+01	-49.45	23.95	4.64e-29	3.66e-15
53000	2.315e+01	1.157e+01	-49.37	24.11	4.13e-30	9.99e-16
54000	2.358e+01	1.179e+01	-49.28	24.28	3.52e-31	3.33e-16
55000	2.402e+01	1.201e+01	-49.20	24.44	2.86e-32	0.00e+00

Performance of BPPM Receiver Using a PIN Photodiode

System Parameters:
Datarate= 20Mbps, Qefficy=0.70, Darkcurrent=2.0e-08
Preampnoisecurrent=1.00e-12 pA/sqrtHz
Loadresistance=28000, Noisetemp= 507K
Backgroundcts= 5.0, Extratio= 20
Wavelength=1300nm

ph/bit	Ppk(nW)	Pav(nW)	Pav(dBm)	SNR0(dB)	BERML	BERTC
2000	1.747e+01	8.735e+00	-50.59	8.66	2.78e-02	1.68e-01
2200	1.922e+01	9.608e+00	-50.17	9.49	1.76e-02	1.32e-01
2400	2.096e+01	1.048e+01	-49.80	10.24	1.08e-02	1.02e-01
2600	2.271e+01	1.136e+01	-49.45	10.94	6.42e-03	7.70e-02
2800	2.446e+01	1.223e+01	-49.13	11.58	3.69e-03	5.73e-02
3000	2.620e+01	1.310e+01	-48.83	12.18	2.05e-03	4.20e-02
3200	2.795e+01	1.398e+01	-48.55	12.74	1.10e-03	3.02e-02
3400	2.970e+01	1.485e+01	-48.28	13.27	5.73e-04	2.14e-02
3600	3.145e+01	1.572e+01	-48.03	13.76	2.87e-04	1.49e-02
3800	3.319e+01	1.660e+01	-47.80	14.23	1.40e-04	1.02e-02
4000	3.494e+01	1.747e+01	-47.58	14.68	6.54e-05	6.83e-03
4200	3.669e+01	1.834e+01	-47.37	15.10	2.96e-05	4.51e-03
4400	3.843e+01	1.922e+01	-47.16	15.51	1.30e-05	2.93e-03
4600	4.018e+01	2.009e+01	-46.97	15.89	5.48e-06	1.87e-03
4800	4.193e+01	2.096e+01	-46.79	16.26	2.24e-06	1.18e-03
5000	4.367e+01	2.184e+01	-46.61	16.62	8.83e-07	7.28e-04
5200	4.542e+01	2.271e+01	-46.44	16.96	3.36e-07	4.42e-04
5400	4.717e+01	2.358e+01	-46.27	17.29	1.24e-07	2.64e-04
5600	4.892e+01	2.446e+01	-46.12	17.60	4.39e-08	1.55e-04
5800	5.066e+01	2.533e+01	-45.96	17.91	1.51e-08	8.94e-05
6000	5.241e+01	2.620e+01	-45.82	18.20	4.98e-09	5.07e-05
6200	5.416e+01	2.708e+01	-45.67	18.49	1.59e-09	2.83e-05
6400	5.590e+01	2.795e+01	-45.54	18.76	4.92e-10	1.55e-05
6600	5.765e+01	2.883e+01	-45.40	19.03	1.47e-10	8.35e-06
6800	5.940e+01	2.970e+01	-45.27	19.29	4.22e-11	4.42e-06
7000	6.114e+01	3.057e+01	-45.15	19.54	1.17e-11	2.30e-06
7200	6.289e+01	3.145e+01	-45.02	19.78	3.14e-12	1.18e-06
7400	6.464e+01	3.232e+01	-44.91	20.02	8.13e-13	5.92e-07
7600	6.639e+01	3.319e+01	-44.79	20.25	2.03e-13	2.93e-07
7800	6.813e+01	3.407e+01	-44.68	20.48	4.90e-14	1.42e-07
8000	6.988e+01	3.494e+01	-44.57	20.70	1.14e-14	6.79e-08
8200	7.163e+01	3.581e+01	-44.46	20.91	2.57e-15	3.19e-08
8400	7.337e+01	3.669e+01	-44.35	21.12	5.57e-16	1.47e-08
8600	7.512e+01	3.756e+01	-44.25	21.33	1.17e-16	6.66e-09
8800	7.687e+01	3.843e+01	-44.15	21.53	2.36e-17	2.97e-09
9000	7.861e+01	3.931e+01	-44.06	21.72	4.61e-18	1.30e-09
9200	8.036e+01	4.018e+01	-43.96	21.91	8.70e-19	5.60e-10
9400	8.211e+01	4.105e+01	-43.87	22.10	1.58e-19	2.37e-10
9600	8.386e+01	4.193e+01	-43.77	22.28	2.78e-20	9.85e-11
9800	8.560e+01	4.280e+01	-43.69	22.46	4.72e-21	4.03e-11
10000	8.735e+01	4.367e+01	-43.60	22.64	7.72e-22	1.62e-11
10200	8.910e+01	4.455e+01	-43.51	22.81	1.22e-22	6.40e-12
10400	9.084e+01	4.542e+01	-43.43	22.98	1.86e-23	2.48e-12
10600	9.259e+01	4.630e+01	-43.34	23.14	2.75e-24	9.48e-13
10800	9.434e+01	4.717e+01	-43.26	23.30	3.91e-25	3.56e-13
11000	9.608e+01	4.804e+01	-43.18	23.46	5.36e-26	1.31e-13
11200	9.783e+01	4.892e+01	-43.11	23.62	7.11e-27	4.76e-14
11400	9.958e+01	4.979e+01	-43.03	23.77	9.10e-28	1.70e-14
11600	1.013e+02	5.066e+01	-42.95	23.92	1.13e-28	6.00e-15
11800	1.031e+02	5.154e+01	-42.88	24.07	1.34e-29	2.00e-15

Photomultiplier Tubes for Use at 1.064 μm Wavelength

Xiaoli Sun

Department of Electrical and Computer Engineering
The Johns Hopkins University
Baltimore, Maryland 21218

November 1992

Photomultiplier tubes (PMT) have long been used to detect very low level light signals.[1] The major advantages of PMTs over photodiodes are the very high photoelectron multiplication gain (10^6) and low dark current (<10 counts/s when cooled). The effect of thermal noise of the subsequent circuit can usually be neglected because of the high photoelectron multiplication gain. PMTs are widely used for detecting light over the spectrum of 115-900nm. It has long been the interest to extend PMT spectral response to the fundamental wavelength of Nd:YAG lasers, =1.064μm.

PMTs detect light by first converting photons into free photoelectrons at the photocathode through photoemission process and then multiply the primary photoelectrons through secondary electron emission at the subsequent dynode chain. The spectral response of a PMT is primarily determined by the property of the photocathode.

Photoemission of a metal photocathode is governed by the following equation[2]

$$E_{max}=h\nu-W \qquad (1)$$

where E_{max} is the maximum energy of the free photoelectrons, hν is the photon energy of the incident light, and W is the work function of the metal which is defined as the energy for an electron to escape from the Fermi level to the vacuum. Equation (1) is known as Einstein's photoemission equation. For photoemission to occur, the left hand of (1) have to be greater than zero, i.e. hν>W. The lowest work function for a metal (Cs) is about 2 eV. Therefore, a pure metal photocathode is only sensitive to light of wavelengths which satisfy

$$h = hc/ > Wq \qquad (2)$$

where c is the speed of light and q is the electron charge. The threshold wavelength is given by

$$_{th} = (hc/q)/W=1242\ (nmeV)/2(eV) = 621\ nm. \qquad (3)$$

Above the threshold wavelength, the photocathode become useless. The spectral response of a photocathode is also limited for wavelengths a few times below the threshold wavelength due to photoelectron reabsorption by the photocathode.[3] Therefore, metal photocathode is only useful for detecting ultraviolet to visible light.

Semiconductors may also be used as photocathodes. The photoemission formula for semiconductors is given by[2]

$$E_{max}=h-(E_g+) \qquad (4)$$

where E_g is the bandgap from the top of the valance band to the bottom the conduction band and is the electron affinity defined as the distance in energy from the bottom of the conduction band to the vacuum level. The energy E_g+ can be as low as 1.4 eV ($_{th}$ = 887 nm) for certain materials (e.g. NaKCsSb).[2] Some semiconductor materials can also have negative electron affinity which results from the downward bending of the conduction and valance bands near the surface such that the conduction band of the bulk material lie above the vacuum level at the surface. Uartinelli and Fisher of RCA.[4] gave a good review about this type of negative electron affinity surface photocathodes.

Negative electron affinity photocathodes made of GaAs can have a nearly flat spectral response with 5-10% quantum efficiencies from = 200-900 nm.[5-7] Materials which have useful quantum efficiency to even longer wavelength are those with lower activated bandgaps, such as InGaAs, In AsP, and InGaAsP.[2,8] The highest reported quantum efficiencies was 9.0% at =1.064m with an InGaAsP photocathode.[9]

Unfortunately, PMTs of these type photocathodes cannot be found in the market today, possibly due to the poor stability and short life time of the photocathodes. Another reason may be the competition from the recent advance in semiconductor photodiodes, which have much higher quantum efficiency and are much easier to use. One of the leading PMT manufacturers, RCA (changed to Burle Industries since 1989), once offered three types of InGaAs photocathode PMTs which had a quantum efficiency of 0.2% at =1.064m,[6] but they discontinued at least before 1984.[10,11] Other leading PMT makers, such as Hamamatsu and EMR, currently do not offer InGaAs or InGaAsP photocathode PMTs.

The only PMTs commercially available now which has useful response to =1.064m and beyond contain a photocathode of multiple layers materials, i.e., Ag-O-Cs (S-1). However, the quantum efficiencies of this type PMTs are only about 0.08% at =1.064 μm.[5] The dark currents are also high, about 1A at room temperature and about 1 nA when cooled to -30 to -40 C.

Conventional PMTs have relatively slow temporal response, typically in nanoseconds, because electrons have to travel through the sizable dynode chain. The latest technology to improve the temporal response is to use microchannel plates (MCP) as the dynodes.[12] A microchannel plate consists of an array of millions of capillaries of internal diameter about 10m and thickness of about 1 mm. The inner wall of capillaries are coated with secondary electron emission material and act as continuous dynodes. Photoelectrons are multiplied when passing through a microchannel plate, just as in a conventional PMT. Since the dimension of microchannel plates are much smaller than that of a conventional discrete dynode chain, the transit time of the photoelectrons are much shorter. Microchannel plate PMTs can have a output pulse rise and fall times of about 100 ps and an electrical bandwidth as high as 3GHz.[12]

Choices between PMTs and Semiconductor Photodiodes at =1.064m

The quantum efficiencies of commercially available PMTs are still too low to be considered at =1.064m for most applications. Semiconductor photodiodes have much higher quantum efficiencies (40%) at this wavelength and faster time response. The overall performance of photodiodes is usually superior in spite of the effects of the circuit thermal noise which is the primary noise source. Avalanche photodiodes (APD) also provide internal photoelectron multiplication gain up to 1000. Silicon APD have been shown to outperform a PMT as photon counters at =1.064m with a quantum efficiency of 0.3% and dark counts of 9000/s at room temperature.[13]

References

1. S. Rodda, *Photo-Electric Multipliers*, Macdonald & Co. (Publishers), LTD., London, 1953.

2. H. R. Zwicker, 'Photoemissive Detectors,' in *Optical and Infrared Detectors*, R. J. Keyes, editor, Springer-Verlag, Berlin, 1977, ch. 5.

3. L. Mandel and D. Meltzer, 'Theory of time-resolved photoelectric detection of light,' *The Physical Review,* Vol. 188, No. 1, pp. 198-212, December 5, 1969.

4. R. U. Martinelli and D. G. Fisher, 'The application of semiconductors with negative electron affinity surfaces to electron emission devices,' *Proceedings of The IEEE,* Vol. 62, No. 10, pp. 1339-1360, Oct. 1974.

5. *Photomultiplier Tubes,* Hamamatsu Corporation, Catalog, Oct. 1990.

6. *Photomultiplier Tubes*, RCA Electronics Components, Harrison, NJ, Catalog, Dec. 1971.

7. R. W. Engstrom, *Photomultiplier Handbook*, RCA Corporation, Solid State Division, Lancaster, PA, 1980.

8. P. N. J. Dennis, *Photodetectors, an Introduction to Current Technology,* Plenum Press, New York, 1986, ch. 4.

9. J. S. Escher, G. A. Antypas, and J. Edgecumbe, 'High-quantum-efficiency photoemission from an InGaAsP photocathode,' *Applied Physics Letters,* Vol. 29, No. 3, pp. 153-155, Aug. 1976.

10. *RCA Photomultipliers,* RCA corporation, Lancaster, PA, Catalog, Jan. 1984.

11. *Photomultipliers*, Burle Industries, Inc., Tube Products Division, Lancaster, PA, Catalog, June 1992.

12. *MCP Assembly,* Hamamatsu Corporation, Technical Information, Sept. 1991.

13. X. Sun and F. M. Davidson, 'Photon counting with silicon avalanche photodiodes,' *J. Lightwave Technology,* Vol. 10, No. 8, pp. 1023-1032, Aug. 1992.